UNIVERSITY OF TECHNOLOGY SYDNEY

STUDY ON TWO-SPEED TRANSMISSIONS FOR BATTERY ELECTRIC VEHICLES

by Yang Tian

Thesis submitted in fulfilment of the requirements for the degree of

Doctor of Philosophy

under the supervision of Nong Zhang

University of Technology Sydney
Faculty of Engineering and Information Technology

June 2020

CERTIFICATE OF ORIGINAL AUTHORSHIP

This research is supported by the Australian Government Research Training Program.

I certify that the work in this thesis has not previously been submitted for a degree nor has it been submitted as part of requirements for a degree except as fully acknowledged within the text.

I also certify that the thesis has been written by me. Any help that I have received in my research work and the preparation of the thesis itself has been acknowledged. In addition, I certify that all information sources and literature used are indicated in the thesis.

Signature of student: Production Note:
Signature removed prior to publication.

Date: 24 June 2020

ACKNOWLEDGEMENT

I'd like to take this opportunity to thank the following people and organizations for their assistance and support during my candidature.

My supervisor Professor Nong Zhang, his knowledge and guidance have been invaluable, and together with co-supervisors Dr. Paul D. Walker has guided me through this research and supported my work.

My UTS colleagues, whose knowledge, advice and experience have encouraged me to do better and better, Jiageng Ruan, Wenwei Mo, Haitao Yang, Jinglai Wu, Shilei Zhou, Shengxiong Sun, Mohamed Awadallah, Jiejunyi Liang, Hanfei Wu, Boyi Xiao, and Weiwei Yang are along with me.

Most importantly my wife, Wang Jiayan, who is always by my side and help me through thick and thin, I couldn't have done this without you. Of course, my parents' advice and encouragement are indispensable.

Financial support for my project is provided by the Australian Research Council and the University of Technology Sydney (UTS).

TABLE OF CONTENTS

LIST OF FIGURES

LIST OF TABLES

GLOSSARY OF TERMS AND NOTATIONS

ABBREVIATIONS USED IN THESIS

EV	Electric Vehicle
BEV	Battery Electric Vehicle
HEV	Hybrid Electric Vehicle
ICE	Internal Combustion Engine
DCT	Dual Clutch Transmission
AT	Automatic Transmission
AMT	Automated Manual Transmission
CVT	Continuously Variable Transmission
VCU	Vehicle Control Unit
SOC	State of Charge
ECE driving cycle	United Nations Economic Commission for Europe (UNECE) urban
NEDC	New European driving cycle
UDDS	Urban dynamometer driving schedule
LA-92	Los Angeles 92 / Unified cycle driving schedule
HWFET	Highway fuel economic test
JP1015	Japan 1015 emission test cycles model
UPAT	Uninterrupted Planet-gear Automatic Transmission
PAMT	Planetary Automated Manual Transmission
CITGS	The constant input torque gearshift strategy
SCOTGS	the semi-constant output torque gearshift strategy
COTGS	the constant output torque gearshift strategy

CHAPTER 3 NOTATIONS

T_i	the applied moment
J_i	the inertia
$\ddot{\theta}_i$	angular acceleration
i	the i^{th} inertia element
C	damping coefficient
K	stiffness coefficient
R	ring gear
C	carrier
SS	small sun gear
LS	large sun gear
IP	inner planet pinion
OP	outer planet pinion
OWC	one-way clutch
r_{SS}	the radius of the small sun gear
r_{IP}	the radius of inner planet pinion
r_{OP}	the radius of outer planet pinion
r_R	the radius of ring gear
r_{LS}	radius of large sun gear
i_{first}	the first gear ratio of UPAT
i_I	the gear ratio of inertia phase during gear shifting
i_{second}	the second gear ratio of UPAT
T_M	the torque of the motor
α_P	accelerator pedal position
$\dot{\theta}_M$	the motor rotational speed

k_1	the spring coefficient
c_1	the damping factor
T_I	the load on the motor
F_{LS}	the applied force
R_D	the band brake drum radius
μ_B	the Coulomb friction coefficient
α_B	the band brake wrap angle.

CHAPTER 4 NOTATIONS

T_{ef}	equivalent vehicle resistance

CHAPTER 6 NOTATIONS

LQR	linear-quadratic regulator
T_{M0}	the initial torque of the motor during torque phase
T_{C0}	the initial torque OWC during torque phase
T_{LS_Max}	the max LS brake torque
T_{M_Max}	the max motor torque in its current speed state.

CHAPTER 7 NOTATIONS

EM	electric machine
S	sun gear
P	planet gear
C	carrier
R	ring gear
GR1	gear ring 1
SH	spline hub
SL	sleeve
GR2	gear ring 2

TDP	the third-degree polynomial
FDP	the fifth-degree polynomial
SDP	the seventh-degree polynomial

ABSTRACT

Due to the shortage of fossil fuel and environment degradation, developing battery electric vehicles (BEVs) has been the irreversible trend in the automotive industry recently. Despite the long-term benefit of BEVs to customers and the environment, the initial cost and limited driving range present the significant barriers for widespread commercialization. At present, BEVs usually adopt a single driving motor with a fixed-ratio transmission in order to simplify the powertrain system; however, the performance requirements of the power battery pack and driving motor are quite high. In order to improve the efficiency of an electric driving system while meeting the requirements of vehicle driveability and reducing manufacturing costs, BEVs can be equipped with multi-speed transmissions. A two-speed transmission system appears to be suitable for BEVs in consideration of dynamic performance, energy efficiency, and cost-saving. It can improve the grade ability at low-speed and efficiency at high-speed, thereby reducing the performance requirements of the power battery pack and driving motor, which reduces the manufacturing costs to a degree.

In this thesis, two different types of two-speed transmissions are proposed. The first is a transmission that is comprised of dual-stage planet gear sets and can achieve a gear shifting without the torque interruption, called Uninterrupted Planet-gear Automatic Transmission (UPAT). The other is made up of a single planet gear set, called Planetary Automated Manual Transmission (PAMT). The proposed 2-speed UPAT takes advantage of its mechanical layout to achieve power-on gearshifts by controlling a band brake to block or unblock the one-way-clutch, which makes the gearshift control easier than

similar transmissions. Although 2-speed PAMT cannot achieve an uninterrupted torque gearshift, it has a simpler structure and an easier gearshift control system than 2-speed UPAT, and a more compact structure than traditional two-speed automated manual transmission (AMT). This thesis focus on the following six research topics: 1) mathematical modeling of 2-speed UPAT; 2) gearshift control strategies' design of 2-speed UPAT; 3) rig development and gearshift strategies' validation of two-speed UPAT; 4) optimal gear shifting control for 2-speed UPAT; 5) torque observer design for 2-speed UPAT; 6) mathematical modeling and gearshift control of 2-speed PAMT.

For two-speed UPAT study, firstly, a mathematical model is developed, including the electric motor, the proposed two-speed UPAT, the vehicle, etc. Secondly, model-based alternative power-on gearshift strategies are developed, and a torque-based gearshift closed-loop controller is proposed. The vehicle jerk and the friction work are taken as the foremost metrics to evaluate the gearshift quality. The simulation results demonstrate that all strategies can achieve power-on gearshifts. The disadvantages and advantages of these strategies are exhibited clearly, which provides beneficial knowledge and reference to the researchers engaged in the development of the transmission controller. Thirdly, to validate the simulation results, a testing rig is developed. The simulation results are well-validated by the experimental results. Fourth, to comprehensively improve the gearshift quality, optimal gearshift control tactics for the torque phase and the inertia phase are proposed to reduce the vehicle jerk and friction work within the fixed gearshift duration. And, the simulation results demonstrate that the proposed multi-objective optimal tactic for the torque phase effectively reduces the vehicle jerk and friction work, and the optimal coordinating tactic for the inertia phase decreases the friction work to a high degree.

Meanwhile, to provide unmeasurable torque information for executing the proposed optimal strategies, sliding mode theory is employed to design the torque observers which are capable of estimating the torque information sufficiently and accurately.

For two-speed PAMT study, to present the transient behaviors during the gear shifting, a detailed and original dynamical model of the electrified powertrain is developed, including an electric machine (EM), a two-speed PAMT, synchronizer mechanisms, driveline, and vehicle, etc. Afterward, the gear shifting control system is devised, and the gearshift process is orderly divided into five stages based on the proposed control strategy. Next, three alternative planning torque trajectories, i.e., the third-degree polynomial (TDP), the fifth-degree polynomial (FDP), and the seventh-degree polynomial (SDP), are proposed to control the EM torque at the first and the fifth stages of the gear shifting respectively. Then, a series of control group simulations are performed to validate which candidate trajectory can obtain the optimal gearshift quality. Simulation results demonstrate that TDP based torque trajectory is the optimal trajectory which is the capacity of not only suppressing the gear shifting jerk but also reducing shift durations. This study will also provide beneficial references for gear shifting control of clutchless automated manual transmission (CLAMT) which is widely adopted in battery electric vehicles.

CHAPTER 1 : INTRODUCTION

1.1 PROJECT STATEMENT

The development and verification of mathematical models and control strategies of Battery Electric Vehicles (BEVs) equipped with two-speed transmissions for achieving the quality gear shifting under a wide range of operating conditions.

1.2 PROJECT OBJECTIVES

In terms of the current state of power battery and driving electric motor technology development, it is necessary to pursue multiple measures for improving the powertrain efficiency to prolong the one-charged mileage and reduce the design requirements of the power battery and the driving electric motor to save the manufacturing costs. Many studies demonstrate that an optimized two-speed transmission system is a kind of effective method to remedy the deficiencies of power battery and driving motor and downsize the powertrain to a great extent. Besides, the motor and transmission system also need optimal strategies and algorithms to work cooperatively to obtain good gear shifting quality. This thesis is focused on the investigation into gear shifting mechanism, transient dynamics, and the control strategies and algorithms of the proposed two-speed transmissions. The main objectives of this project are:

1. Build the dynamic model of the main components of a two-speed UPAT and integrate it into a vehicle powertrain model for predicting the transient characteristics during gear shifting.

2. Design model-based gearshift control strategies of the two-speed UPAT for achieving the power-on gearshifts.
3. Develop the experimental rig for validating the gear shifting control strategies.
4. Develop optimal gearshift controller of the two-speed UPAT for comprehensively improve the gear shifting quality, and torque observer is designed for power-on gearshift control to provide necessary torque information for closed-loop torque control.
5. Build the model of key mechanical parts of the two speed PAMT and integrate it into a full vehicle powertrain model to obtain the transient dynamics in the gear shifting process and develop the gear change algorithms for two speed PAMT.

1.3 PRESENTATION OF THIS THESIS

The thesis will consist of 8 chapters, organized as follows, subject to change if necessary.

Chapter 1:

In the first chapter, the project statement and objectives will be presented. And the project's main contents, presentation of this thesis, and publications will be included as well.

Chapter 2:

This chapter provides the framework for the research of this thesis. Initially, the required background information on relevant aspects of the advantages of multi-speed transmissions equipped BEVs is presented to introduce the topics for research. This is followed by a detailed literature review that identifies the state-of-the-art in multi-speed

BEVs, the gearshift schedules, torque observer design, and gearshift control methodologies. To complement this work, a brief exploration of literature is performed in each relevant chapter to identify the important aspects of relevant research, as necessary.

Chapter 3:

The mathematical model of the full vehicle powertrain with two-speed UPAT is developed in this chapter using conventional dynamic theories. This model is applied to Matlab and Simulink environments to investigate the transient response of the powertrain system during gear shifting.

Chapter 4:

Model-based gear shifting strategies for two-speed UPAT will be designed to achieve the power-on gear shifting, and the corresponding simulation results will also be presented to evaluate which strategy is optimal among these shift strategies.

Chapter 5:

The configuration of the lab powertrain testing rig is presented. Vehicle control unit, motor control unit, and transmission control unit are demonstrated. And, the experimental results according to alternative model-based gear shifting strategies are also analyzed in this chapter.

Chapter 6:

In this chapter, the optimization control theory is applied to design a limited-time linear-quadratic regulator. A series of simulation results' comparisons from different control algorithms are shown and demonstrate that the limited-time linear-quadratic regulator can improve the gear shifting quality comprehensively. The sliding observers are designed to estimate the key torque information for achieving the power-on gear shifting strategies. And, the observer robust is also demonstrated.

Chapter 7:

In this chapter, to present the transient behaviors during the gear shifting, a detailed and original dynamical model of the electrified powertrain is developed, including an electric machine (EM), a two-speed PAMT, synchronizer mechanisms, driveline, and vehicle, etc. Afterward, the gear shifting control system is devised, and the gearshift process is orderly divided into five stages based on the proposed control strategy.

Chapter 8:

The concluding chapter reviews and summaries each of the previous chapters, presenting significant and novel results of this thesis as well as identifying the important areas for further research.

1.4 PUBLICATIONS

Journals

[1] **Y. Tian,** J. Ruan, N. Zhang, J. Wu, and P. Walker, "Modelling and control of a novel two-speed transmission for electric vehicles," Mechanism and Machine Theory, vol. 127, pp. 13-32, 2018.

[2] **Y. Tian**, H. Yang, W. Mo, S. Zhou, N. Zhang, and P. D. Walker, "Optimal coordinating gearshift control of a two-speed transmission for battery electric vehicles," Mechanical Systems and Signal Processing, vol. 136, 2020.

[3] **Y. Tian**, N. Zhang, S. Zhou, and P. D. Walker, "Model and gear shifting control of a novel two-speed transmission for battery electric vehicles," Mechanism and Machine Theory, p. 103902, 2020.

[4] S. Zhou, P. Walker, **Y. Tian**, and N. Zhang, "Mode switching analysis and control for a parallel hydraulic hybrid vehicle," Vehicle System Dynamics, pp. 1-21, 2020.

Conference Proceedings:

[1] **Y. Tian**, J. Ruan, P. D. Walker, N. Zhang, An optimized speed synchronization control for Clutchless Automated Manual Transmission in pure electric vehicles. The 2017 International Conference on Advanced Vehicle Powertrains, China.

[2] S. Zhou, P. Walker, **Y. Tian**, and N. Zhang, "Parameter Design of a Parallel Hydraulic Hybrid Vehicle Driving System Based on Regenerative Braking Control Strategy," SAE Technical Paper, 0148-7191, 2019.

CHAPTER 2 : BACKGROUND INFORMATION AND LITERATURE REVIEW

2.1 BACKGROUND

Automobiles have made great contributions to the growth of modern society by satisfying many of the needs for mobility in the daily activities of human beings [1]. The rapid development of the automotive industry has prompted the progress of human beings from primitive society to a highly developed industrial one [2].

At present, most vehicles still rely on the combustion of fossil fuels to derive the energy necessary for their propulsion. However, the combustion of fossil fuels yields carbon dioxide (NO_2), nitrogen oxides (NO_x), carbon monoxide (CO), and unburned HCs, some of which are toxic to human health and the environment [3-6]. Beyond all doubt, the large number of automobiles in use around the world has caused and continues to cause air pollution, global warming, and the rapid depletion of the Earth's petroleum resources [7-9]. Historical and current data all show that the discovery of oil reserves grows slowly [10, 11]. However, consumption data shows a high and continuous growth rate. If oil discovery and consumption follow the current trends, the world oil resource will be used up in around forty years [10].

In the future, BEVs with their low local-emission status and potential independence from fossil fuels will provide a valuable and sustainable addition to the mobility landscape to replace the current conventional combustion engine vehicle [12-14]. To encourage the

sustained increase in the demand for BEVs, major economies in the world (e.g., United States, European Union, China, and Japan) are releasing increasingly financial and policy incentives [15]. BEVs are distinguished with superior features such as high-efficiency and a more flexible powertrain configuration as well as harmful emission reduction. As the most promising transportation, BEVs obtain wide concern of traditional automotive industries and emerging automakers from all over the world. A great quantity of commercial BEVs and concept BEVs have been made and launched, e.g. General Motors, Renault–Nissan alliance, Mitsubishi, Audi, Ford, BMW, Volvo, Fiat, Mercedes-Benz [16].

The following sections review the current research state of multiple speed transmission systems used in BEVs, the gearshift schedules, torque estimation in the gearshift process, and gearshift control methodologies.

2.2 LITERATURE REVIEW

2.2.1 The benefits of multiple speed transmission systems for BEVs

Current electrified powertrain solutions normally consist of an electric machine combined with a fixed-ratio transmission and differential gear, e.g. VW e-Golf, Nissan Leaf, BYD e6, Renault Zoe, and Ford Focus. Permitting a relatively low level of integration, their hill-climbing ability, accelerating performance, and efficiency are limited too. With the increasing demands, BEVs must satisfy without compromise regarding lightweight, recharge mileage, and price, while also providing a high level of safety, reliability, and ride comfort [17]. To meet these requirements, further exploiting the potential benefits of

the electrified powertrain is essential [18]. Many investigations indicate that integrating a multiple speed transmission into the electric-drive system can make optimum use of high-efficiency motor operating ranges, improve drivability and cut energy consumption compared to a single-speed equivalent [16, 19-28].

A multiple speed transmission for an electric vehicle is proposed in [29]. In this research, the first gear ratio helps the vehicle to improve the maximum acceleration performance and the maximum climbing road grade performance. This means that the maximum torque of the electric motor can be decreased due to the maximum wheel torque increased or unchanged by increasing the first gear ratio. When the maximum torque becomes smaller, the volume and weight of the electric motor will be reduced, which contributes to saving the manufacturing costs. When the second gear is adopted, the maximum vehicle speed is greatly increased by about 17% (from 120km/h to about 140km/h). And, this research also shows a comparison of the operating point for a single and two-speed electric drivetrain. The results theoretically illustrated that when the vehicle speed and required wheel torque are given, the motor would be operating in a lower efficiency region in the first gear than in the second gear. The reason is that the high-efficiency region of a motor is generally in the low-speed high torque region as opposed to the high-speed low torque region. In 2010, more detailed research is presented by the same research group [30]. In this research, two electric motors with the same power were chosen for the two powertrains. The two-speed powertrain was powered by a low torque high-speed motor as opposed to a high torque low-speed motor for the single-speed powertrain. The first advantage form adopting a low torque high-speed motor is that the weight and volume were saved by 51 kg and 15 litres separately. Furthermore, the authors

found that 0-100 km/h acceleration time for the two-speed vehicle was 7.4s which is less than 8.4s for the single-speed vehicle and compared to the single-speed vehicle.

A three-speed dual-clutch transmission for a BEV was developed by Antonov Plc [31]. The three-speed transmission shows merits over a single-speed for an electric vehicle, e.g. reducing powertrain weight and cost due to the motor downsized and improving powertrain efficiency and range. The benefits of adopting a three-speed transmission over a two-speed were also discussed. The energy consumption for single, two, three, and four-speed transmissions were compared by using a drive cycle analysis tool, where the motor size and gear ratios of all study cases were optimized, with regenerative braking considered. The two-speed transmission has a more significant efficiency improvement than the single-speed equivalent. However, only smaller efficiency improvement can be obtained by the three and four-speed powertrains over the two-speed equivalent.

A two-speed automated manual transmission with a rear-mounted dry clutch is proposed in [21]. In this research, it had a vehicle performance comparison with fixed-ratio gearbox and the proposed 2-speed automated manual transmission. To achieve better drivability and economic performance, firstly the gear ratio and the gearshift schedules were optimized by using a dynamic programming method where three different kinds of driving cycles were used, including NEDC, UDDS, and 1015. The comparison results show that the acceleration time from 0 to 80 km/h is reduced by 1.1 s and the top speed is improved from 113 km/h to 148 km/h which is significantly increased by about 31.1%. Also, the average energy consumption is saved by about 7–11% under three drive cycles, which means that the driving range can be extended with the same battery pack. Furthermore, this study also had a consideration into the slip friction work of clutch in

the gearshift process of the proposed two-speed transmission due to its negative impact on the energy efficiency of the vehicle.

Two redesigned multi-speed transmission systems are proposed in [32], a two-speed DCT, and a CVT without a torque converter. Firstly, this study gave an inclusion of previous research and pointed out some limitations of those research, such as the lack of the analysis for additional manufacturing cost due to adopting multiple speed transmissions to battery electric vehicles, the lack of experiment validations of the proposed multiple speed transmissions and so on. Then, the powertrain backward-facing models, including different transmissions, e.g. single-speed, two-speed DCT, and CVT without a torque converter, were built in detail. Besides, the gear ratios and gearshift schedules for multiple speed gearboxes were designed and optimized. After that, simulations were run for the Urban Driving Cycle (ECE-15), Highway Fuel Economic Test Cycle (HWFET), and LA92. Simulation results show that CVT improves motor efficiency by 5–16% and reduce power consumption 6–10%, compared to a BEV equipped with a single reducer transmission system. Less improvement was achieved in a two-speed DCT scenario with raising motor efficiency 2–10%. However, the authors also think that this advantage of CVT will disappear in the practice when compared to 2-speed DCT because CVT itself has more energy dissipated. The dynamic performance simulation results show that the same acceleration time is achieved in single-speed reducer and two-speed DCT due to their same highest gear ratio. The CVT system with a higher gear ratio helps increases the acceleration time by one second and the maximum driving road grade by 25%. The two-speed DCT improves top speed by 57% comparing with a single-speed equivalent. The performance of single-speed reducer and two-speed DCT is also verified by a

powertrain-testing rig in HWFET and ECE driving cycles. In the HWFET cycle testing, comparing with the single-speed system, the two-speed DCT system had about 7.4% average motor efficiency improvement. In the ECE cycle, most of the testing is acceleration and braking at a low speed. Therefore, the 2nd gear of two speeds DCT has far less opportunity to use in this cycle, which will influence the overall motor efficiency. The average motor efficiency is 82%, 5.6% higher than that of SR scenario. At the end of this paper, the authors evaluated the increased manufacturing cost and reduced daily-use cost for three transmissions, which is the largest highlight in the research. It can be found that adding a multi-speed transmission system to BEVs can save thousands of dollars. This paper is systematic research into multiple speed transmission and provides a good reference to the other researchers and BEV manufacturers. However, there still exist some problems which need to be further considered and researched. For example, the friction work in the gear shifting process should be considered and the gearshift schedules are only based on the economy performance, which may not be accepted in transmission products.

According to the above research results, it can be found that when BEVs equipped with multispeed transmissions presents advantages in many aspects compared to single-speed equivalent, e.g. dynamic enhancement, operation efficiency improvement of the electric motor, downsizing the weight and volume of powertrains and manufacturing cost reduction. In the following part, different kinds of multispeed transmissions applied in BEVs will be reviewed, including their layouts and structure, the gear shifting principle, gearshift actuators, etc.

2.2.2 Alternative transmissions used in BEVs

In this section, different multiple-speed transmission layouts proposed for or used in modern BEVs are reviewed. Currently, a variety of multispeed transmissions adopted in BEVs are widely studied. However, both advantages and disadvantages of each transmission configuration coexist. These multiple speed transmissions are generally divided into two types, i.e., power-on and power-off [33]. These transmissions with power-on gearshift capacity consist of dual-clutch transmission (DCT) [22, 34], planetary automatic transmission (AT) [35-37], torque-assist automated manual transmission (AMT) [20, 38, 39] and Continuously Variable Transmission (CVT) [16]. The other style of transmission is without power-on gearshift capacity, i.e., clutchless automated manual transmission (CLAMT) regarded as the traditional AMT variant. All of these multi-speed transmissions utilized in BEVs were initially designed for internal combustion engines (ICE) vehicles [26], and Since ICE cannot work below idle speed and its precise speed control in the gear shifting process is also a difficult task, clutches or torque converters are necessary for some scenarios of start-up, idle speed, and gear shifting. However, the operating speed of electric motors for BEVs is easily controllable in a wide range and the electric motors exhibit a high constant torque from zero to base speed. Especially, the electric motors for BEVs do not need the idle speed function of ICE. These benefits from electric motors provide an opportunity for redesigning the previous transmissions for BEVs.

2.2.2.1 AMT

AMT is of great merits due to its lower cost, easier manufacture, and higher efficiency in comparison with other types of transmissions such as AT, CVT, and DCT [40, 41]. However, the torque interruption during gear changing operation always causes uncomfortable accelerations and jerks. The uncomfortableness is mainly dominated by the control of ICE, clutch, and gearshift actuator. The standard form of AMT is one that uses a standard manual transmission and installs automated actuators on the shift forks and clutch [42]. These actuators can be driven by the pneumatic, hydraulic, or electric source to replace the drivers' operations during start-up and gear shifting.

A conventional AMT for vehicles powered by an internal-combustion engine (ICE) requires a clutch controlled by a corresponding electronic control unit to isolate and engage the engine power for smooth gear changes or start-up, because of the big inertia of the ICE. This not only makes the system complicated and expensive but also causes power loss due to the slip friction process of clutch surfaces, and increases the gear shifting duration. However, when AMT is used in the BEVs, the clutch can be removed due to the following reasons [43]: firstly, the electric motor has smaller inertia than an ICE and excellent low-speed control capability, and so the vehicle can be launched by controlling the motor smoothly; secondly, during gear shifting, the electric control unit (ECU) can quickly control the motor operation when the motor is switched between the torque mode and the speed mode. At this moment, the motor speed is controlled to be synchronous with the connected input shaft of AMT. Then, the gear actuators can be operated at this time when finishing the gear-shift operations. For these reasons, a clutch is unnecessary when integrating AMT into a driving electric motor system. After the

elimination of clutch, the manufacturing cost could be reduced to a great degree and the level of control difficulties is also reduced. Furthermore, the powertrain mass and volume are reduced to free up more space for layout, and maintenance costs of the clutch are also saved.

The GKN Plc developed a two-speed AMT, shown in Figure 2-1 [44]. It was applied to BMW i8 and was used to drive the front wheels of the car via connecting its input shaft to the traction motor. Giving the electric motor an additional gear ratio improves acceleration and pure electric range, benefiting both driving dynamics and CO_2 emissions, according to GKN. On November 16, 2016, BorgWarner also declared that its electric drive module (eDM) with integrated AMT eGearDrive® gearbox would be developed and used in pure electric vehicles from a major Chinese automaker. The propulsion system is produced in China [40].

Figure 2-1: GKN's two-speed AMT [44]

Figure 2-2 shows the workflow of a Clutchless AMT (CLAMT) control system [43]. In this research, firstly, the authors analyzed the gear-shifting procedure and then found traction motor speed control and actuator motor position control play a key role in the whole shift process. In the end, they designed a traction motor controller based on the sliding-mode method to achieve quick and smooth gearshift operation, which is verified by simulation and experimental results.

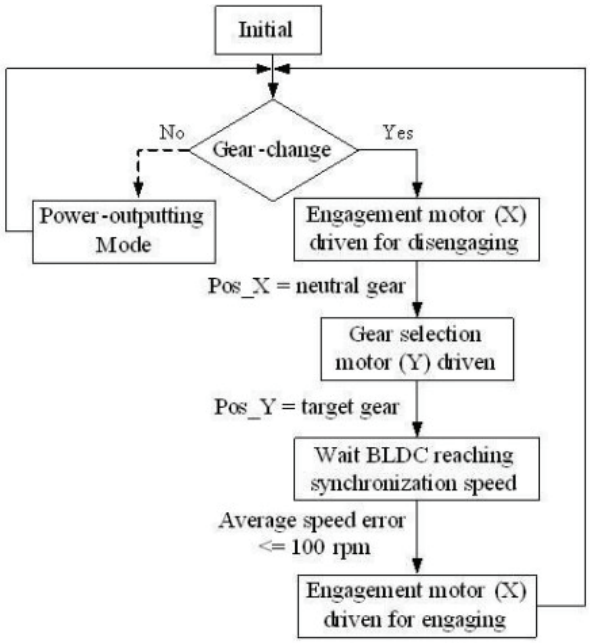

Figure 2-2: The workflow of the CLAMT control system [29]

In Ref. [22], a robust speed controller was designed to control the motor speed at the third stage of gear shifting. Refs. [23–26] focused on the dynamics and control of gearshift actuators. Torque observers were designed to improve oscillation damping performance and gear shifting quality [27,28]. These studies achieve splendid results corresponding to their research topics, but do not consider transient jerk response of the powertrain during

the whole gear shifting. This problem was addressed by Walker et al. [29]. Their research demonstrated that motor torque reduction and reinstatement stages have the most significant effect on the longitudinal vehicle jerk response. However, this study does not propose methods to reduce the vehicle jerk.

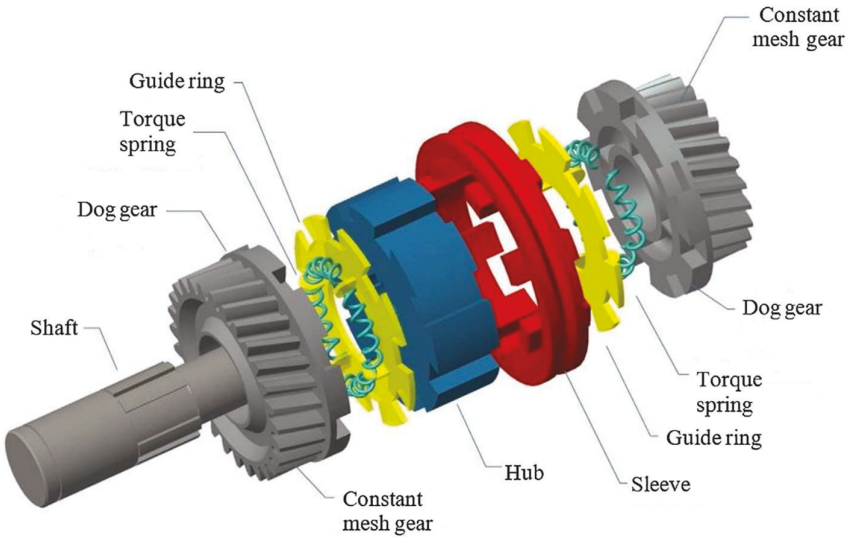

Figure 2-3: Exploded view of the Harpoon-Shift concept [45]

The synchronizer as one of the key components of AMT is also widely investigated. In Ref. [45], this study proposes a novel synchronizer which is named as 'Harpoon-Shift', as shown in Figure 2-3. The gearshift process is displayed in Figure 2-4. This novel synchronizer aims at improving comfort during the gear shifting, meanwhile, simplifying the shifting control strategy for multispeed battery electric vehicles. It will overcome one of the biggest shortcomings of the traditional synchronizer system with a frictional cone clutch. At last, the simulation and experimental results present the significant improvement of the proposed synchronizer compared to the conventional cone clutch synchronizer. In order to improve the gear shifting performance of the proposed novel

synchronizer, Wenwei et al. [46] built an original dynamic model of the powertrain integrating the model of the Harpoon-shift mechanism to investigate the transient responses of driveline system during the gear shifting process. Besides, they proposed a shifting control method based on a special step function to improve driving comfort. Upshift and downshift simulation results validate the effectiveness of the proposed mathematic model and control strategy. Then, this study also optimizes the torque spring stiffness of Harpoon-shift for each gear, rotating inertia and speed difference, which helps to reduce the shifting jerk. Study results show that the jerk is reduced considerably during engagement using the optimized torque springs, which again validated the significant advantages of the Harpoon-shift synchronizer compared to traditional synchronizers.

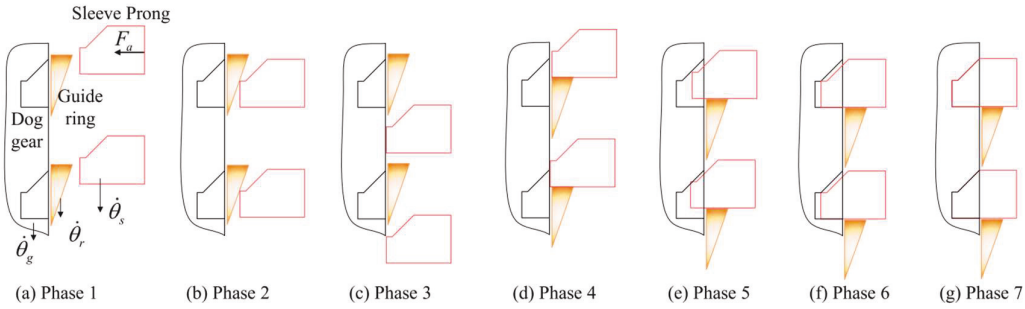

Figure 2-4: Engaging process of Harpoon-shift [46]

Chen and co-author [47] developed a high-fidelity model to capture the trajectories of the parts in the transmission. This model treated the engaging process of synchronizer as a two-phase process-sleeve first interacting with synchro ring and then with clutch gear, described mechanical part movements under a certain constraint by multibody dynamics, and the speed jumps caused by impacts by applying the Poisson coefficient of restitution. This study found that this model can be used for the characteristic analysis of the

engagement process with multiple interaction cases between the engaging-related parts, and the simulation results can be is well validated by bench tests. This study validated two key conclusions: firstly, that the relative position of sleeve and clutch gear has a significant effect on the interaction way of sleeve and clutch gear; secondly, increasing the shifting force can decrease the engaging duration but increase the maximum impact impulse. Piracha et al.[48, 49] developed model-based control strategies aimed to reduce noise and wear during gearshifts.

2.2.2.2 Torque-assist AMT

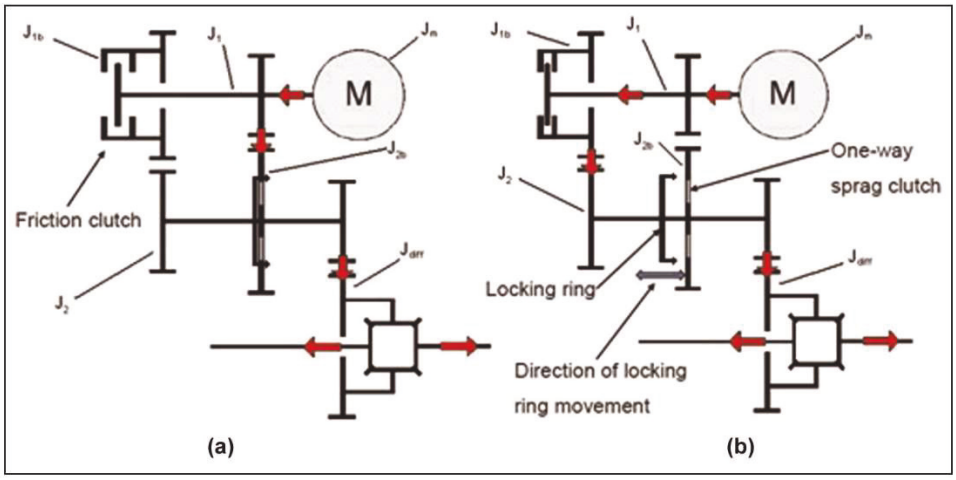

Figure 2-5: Schematic of the transmission operation in (a) 1st gear and (b) 2nd gear [37]

Although the benefits of the CLAMT are obvious, the uncomfortableness of passengers during gear changing operation is still investable during the torque interruption. To address this issue, the AMT with a rear-mounted clutch was proposed. AMT with a rear-mounted clutch is not a newly invented architecture [20, 50] and LuK company and HITACHI company have already researched it for many years for traditional vehicles

with IC engines [51]. Figure 2-5 [37] displays the schematic of the transmission in first gear and second gear. The two-speed transmission can obtain a clutch-to-clutch gearshift without torque interruption. Its primary elements include a one-way sprag clutch (OWC) and a friction clutch, which are installed on the secondary shaft and the primary shaft, respectively. The motor input torque is transmitted by OWC while in first gear, and by the friction clutch while in second gear. The friction clutch is applied to transfer torque from OWC during an upshift and is released to allow OWC to engage to accomplish a downshift. To obtain regenerative energy recovery when decelerating or braking in first gear, a locking ring is engaged to prevent the OWC from overrunning. Also, the gearshift mechanism can be used as a park lock by simultaneously engaging the locking ring and closing the friction clutch, which helps to remove the separate park lock mechanism and actuator.

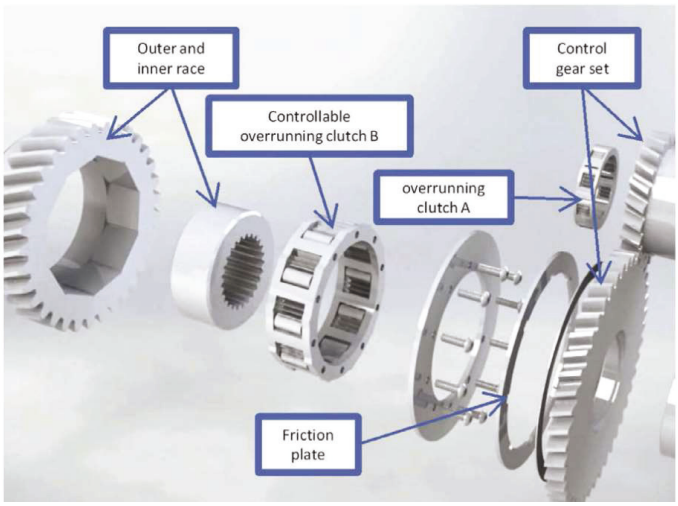

Figure 2-6: Controllable overrunning clutch system [52]

Gao et al. [52] propose an overrunning clutch for torque-assist AMT, which helps to remove synchronizer and shift fork. By applying a controllable overrunning clutch system shown in Figure 2-6, traction interference during the inverse gear process is avoided. A novel inverse dry clutch actuator using worm gear and camshaft is also designed as shown in Figure 2-7. The experimental results show that the actuator can control the clutch position accurately.

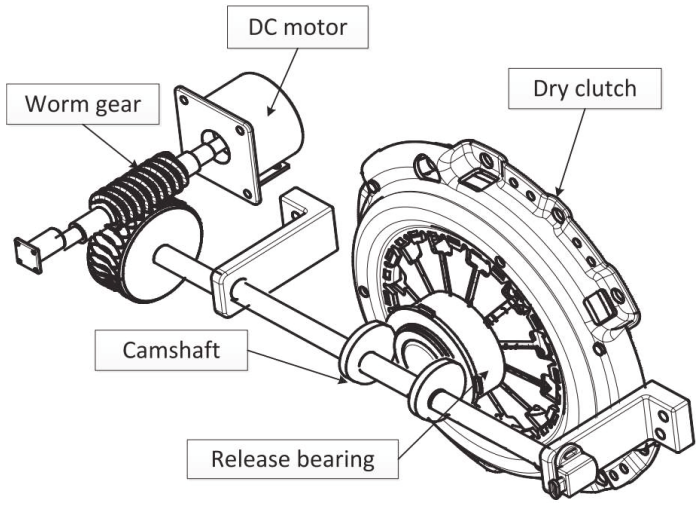

Figure 2-7: Inverse dry clutch actuator [52]

2.2.2.3 DCT

DCT is a modern evolution AMT [53-55], A DCT schematic is shown in Figure 2-8. It is often regarded as two manual transmissions joined together and made of a quill shaft with the inner shaft and the outer shaft connected to two different clutches, respectively. Either the odd or even gears are installed on the inner shaft or the outer shaft. When the torque is being transferred through the inner shaft and the next gear on the outer shaft can be pre-selected. The gearshift can occur through disengaging selected gear clutch and engaging

the pre-selected gear clutch, which helps to achieve a seamless gearshift by transferring the torque from one input shaft to the other. The DCT has many benefits such as high efficiency, seamless gearshift however it is costly to manufacture.

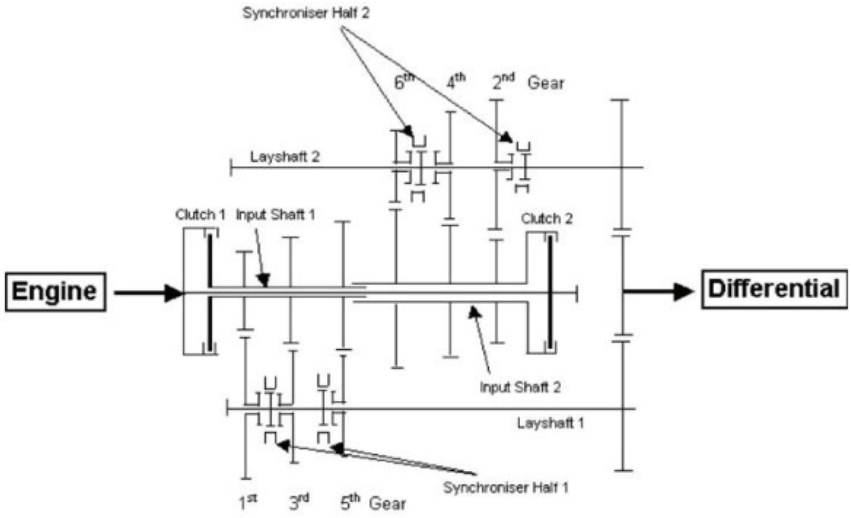

Figure 2-8: A DCT schematic [53]

UTS and BJQ developed a prototype of two-speed wet DCT transmission for a purely electric, the diagram of two speed DCT electric powertrain [56], shown in Figure 2-9. Due to adopting the two-speed design by considering the speed and torque characteristics of electric motors, the synchronizers are eliminated. The different gear-changing control algorithms are designed and validated by simulation and powertrain rig tests [34]. The results illustrate that the designed control program can realize the transient shifting control and obtain a good gear shifting quality. In their research, dynamic and economic shift schedules are developed for the two-speed DCT electric vehicle and the design methods are introduced in detail. The effectiveness of economic schedule was verified by simulation and experiment in NEDC and UDDS cycles. The simulation results and can

match experiment results well, which demonstrates the effectiveness of economic schedule [19]. A dry-type two-speed DCT for EVs is also developed in [57].

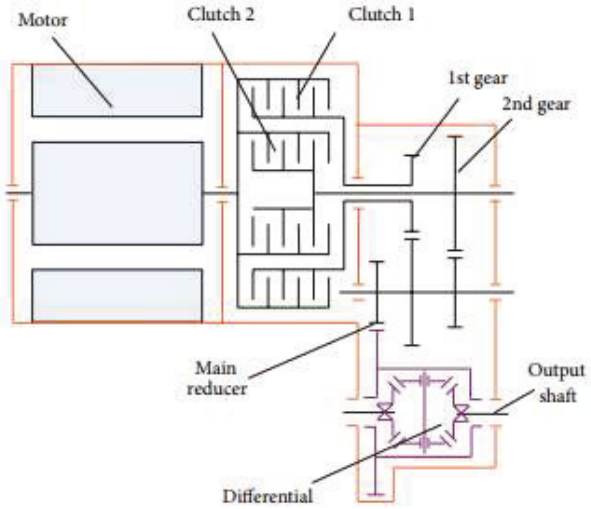

Figure 2-9: Two-speed DCT electric powertrain [56]

Antonov PLC developed a three-speed DCT for a purely electric vehicle [31], shown in Figure 2-10. By adopting the three-speed, Antonov Plc illustrated that it is for "significantly improved performance" over a two-speed system, however, no performance comparison data was given to verify their conclusion. The added complexity of a three-speed over a two-speed increases the cost and production time so it is questionable whether this prototype is the optimum solution.

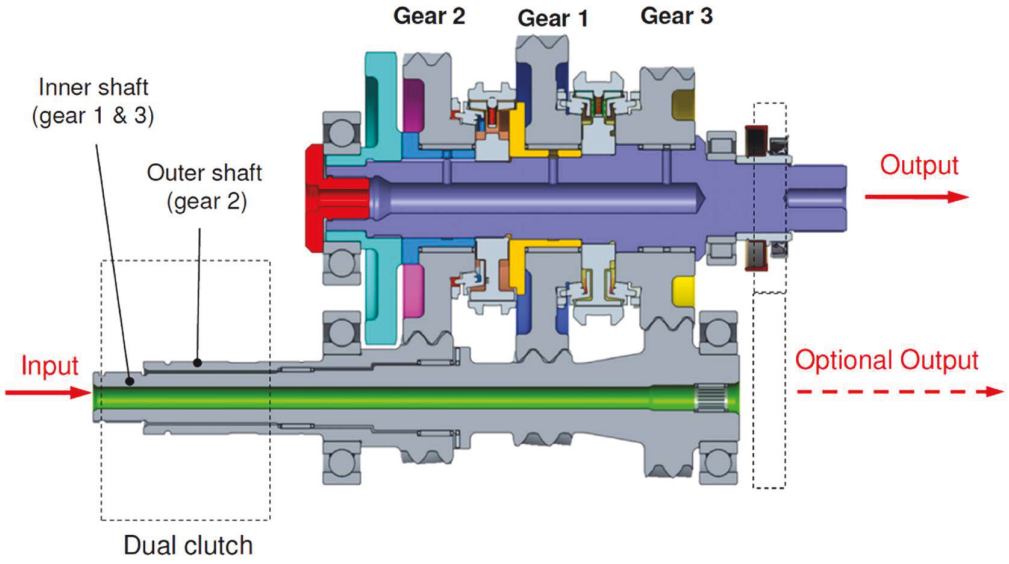

Figure 2-10: Antonov three gear DCT [31]

2.2.2.4 AT

The development of automatic transmission revolutionized the transmission industry as it automated the gear shift process alleviating the need to manually change gear. The standard automatic transmission is comprised of a complex series of planetary gear sets, clutch packs, and bands to change the gear ratio. Besides, the automatic transmission has a torque converter to replace the friction clutch of the manual transmission and smooth the transfer of torque from the engine to the transmission during gear changes. The main drawback of the automatic transmission is the poor efficiency of the torque converter during gearshifts, although locking clutches are now adopted when the input and output speeds are equal. So automatic transmission with hydraulic torque converter is lower efficiency, and not suitable for the high-efficiency electric vehicle [58-60]. However, for

a fully electric vehicle application, a torque converter is not necessarily due to the speed and torque nature of electric motors.

An early design of an AT developed specifically for a fully electric vehicle was put forward in 1985 [61]. The two-speed transmission used in an electric vehicle was expected to attain 30% grade ability, 0-80km/h in less than 20 seconds, a top speed of 96km/h, and 0.16kwh/km energy consumption by Ford Motor Company. The design architecture of the powertrain is comprised of the traction motor and transmission built concentrically around the drive axle. The transmission has two planetary gear sets, a one-way-clutch (OWC) and two friction clutches (CL1 and CL2) as shown in Figure 2-11. The output of the first gear set is the input to the second gear set. The input shaft of this transmission connects the traction motor and S1. The output shaft is connected to wheels via the differential.

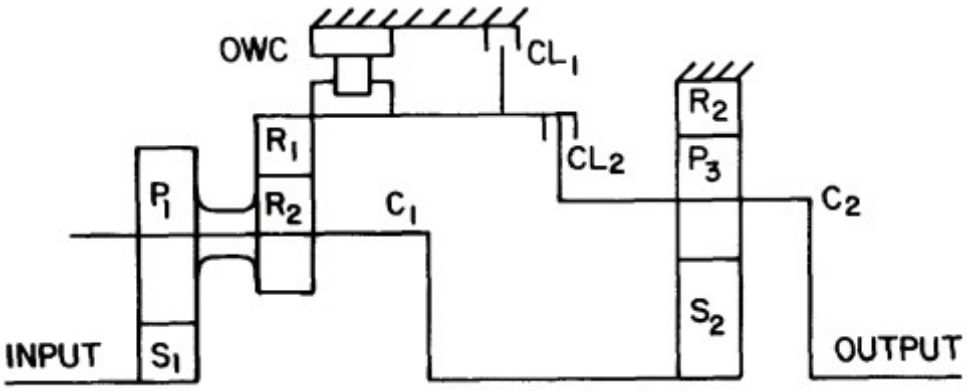

Figure 2-11: The schematic of an early two-speed AT for EVs [61]

In the first gear, two friction clutches do not work. OWC prevents R1 from turning backward and provides the reaction torque. And R2 is also grounded. When the

regeneration takes place CL1 will be locked to ground R1 to prevent freewheeling. When the 2nd gear works, is accomplished through applying the clutch CL2 will be applied to directly connect the R1 to C2, at this time, the reaction torque of R1 is removed by unloading OWC. The shifting process is particularly simplified due to only requiring operating one gearshift actuator.

An innovative two-speed Uninterrupted Mechanical Transmission (UMT) presented in [36], which consists of an epicyclic gearing system, a centrifugal clutch, and a brake band, allowing the seamless shifting between two gears, shown in Figure 2-12.

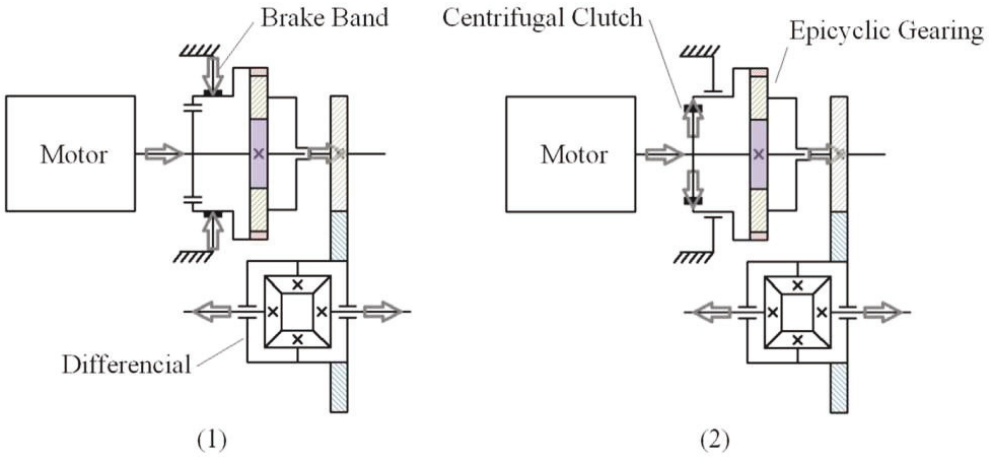

Figure 2-12: Schematic of the two-speed transmission [36]

The UMT adopts a single-stage epicyclic gear system and an uninterrupted gearshift system. The single-stage epicyclic gear system consists of a sun gear, a ring gear, and a couple of planet gears amounted on a carrier. The sun gear is used as input and driven by an input torque from the drive motor, while the carrier transmits the output torque to the differential. A centrifugal clutch and a brake band compose the gearshift system. As shown in Figure 2-12, when the first gear works, the ring gear is grounded to the

transmission case by the brake band. And the clutch shoes have no contact with the drum of the clutch system and no friction torque is applied. When the second gear works, the centrifugal clutch will be engaged, and the brake band will be released. The same research group also proposed a different UMT structure [62], shown in Figure 2-13. Comparison with the above structure, the difference is that the centrifugal clutch is installed on the Carrier instead of on the sun gear. The gearshift process is similar to each other.

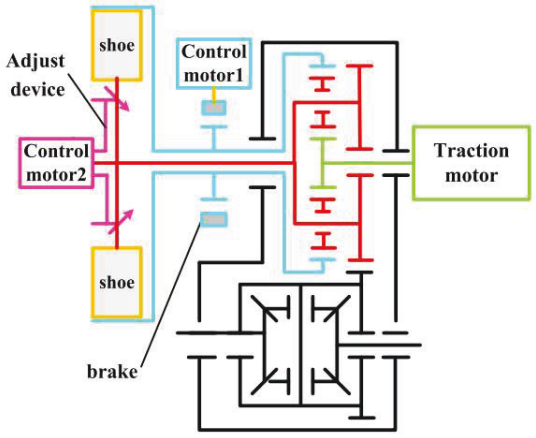

Figure 2-13: The novel two-speed uninterrupted transmission [62]

Dual-stage planetary gear transmission is proposed in [35]. Figure 2-14 shows the schematic view of the driveline of an electric vehicle equipped with the proposed two-speed transmission. As can be seen in Figure 2-14, the input of the transmission is the carrier of the first stage of the two-stage planetary gear set, which is attached to an electric motor. The output of the mechanism is the carrier of the second stage which is connected via the final drive to the wheels. Two different gear ratios can be obtained by braking the sun or the ring gears. By braking ring gear with sun gear released, the first gear is achieved.

When the second gear works, the sun gear is grounded by Sun Brake with no torque transferred by Ring Brake.

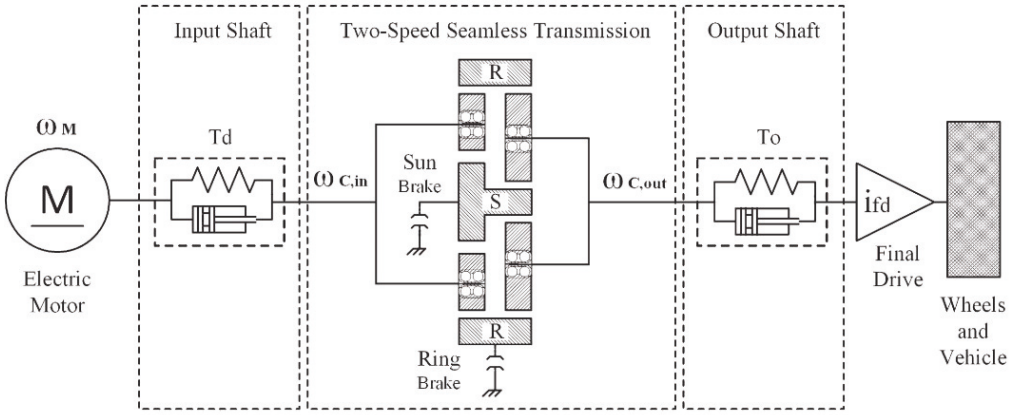

Figure 2-14: The powertrain of an EV equipped with two-speed transmission [35]

2.2.2.5 CVT

CVT has aroused a great deal of interest in the automotive sector due to the potential of lower emissions and better performance. A CVT is an emerging automotive transmission technology that offers in theory a continuum of gear ratios between high and low extremes. This consequently enhances the fuel economy and acceleration performance of a vehicle by allowing the better matching of the engine operating conditions to the variable driving scenarios. However, despite the several advantages proposed by a CVT system, the goals of higher fuel economy and better performance have not been realized significantly in a real production vehicle. There are many kinds of CVTs, each having their own characteristics, e.g. Spherical CVT [63], Hydrostatic CVT [64], Toroidal CVT [65], Belt CVT, Chain CVT, etc. However, belt and chain types are the most commonly used CVTs, among all, in automotive applications.

The CVT is also a form of transmission that should be considered for an electric drivetrain. Through having the ability to smoothly transition between any number of gear ratios between its higher and lower limit it can in theory keep the drivetrain operating in the high-efficiency area. Torque transfer is accomplished through various methods such as a chain between two moveable gears, two helical gears that rotate to change the gear ratio and various other methods. However, this transmission typology suffers from low efficiency due to the way the torque is transferred in the transmission, i.e. by pressure which generates slip and friction [35, 62]. And, because the set of efficient operating points for electric motors is rich enough, the multiplicity of gear ratios or a continuously variable transmission are not necessary for EVs [35]. The research in [66] shows that the CVT is generally a poor choice if in real-world applications it suffers from low efficiency and as such a manual transmission or even a single-speed is more beneficial in terms of energy consumption. So CVT maybe not the best choice for BEVs due to the nature of torque and speed of traction motor.

2.2.3 The gearshift schedule

For the development of the gearshift event control system of multiple speed gearboxes, the gearshift schedules determine which gear ratio should be selected when the drivers' demand， drive quality, drivability, and energy economy are considered. According to the current literature review, the shift schedule is often divided into three categories. The first one is called the single-parameter shift schedule. In this schedule, the gear shifting events are only triggered according to vehicle speed. This presents the main shortcoming of the driver demand not being considered in vehicle gearshifting operations. And, the

most key disadvantage of the single-parameter schedule is easy to develop and implement [67, 68]. The second one is called the dual-parameter shift schedule. Compared to the single-parameter one, it is a more comprehensive control strategy due to taking into account the drivers' demand by introducing a throttle position signal to the control system. Currently, this schedule is widely used in practical transmission control units. However, the dual-parameter shift schedule also has some limitations. For example, frequent and undesired gear shifting can occur because of sharp changes in acceleration or fast-changing road conditions unpredicted [19]. At last, the three-parameter shift schedule is proposed to consider not only the vehicle speed and throttle position but also the vehicle acceleration to deliver a more accurate prediction of the drivers' requirements [69]. However, this system is also limited since the same inputs may relate to different driving conditions for a full-loaded vehicle on a flat road or an unladen vehicle on a slope. There are mainly three control methods being adopted in this field, including throttle position-based shift maps, dynamic programming based shift maps generation, and artificial intelligence-based shift scheduling system. They will be reviewed in the following sections.

In [19], the purely dynamic and economic shift schedules based on the torque and efficiency nature of an electric motor is designed by the graphical method based on a dual-parameter shift map. Firstly, according to the acceleration equation the vehicle, the dynamic upshift schedule is designed. To avoid the frequent gear shift, a buffer region between the upshift and the downshift is used. Then, the design procedure of the economic shift strategy is introduced and the original economic shift schedule is adjusted for voiding the frequent gearshift. The authors evaluated the dynamic performance of two

different shift schedules by using an acceleration test from 0 km/h to100 km/h. The results demonstrate that the dynamic shift schedule achieves a better acceleration performance. Meanwhile, the economic performance comparison between two different control strategies is also given in the New European Driving Cycle (NEDC) and the Urban Dynamometer Driving Schedule (UDDS) cycle. Compared to the dynamic gear schedule, a longer running range can be achieved by the economic shift schedule in both the NEDC and the UDDS cycles, with the improvement of 7 km and 5 km running ranges respectively. A similar design method is also uesd in [70, 71]. Although these papers provide theoretical support to BEV powertrain system matching, the downshift control strategy does not consider optimizing the regeneration of energy in braking by simply defining the downshift map as less speed value than the upshift map.

In [72], the authors presented their research on the development of a pure electric bus which was to be introduced for the Beijing Olympics. For this application, the authors used a dual-parameter shift map using vehicle speed and accelerator pedal position as the inputs to the shift table. The shift map was designed by optimizing the battery and electric motor/transmission efficiency point whilst considering the vehicle dynamics. Besides, the authors suggested that the shift map is designed to help maintain the battery charge level through optimizing the gearshift points to maximize regenerative braking. However, the technique used to derive the gearshift map is not quantitatively explained.

Dynamic programming, as first stated by Bellman [73], is a global optimization technique that is used to solve multi-stage decision-making and control problems. The main idea of dynamic programming is that a large problem can be decomposed into small sections which can be optimized individually. Dynamic programming works retrospectively so in

this case the gearshift strategies are optimized over a driving cycle starting from the end working to the start instead of running a simulation calculating the fuel consumption for every possible combination of gearshift changes over the drive cycle (i.e. N gear transmission with running in T second drive cycle and at second-time step would require $N^{T/t}$ iterations). In [74], to minimize fuel consumption, the researchers proposed a method based on dynamic programming to optimize the gearshift schedules at each sampling point of a driving cycle. In this paper, a transmission called Power Shift AMT (PS-AMT) was applied to the powertrain. The results of the dynamic programming showed a 15.4% fuel consumption improvement over the "normal shifting" using a backward-facing model for comparison. The authors then went on to compare the two gearshift schedules in a forward-facing model and confirmed an improvement of 15.7%. Experimental validation was carried out with the roller bench where an 11.2% improvement was found. A similar method is also applied in [75], but the detailed design process is not provided. In this paper, the driver's accelerator pedal position is interpreted as a power request, which is to be satisfied by coordinating the transmission gear shift and the throttle opening in an optimal fashion. In [21], a novel 2-speed I-AMT is proposed, and the dry clutch is located at the rear of the transmission without traction torque interruption. To optimize the gear ratios, discrete dynamic programming was used for designing the gear changing control strategy with regenerative braking considered. While only for optimizing the gear ratios, there is no comparison against other shift schedules. Dynamic programming is an excellent tool to find the optimal solution for a finite horizon control problem however it is not practical for real-world applications. This is due to dynamic programming working backward and requiring knowledge of the velocity profile prior to the optimization so no

online optimization can take place. Essentially it is a good method to find the global optimal solution using less computational power compared to other methods. In addition, dynamic programming can be used to find the optimal solution by which other control methods can be compared. The question is whether this simply need a local optimum or a global solution to the specific problem of a two-speed electric vehicle energy management.

In [76], a more complex method for developing a gearshift map is proposed based on a combination of fuzzy control [68] and neural network control, namely neuro-fuzzy control. In this paper, the authors firstly introduced an empirical gearshift map which is used as a base to have a comparison with the proposed new control system. This gearshift map differs from the previous papers mentioned because it is not only based on vehicle speed and throttle position but also on the changing rate of the throttle position which helps give some indication of the driver's intention. The experiment results show that the vehicle tested with the conventional shift map experienced more frequent shift gears which leads to vehicle speed oscillations. The vehicle with the shift map created by neuro-fuzzy control only shifts gear once which helps the vehicle maintain a steady speed. In this paper, the energy consumption between the two gearshift maps was not discussed. The research on neuro-fuzzy control is novel due to the intelligent use of adopting neural network control theory to tune fuzzy logic membership functions. However, it is only a method to tune the membership functions faster than tuning them on a test rig (or other manual methods) through trial and error. The control system still needs to use test data which can be imperfect as the driver may not be driving most efficiently or in the most desirable fashion relative to the requirements of the passenger. Essentially it is only suited

to generating a gearshift map that can accurately simulate that of a real-world driver and potentially have the advantage of increasing the enjoyment of the driver.

2.2.4 Torque estimation in the gearshift process

In the clutch-clutch transmissions, At and DCT, speed ratio change is regarded as the process of the torque on one clutch/brake transmitted to the other, which are also called as the clutch-to-clutch shift [77]. Compared to AMT, the most obvious advantage of clutch-to-clutch shift transmissions can achieve gear shifting without torque interruption. To completely obtain the advantage of the clutch-clutch gearshift control system, firstly, torque coordination based control strategy must be developed for shifting performance improvement, which mainly includes reductions of jerk, friction work, and shifting duration [78]. Then, a clutch or brake actuator needs to be precisely controlled to achieve the gearshift algorithms. In the torque phase of gear shifting, the engine/motor output torque is simultaneously transmitted from one clutch or brake to the other. This process is also called torque hand-over [77]. If the coordination of the two clutches or brakes cannot be controlled well, the power cycle or torque interruption will occur to deteriorate the shifting quality. Considering the closed-loop control, when the clutch or brake transmits torque, the friction coefficient always varies with the speed difference between the driven plate and driving plate [79, 80], and is influenced by factors such as wear and surface temperature [81, 82]. This will result in that the actual transmitted torque calculated by the model doesn’t match the demand torque of the clutch or brake. Therefore, the key issue to improving the shifting quality is to precisely estimate the transmitted torque by clutch or brake in real-time. According to the accurate estimation

of transmission, the clutch/brake actuator can achieve the desired control algorithms to obtain quality gear shifting.

Some studies on estimating the transmission output torque and clutch torque have been conducted by adopting the equivalent linear model of a powertrain model. [83] and [84] estimated the half shaft torque by considering the flexibility of the shaft. In [85], the engine speed, wheel speed, and torsional angular displacement of a drive shaft were regarded as state variables to conduct a linear driveline model by applying the difference between the engine speed and transmission output speed as input and designed a Luenberger observer to estimate the output torque of a drive shaft. However, in the real powertrain system, the nonlinear characteristic is inevitable, the established linear model cannot accurately estimate the corresponding torque. In [53], authors considered the uncertainties and nonlinearities of the clutch transmitted torque during the gear shifting, and proposed a clutch friction coefficient model that was represented by a higher-order polynomial as a function of the sliding speed. Ahlawat [86] built a clutch model that was comprised of a hybrid system containing two discrete states, a slip state, and a locked state. In [87], researchers estimated the clutch-transmitted torque in DCT during the gear shifting based on a novel observer. However, in this study, the observation precision is mainly dependent on the accuracy of sensor signals and model parameters. A sliding mode observer was developed to estimate the torque of half shafts of a powertrain [88]. An adaptive sliding mode algorithm was also proposed to estimate the turbine torque of automatic transmissions in [89]. Furthermore, [90] applied the sliding mode theory to estimate the clutch pressure in a hydraulically powered automatic transmission. The extended Kalman algorithm in [91] is used to estimate the clutch actuator pressure and

the transmission output shaft torque simultaneously. In [92], a neural network based observation method was proposed to estimate the turbine torque by taking engine speed, turbine speed, and oil temperature as inputs. Zhao et al.[93] built a detailed dynamic model of powertrain system with a seven-speed DCT and estimate the torque transmitted by a twin-clutch during the gear upshifting based on UKF. The torque estimation algorithm is verified using a DCT prototype vehicle installed with torque sensors on the drive half-shafts. In [94], a four degrees of freedom DCT powertrain system is established and extended Kalman filter (EKF), joint extended Kalman filter (JEKF), and dual extended Kalman filter (DEKF) were used to estimate the target torque. The simulation results showed that DEKF and JEKF provide much higher accuracy in the estimation of target torque than that of EKF when model parameters are uncertain, so as to improve ride performance during gear shifting, i.e. reduction of torque hole and shifting time. Furthermore, DEKF obtained higher estimation accuracy than the JEKF in estimating uncertain parameters. However, this research is a lack of experimental verification. To improve the estimation precision of the clutch pressure of the automatic transmissions with clutch-to-clutch shift control, the rotational freedom of the drive axle shaft is introduced into the model-based observer design [95]. The proposed observer adopted easily and precisely measured speed signals to formulate a correction term where the unknown nonlinear characteristics of powertrain systems used as their original form of lookup tables. Model uncertainties including steady state errors and unknown dynamics were considered as additive disturbance inputs, and the observer was designed such that the error dynamics is input-to-state stability. The designed observer is tested on an AMESIM software environment including the speed sensor models. Through continuous

and discrete implementation comparisons, it was illustrated that the estimation error can be limited in the required bound range though a large extent of model errors exists.

2.2.5 Gearshift control methodologies

Gear shift quality requires short shift duration and smooth torque delivery, however, these two are often in conflict with each other. Therefore, the gearshift process should be properly controlled to achieve the balance of smoothness and shift duration. There is a lot of available researches in this field, such as model predictive control [96] and back-stepping technique [97]. Randomized algorithm was applied to develop an open-loop controller for power-on gear shifting of automatic transmission [98]. Genetic algorithm [99] was used to obtain the comprehensive optimization of gear shifting performance of double clutch transmission, i.e. reducing the longitude vehicle jerk, sliding friction work and shift duration. Fuzzy control [100], sliding mode control [101] and adaptive control [102] were also used to optimize the control process of the gearshift. The gearshift actuator control is also key issue for obtaining the quality gear shifting. In [41, 103], the gearshift actuator was controlled according to a planning speed trajectory of clutch. In general, the planning speed trajectory of the actuator is often devised based on experience or real vehicle test results. The reference trajectory of clutch speed difference was presented in the style of exponential decay in [104, 105]. And the reference trajectory for actuator output speed was designed by the optimal control theory to meet in the style of a cubic polynomial [106]. Also, optimization based control algorithm [107] was also widely used to develop the controller for the gear shifting actuator. This method uses penalty function to simultaneously formulate multiple control objectives, since the

performance of gearshift actuator control is generally expected to meet three main indexes, including minimizing the engagement time, the friction losses, and the longitude vehicle jerk. Researches in [108] and [109] utilized a linear quadratic method to obtain quality gear shifting control, which makes use of the slipping time of clutch and the change rate of clamp force as cost function. In [110], [111], and [112], a dynamic programming method was applied for clutch control during the gear shifting process of automatic transmission. An optimal control technique was also used for tracking a predefined reference signal [113, 114]. However, the disadvantage of using optimal control techniques is its heavy computation burden.

2.3 CHAPTER CONCLUSIONS

This chapter reviews the current research state of multiple speed transmission systems used in BEVs, the gearshift schedules, torque estimation in the gearshift process, and gearshift control methodologies. Although a very large number of similar studies can be found, some limitations of the studies above are:

1. The lack of the analysis of uninterrupted planet-gear automatic transmission for electric vehicles.

2. The lack of the analysis and experiment validation of different gear shifting strategies' characteristics.

3. The lack of the analysis of gear shifting strategy based optimal control method. The design process of optimal gearshift control will be simplified by adopting the specific shift strategy.

4. The lack of the analysis of planet automated manual transmission for electric vehicles.

Based on the achievements and limitations in previous work, two different types of two-speed transmissions proposed for BEVs is presented in this thesis in the following parts:

1. A detailed and original mathematical model of electrified powertrain equipped with two-speed UPAT is developed to present the transient response during gear shifting.

2. Three model-based power-on gearshift control strategies are proposed for the novel two-speed UPAT, termed as CITGS, SCOTGS, and COTGS. And the influence on gear shifting quality is analyzed according to these three strategies.

3. The experiment test rig is built to validate the proposed gearshift strategies.

4. Gear shifting strategy based optimal controller is developed to achieve the comprehensive improvement of gearshift performance.

5. To capture the powertrain transient responses, a comprehensive and original electrified powertrain system equipped with two-speed PAMT is modeled. To achieve gear shifting, a control strategy is designed, and divided into five stages orderly. And the corresponding controllers for the different stages are also developed respectively to achieve this strategy. To control the motor torque reduction and reinstatement at the first and the fifth stages, three alternative torque trajectories are proposed.

CHAPTER 3 : DYNAMIC MODELING OF THE POWERTRAIN SYSTEM WITH THE TWO-SPEED UPAT

3.1 INTRODUCTION

In this chapter, lumped stiffness-inertia torsional models of the powertrain will be developed for different powertrain states to investigate transient response during the gearshifts. These models can be used for gearshift transient studies. The major powertrain components such as electric motor, transmission, main reducer, or differential are lumped as inertia elements, interconnected with torsional stiffness and damping elements to represent a multi-degree of freedom powertrain model.

This chapter is then divided into four sections covering the development of a lumped mass model of the powertrain. The first section is devoted to the introduction of modeling theory. In the second section, the different states of the powertrain are identified through the combination of open and closed band brake. Next, in section three, the lumped inertial powertrain is presented and specific assumptions regarding the model development are identified. Finally concluding remarks are made.

3.2 LUMPED MASS MODELLING THEORY AND APPLICATION

Applying the torsional lumped inertia models to complex dynamic systems such as vehicle powertrains is a traditional and popular method for simulating powertrain

characteristics such as damped natural frequencies and modal shapes or studying the transient response of the powertrain under different operating scenarios [115]. Methods for applying these modeling techniques can be found in many sources of literature. For inertial elements, the equations of motion are derived according to *Newton's Second Law* [116]. These equations can be mathematically presented as follow

$$\sum T_i = J_i \ddot{\theta}_i \tag{3.1}$$

where T_i is the applied moment, J_i is the inertia, $\ddot{\theta}_i$ is angular acceleration, and i stands for the i^{th} inertia element.

A two degree of freedom system is a good example to demonstrate the process for building a lumped inertia model. Figure 3-1 shows the generic model of a two degree of freedom system, applying *Newton's Second Law* to inertias J_1 and J_2 separately, and using two independent coordinates θ_1 and θ_2.

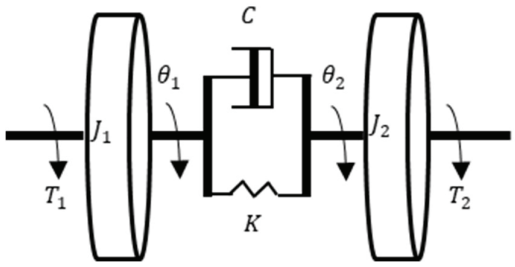

Figure 3-1: Two degree of freedom system

The equations of motion of this system are described by using the linear analog of Eq. (3.1), as follows

$$J_1\ddot{\theta}_1 + C\left(\dot{\theta}_1 - \dot{\theta}_2\right) + K(\theta_1 - \theta_2) = T_1 \tag{3.2}$$

$$J_2\ddot{\theta}_2 + C\left(\dot{\theta}_2 - \dot{\theta}_1\right) + K(\theta_2 - \theta_1) = T_2 \tag{3.3}$$

where θ is angular displacement, $\dot{\theta}$ is angular speed, $\ddot{\theta}$ is angular acceleration, J is component inertia, C is damping coefficient, K is stiffness coefficient, and T is the torque applied to this two degree of freedom system. And, the equations of motion of this system are also rearranged in matrix form, as following

$$\begin{bmatrix} J_1 & 0 \\ 0 & J_2 \end{bmatrix}\begin{bmatrix} \ddot{\theta}_1 \\ \ddot{\theta}_2 \end{bmatrix} + \begin{bmatrix} C & -C \\ -C & C \end{bmatrix}\begin{bmatrix} \dot{\theta}_1 \\ \dot{\theta}_2 \end{bmatrix} + \begin{bmatrix} K & -K \\ -K & K \end{bmatrix}\begin{bmatrix} \theta_1 \\ \theta_2 \end{bmatrix} = \begin{bmatrix} T_1 \\ T_2 \end{bmatrix} \tag{3.4}$$

According to above these equations, the angular acceleration of the two rotary inertias is dependent on the coupled stiffness and damping of the system as well as the applied torque. Besides, it is clear that the vibration response of inertia 1 will influence inertia 2, and vice versa.

So, the main components of the powertrain in this study can be simplified to a series of lumped inertias connected via torsional stiffness and dampers. Thus, it is possible to provide a reasonable approximation of the response of the powertrain system through the use of lumped inertia multi-degree of freedom models. The complex nature of powertrains structured with multiple branches and gear pairs are all defined using interconnected elements. For transient analysis, loading exists in the form of externally applied torques from traction electric motor, band brake, and vehicle resistance.

3.3 THE LAYOUT AND WORKING PRINCIPLES OF UPAT

The novel two-speed transmission is shown in Figure 3-2. The powertrain system of the BEVs consists of an electric motor, a two-speed transmission, final drive, differential, half shafts, and wheels. As shown in this figure, the input of the transmission is the small sun gear, which is connected to the electric motor through the input shaft. The output of the transmission is the ring gear which is attached via the final drive and differential to the wheels.

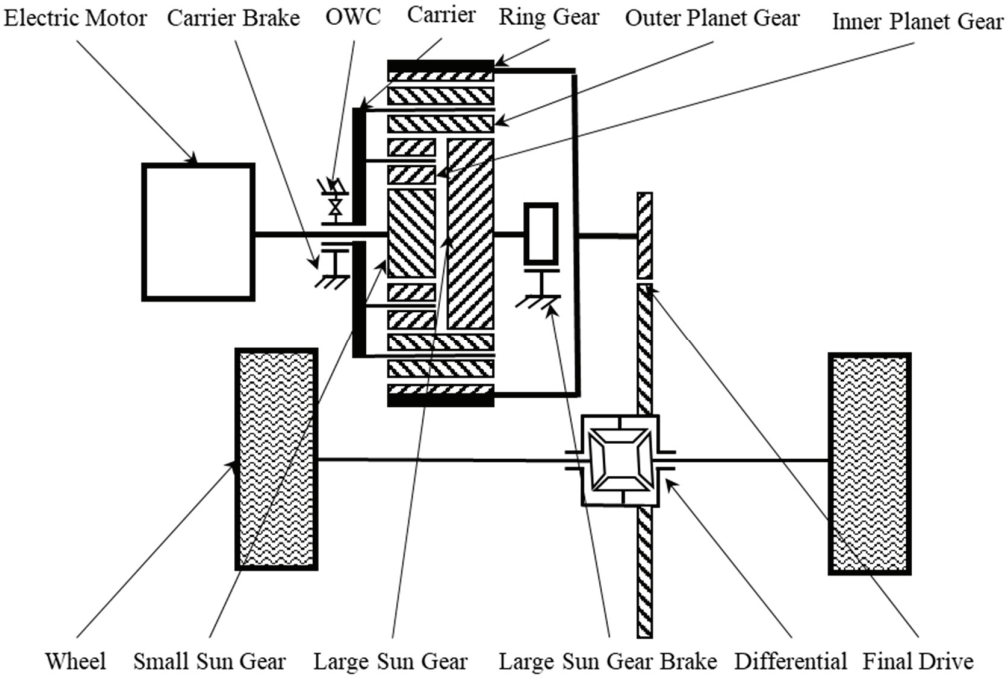

Figure 3-2: Schematic diagram of a BEV equipped with the 2-speed UPAT

The transmission is comprised of a compound planetary gear system with a double pinion planetary gear set and a single pinion planetary gear set. The compound planetary gear consists of a ring gear (R), a carrier (C), a small sun gear (SS), a large sun gear (LS), three

inner planet pinions (IP), and three outer planet pinions (OP). Although the mechanical layout is similar to the traditional AT, it adopts electric actuators (a motor using a screw-nut pair) to control the band brake, while traditional AT usually uses hydraulic actuators. The electrified actuator is efficient, easy to control, and quick response [117].

To ensure the power-on gearshift, a gearshift system featuring both low-cost and easy to control is applied. A one-way clutch (OWC) and two band brakes (C brake and LS brake) are adopted in the gearshift system. C brake is only taken as on-off control based on a switched component and does not work in the gearshift process. Different from C brake, LS brake, the only controlled actuator during gearshifts, needs to be precisely operated. LS brake can enable the torque applied to OWC to decrease or increase by increasing or decreasing the torque exerted on itself during the gearshifts. When the torque exerted on OWC reaches 0, C will be automatically released at the end time of the torque phase of power-on upshifts. Analogously, OWC can automatically hold C at the start time of the torque phase of power-on downshifts. Once OWC is replaced by other corresponding gearshift components that need to be actively controlled to mimic the characteristic of OWC, the transmission will require two elements to cooperate with each other to accomplish the gear changing, which will further improve the gear control complexity. Furthermore, when two gearshift components can not cooperate well, the untimely releasing or engaging of these components will occur, which will impair the gearshift quality [33, 117]. Therefore, adopting OWC as the gearshift element will reduce the gearshift control complexity of the proposed novel transmission when in comparison with some transmissions studied in [34-36].

Due to the two degrees of freedom of the compound planetary gear system, two different gear ratios can be achieved. The working principles of the gearshift system are presented in Table 3-1. In the table, ’0’ indicates the element does not work, and ‘1’ means the element is in operating. When C is grounded by OWC with C brake engaged, the first gear is achieved. The reason to engage C brake in the first gear is to prevent OWC overrunning when regenerative energy recovery condition happens. When the upshift event happens, firstly, C brake must be fully disengaged quickly, and then LS brake is controlled to engage gradually until LS speed reaches zero, which means the upshift process is finished. Therefore, only LS brake is applied in the second gear. When shifting the second gear to the first gear, the LS brake is released gradually until the torque applied on itself is zero, which means the downshift is achieved. Simultaneously, C brake should be controlled to engage quickly. In the condition of reverse gear driving, C is grounded by C brake to prevent from overrunning of OWC with the counter-clockwise ration of the traction motor. Parking gear can be obtained by engaging both C brake and LS brake.

Table 3-1: Gear-shifting Applied Elements

Gear	OWC	C Brake	LS Brake
1st	1	1	0
2nd	0	0	1
Reverse	0	1	0
Parking	0	1	1

3.4 POWERTRAIN MODEL

3.4.1 Kinematic analysis of the transmission

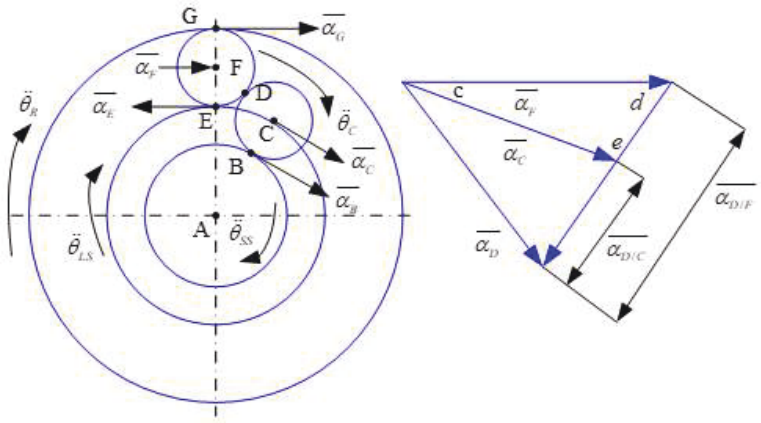

Figure 3-3: Acceleration relationships for planetary gear sets

Figure 3-3 shows the tangential acceleration relationships for planetary gear sets. In this section, the kinematic equations of this transmission, shown in Eqs. (3.5)-(3.8), are reported through the analysis of acceleration relationships shown in Figure 3-3. And, the gear ratios of different stages are derived from the kinematic equations.

$$\ddot{\theta}_{SS} r_{SS} = \ddot{\theta}_C (r_{SS} + r_{IP}) - \ddot{\theta}_{IP} r_{IP} \tag{3.5}$$

$$\ddot{\theta}_{LS} r_{LS} = \ddot{\theta}_C (r_{LS} + r_{OP}) - \ddot{\theta}_{OP} r_{OP} \tag{3.6}$$

$$\frac{\ddot{\theta}_C (r_{SS} + r_{OP})}{\sin e} = \frac{\ddot{\theta}_{OP} r_{OP} + \ddot{\theta}_{IP} r_{IP}}{\sin c} \tag{3.7}$$

$$\ddot{\theta}_R r_R = \ddot{\theta}_C (r_{LS} + r_{OP}) + \ddot{\theta}_{OP} r_{OP} \tag{3.8}$$

where each gear radius and acceleration is presented by r_{SS}, r_{IP}, r_{OP}, and r_R, and $\ddot{\theta}_{SS}$, $\ddot{\theta}_{IP}$, $\ddot{\theta}_{LS}$, $\ddot{\theta}_C$ and $\ddot{\theta}_R$.

The transmission has two degrees of freedom in the inertia phase. The angular velocities of all transmission elements can be regarded as functions of $\ddot{\theta}_{LS}$ and $\ddot{\theta}_C$.

According to Eqs. (3.5)-(3.8), $\dot{\theta}_{SS}$ and $\dot{\theta}_R$ can be derived as $\dot{\theta}_{LS}$ and $\dot{\theta}_C$ as followings

$$\dot{\theta}_{SS} = \frac{\dot{\theta}_C \left[(r_{SS} + r_{OP}) \frac{\sin e - \sin c}{\sin e} + r_{LS} + r_{OP} \right] - \dot{\theta}_{LS} r_{LS}}{r_{SS}} \tag{3.9}$$

$$\dot{\theta}_R = \frac{2\dot{\theta}_C (r_{LS} + r_{OP}) - \dot{\theta}_{LS} r_{LS}}{r_R} \tag{3.10}$$

According to Eqs. (3.9) and (3.10), the gear ratio of the transmission can be expressed as follows

$$i = \frac{\dot{\theta}_{SS}}{\dot{\theta}_R} = \frac{r_R}{r_{SS}} \frac{\dot{\theta}_C \left[(r_{SS} + r_{OP}) \frac{\sin e - \sin c}{\sin e} + r_{LS} + r_{OP} \right] - \dot{\theta}_{LS} r_{LS}}{2\dot{\theta}_C (r_{LS} + r_{OP}) - \dot{\theta}_{LS} r_{LS}} \tag{3.11}$$

where i is the gear ratio of UPAT.

According to Eq. (3.11), three different gear ratios are achievable.

1) when C is completely held by OWC and C brake, the first gear and reverse gear are achieved. The gear ratio can be expressed as follows

$$i = \frac{\dot{\theta}_{SS}}{\dot{\theta}_R} = \frac{r_R}{r_{SS}} = i_{first} \tag{3.12}$$

where i_{first} is the first gear ratio of UPAT.

2) During the torque phase, $\dot{\theta}_C = 0$. Thereby, there is no gear ratio change compared to the first gear in the torque phase.

3) During the inertia phase, neither C nor LS is grounded. The gear ratio can be expressed as

$$i = \frac{\dot{\theta}_{SS}}{\dot{\theta}_R} = \frac{r_R}{r_{SS}} \frac{\dot{\theta}_C \left[(r_{SS} + r_{OP}) \frac{\sin e - \sin c}{\sin e} + r_{LS} + r_{OP} \right] - \dot{\theta}_{LS} r_{LS}}{2\dot{\theta}_C (r_{LS} + r_{OP}) - \dot{\theta}_{LS} r_{LS}} = i_I \qquad (3.13)$$

where i_I is the gear ratio of the inertia phase during gear shifting.

4) When LS is completely grounded by LS brake, the second gear works. The gear ratio is

$$i = \frac{\dot{\theta}_{SS}}{\dot{\theta}_R} = \frac{r_R}{r_{SS}} \frac{\left[(r_{SS} + r_{OP}) \frac{\sin e - \sin c}{\sin e} + r_{LS} + r_{OP} \right]}{2(r_{LS} + r_{OP})} = i_{second} \qquad (3.14)$$

where i_{se} is the second gear ratio of UPAT.

3.4.2 Modelling of the powertrain system

Schematically, the powertrain system in this study is shown in Figure 3-4. The BEV powertrain is based on a front-drive vehicle. The system is connected by shaft elements or frictional contact. It includes mainly an electric motor, a novel two-speed transmission, brakes and OWC, final drive set, differential, wheels, etc. The main variation from conventional vehicles is the electric motor and torque converter. For the BEV powertrain,

the torque converter is removed completely, which reduces the rotating inertia and energy loss. In this section, the modeling methods used in this study follow traditional methods such as [53, 118] with the major powertrain components modeled as lumped inertia elements connected with corresponding stiffness and damping components. The main elements of the powertrain are presented in Figure 3-4. Some assumptions are made to reduce model complexity:

a. All rotating elements of the transmission are rigid

b. All links have only one rotational degree of freedom

c. Gears exhibit no backlash and bearings have no play

d. Linear stiffness and damping model for tires

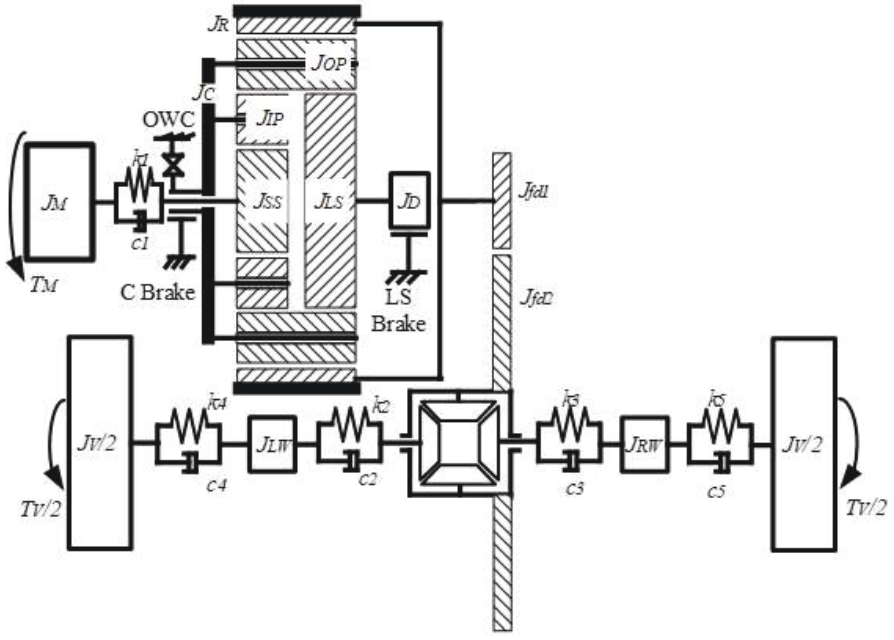

Figure 3-4: Lumped powertrain model schematic for a front-drive BEV

3.4.2.1 Electric motor model

The electric motor is modeled as a rotating rigid body, neglecting the high-frequency vibrations. The torque of the motor T_M can be obtained from a lookup table and taken as a function of the accelerator pedal position α_P and the motor rotational speed $\dot{\theta}_M$. The dynamic of the motor can be expressed by using the torque balance equation as following

$$J_M \ddot{\theta}_M = T_M - T_I \tag{3.15}$$

Where $T_M = f(\alpha_P, \dot{\theta}_M)$

The relationship of the maximum motor torque and the motor speed is from a measured characteristic map as shown in Figure 2-1.

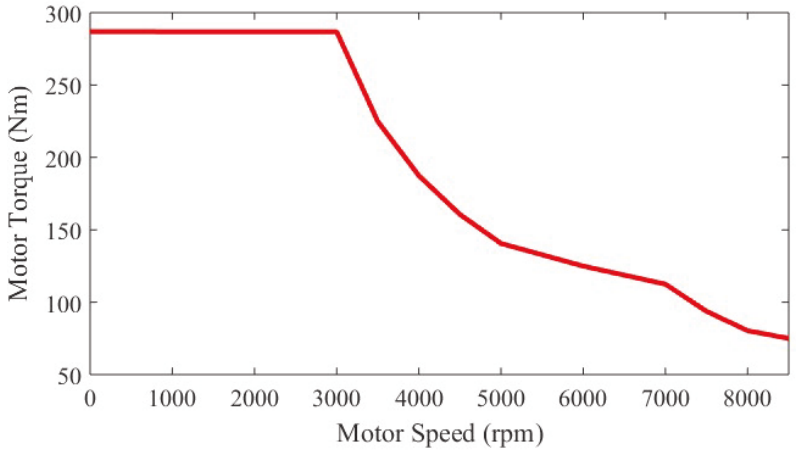

Figure 3-5: The electric motor torque characteristic map

The transmission input shaft is modelled as a spring-damp system with the spring coefficient k_1 and the damping factor c_1 . Here, T_I can be considered as the load on the motor and expressed as following

$$T_I = k_1(\theta_M - \theta_{SS}) + c_1\left(\dot{\theta}_M - \dot{\theta}_{SS}\right) \tag{3.16}$$

3.4.2.2 Transmission model

These components are represented as individual bodies in the mechanical model of the transmission, depicted in Figure 3-6. Using the Newtonian mechanics, the transmission model can be derived in detail as followings

$$J_{SS}\ddot{\theta}_{SS} = T_I - 3F_{IP}r_{SS} \tag{3.17}$$

$$3J_{IP}\ddot{\theta}_{IP} = 3F_{OP}r_{IP} - 3F_{IP}r_{IP} \tag{3.18}$$

$$3J_{OP}\ddot{\theta}_{OP} = 3(F_{OP} - F_{LS} - F_R)r_{OP} \tag{3.19}$$

$$(J_{LS} + J_D)\ddot{\theta}_{LS} = -3F_{LS}r_{LS} + T_{LS} \tag{3.20}$$

$$\begin{aligned} J_C\ddot{\theta}_C = {} & 3F_{IP}(r_{SS} + r_{IP}) - 3F_{OP}(r_{OP} + r_{IP}) + 3F_{LS}(r_{LS} + r_{OP}) \\ & - 3F_R(r_{LS} + r_{OP}) + T_C \end{aligned} \tag{3.21}$$

$$\left(J_R + J_{fd1} + \frac{J_{fd2}}{i_f^2}\right)\ddot{\theta}_R = 3F_R r_R - T_{TO} \tag{3.22}$$

where $T_{TO} = \frac{1}{i_f}\left[k_2\left(\frac{\theta_R}{i_f} - \theta_{LW}\right) + c_2\left(\frac{\dot{\theta}_R}{i_f} - \dot{\theta}_{LW}\right) + k_3\left(\frac{\theta_R}{i_f} - \theta_{RW}\right) + c_3\left(\frac{\dot{\theta}_R}{i_f} - \dot{\theta}_{LW}\right)\right]$.

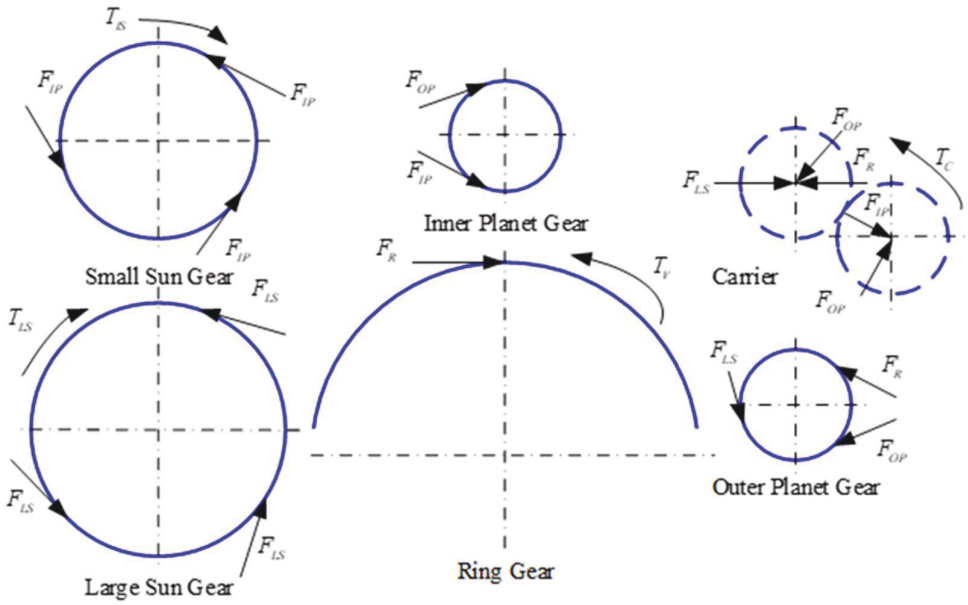

Figure 3-6: Forces and Torques acting on the components of planetary gear sets

The one-way-clutch (OWC) allows a relative motion in one direction and blocks it up in the other direction. By defining this free direction as positive, the two operating states can be described as followings

$\dot{\theta}_C = 0$, one-way clutch blocks, and

$\dot{\theta}_C > 0$, one-way clutch unblocks

Also, the band brake torque depends on whether the band is in the energized mode or the de-energized mode. In the energized mode, the following formula provides the braking torque as a function of the external brake actuation force that tightens the belt [119].

$$T_{LS} = F_{LS} R_D (e^{\mu_B \alpha_B} - 1) \tag{3.23}$$

And in the de-energized mode, the band torque can be expressed as

$$T_{LS} = F_{LS} R_D (1 - e^{-\mu_B \alpha_B}) \tag{3.24}$$

Where F_{LS} is the applied force, R_D is the band brake drum radius, μ_B is the Coulomb friction coefficient, and α_B is the band brake wrap angle.

3.4.2.3 The vehicle and tires

This sub-model is a simplified description of the differential output from the half shafts to the wheels and chassis of the vehicle.

$$J_{LW}\ddot{\theta}_{LW} = \left[k_2\left(\frac{\theta_R}{i_f} - \theta_{LW}\right) + c_2\left(\frac{\dot{\theta}_R}{i_f} - \dot{\theta}_{LW}\right)\right] - \left[k_4(\theta_{LW} - \theta_T) + c_4(\dot{\theta}_{LW} - \dot{\theta}_T)\right] \tag{3.25}$$

$$\frac{J_V}{2}\ddot{\theta}_T = \left[k_4(\theta_{LW} - \theta_T) + c_4(\dot{\theta}_{LW} - \dot{\theta}_T)\right] - \frac{T_V}{2} \tag{3.26}$$

$$J_{RW}\ddot{\theta}_{RW} = \left[k_3\left(\frac{\theta_R}{i_f} - \theta_{RW}\right) + c_3\left(\frac{\dot{\theta}_R}{i_f} - \dot{\theta}_{RW}\right)\right] - \left[k_5(\theta_{RW} - \theta_T) + c_5(\dot{\theta}_{RW} - \dot{\theta}_T)\right] \tag{3.27}$$

$$\frac{J_V}{2}\ddot{\theta}_T = \left[k_5(\theta_{RW} - \theta_T) + c_5(\dot{\theta}_{RW} - \dot{\theta}_T)\right] - \frac{T_V}{2} \tag{3.28}$$

The vehicle resistance torque is the combination of the rolling resistance force, incline load, and air drag. It is expressed as

$$T_V = \left(mg\sin\alpha + \mu mg\cos\alpha + \frac{1}{2}\rho C_D A\left(\dot{\theta}_T r_T\right)^2\right) r_T \tag{3.29}$$

Where μ is rolling resistance coefficient, g is gravity acceleration, α is incline angle, C_D is drag coefficient, ρ is the air density, and A is the vehicle frontal area and r_T is the wheel radius.

To summarise powertrain elements: inertia elements represented by $J_M, J_{SS}, J_{IP}, J_{OP}, J_{LS}, J_C, J_R, J_D, J_{fd}$, J_{fd2}, J_{LW}, J_{RW} and J_V are the electric machine, small sun gear, inner planetary gear, outer planetary gear, large sun gear, carrier, ring gear, brake drum of the large sun gear, driving side of final drive, driven side of final drive, left wheel hub, right wheel hub, and vehicle, with θ , $\dot{\theta}$ and $\ddot{\theta}$ used to stand for the rotation displacement, velocity, and acceleration for corresponding components. F_{IP}, F_{OP}, F_{LS} and F_R are the interaction force of small sun gear and inner planet gears, inner planet gears and outer planet gears, large sun gear and outer planet gears, and outer planet gears and ring gear. Stiffness and damping elements are represented as k_1 and c_1, k_2 and c_2, $k_3$and c_3, k_4 and c_4 , k_5 and c_5 as the motor output shaft, left half shaft, right haft shaft, left tire, and right tire respectively. The final drive ratio is i_f.

3.4.2.4 Model Parameters

In this section, it is most useful to define the parameters that are employed in this model to represent the powertrain model. The lumped mass, stiffness, damping, and gear ratios for the finite element model are then presented in Table 3-2.

3.5 CHAPTER CONCLUSIONS

The objective of this chapter is the development of a model of two-speed UPAT equipped BEV powertrain which provided a simulation platform for the transient gear shifting

process. The powertrain is characterized as a front-wheel drive, UPAT with band brake to engage or disengage for gear shifting between the first gear and the second gear. During the modelling, some assumptions have employed to simplify the model complexity. These assumptions have allowed the development of a simplified powertrain model of two-speed UPAT while still capturing the important characteristics of the powertrain, particularly with regard to transient vibration, and damping of the powertrain system.

Table 3-2: Model parameters used in Powertrain equipped with UPAT

Parameter	Value	Unit	Parameter	Value	Unit
r_{SS}	0.022225	m	J_{fd2}	0.1444	kg·m^2
r_{IP}	0.0127	m	J_{LW}, J_{RW}	1	kg·m^2
r_{OP}	0.0127	m	J_V	71.5222	kg·m^2
r_{LS}	0.0279	m	k_1	5×10^5	Nm/rad
r_R	0.05333	m	k_2, k_3	5×10^5	Nm/rad
e	38.385	°	k_4, k_5	1×10^5	Nm/rad
c	82.989	°	c_1	0.03	Nm·s/rad
i_{first}	2.398	–	c_2, c_3	50	Nm·s/rad
i_{second}	1.48	–	c_4, c_5	100	Nm·s/rad
i_f	3.8	–	R_D	0.0725	m
J_M	6.5×10^{-2}	kg·m^2	μ_B	0.3	–
J_{SS}	2.3×10^{-4}	kg·m^2	α_B	320	°
J_{IP}	7.23×10^{-6}	kg·m^2	m	1400	kg
J_{OP}	1.29×10^{-5}	kg·m^2	g	9.81	m/s^2
J_{LS}	2×10^{-4}	kg·m^2	α	0	°
J_D	5.7×10^{-3}	kg·m^2	μ	0.013	–
r_W	0.2260	m	ρ	1.127	kg/m^3
J_C	1.7×10^{-2}	kg·m^2	C_D	0.3	–
J_R	3.5×10^{-3}	kg·m^2	A	2.08	m^2
J_{fd1}	6.25×10^{-4}	kg·m^2			

CHAPTER 4 : DESIGN AND VALIDATION OF MODEL-BASED GEARSHIFT CONTROL STRATEGIES OF TWO-SPEED UPAT

4.1 INTRODUCTION

Generally, the gear shifting in AT can be categorized into four types: power-off upshifts, power-off downshift, power-on upshifts and power-on downshifts. Power-off gearshifts will introduce power interruption. On the contrary, the interruption will be avoided in power-on gearshifts. This section only takes the power-on gearshift process as an example to reveal the gearshift effects of the proposed alternative power-on gearshift tactics. Typically, the power-on gearshift is divided into two phases [33, 53]. The first phase is the torque phase where the torque is transferred from OWC to LS brake for the proposed transmission. The torque phase is started from T_{LS} increase. As T_{LS} increases, T_C will decrease. When the torque phase ends, the torque exerted on C becomes zero. At the end of the torque phase, the torque is transferred through LS brake rather than OWC. The second phase is the inertia phase. During the inertia phase, the slip speed of LS will change from a negative value to zero, the slip speed of C will change from zero to a positive value and the transmission input speed decreases from first gear level to the second gear level. To achieve this speed change, the torque needs to be exerted by LS brake. Due to the difference between the torque phase and the inertia phase, the design of gearshift control strategy will be divided into two steps in the whole gear shift process

[120-122]. Due to the strongly nonlinear behavior of these processes, strategies to control the power-on shifting process become the key technology, with the ultimate objective of balancing the shifting duration, vehicle longitudinal jerk, and friction work from clutch or brake [123, 124].

This chapter is then divided into four sections. The first section is devoted to simplifying the dynamic model for the design of gear shifting control strategies. In the second section, three different model-based gearshift control strategies will be designed to achieve the power-on gearshift for the proposed two-speed UPAT. Next, in section three, results and discussion are presented. Finally concluding remarks are made.

4.2 SIMPLIFYING THE DYNAMIC MODEL

To simplify the model-based control strategy design procedure, the powertrain system model can be regarded as a rigid body by neglecting the stiffness and damping of the system [20, 35, 36, 39]. Consequently, according to Eqs. (3.15)-(3.29), the rigid body model of this powertrain is presented from Eq. (4.1) to Eq. (4.6).

$$J_{M+SS}\ddot{\theta}_M = T_M - 3F_{IP}r_{SS} \tag{4.1}$$

$$3J_{IP}\ddot{\theta}_{IP} = 3F_{OP}r_{IP} - 3F_{IP}r_{IP} \tag{4.2}$$

$$3J_{OP}\ddot{\theta}_{OP} = 3(F_{OP} - F_{LS} - F_R)r_{OP} \tag{4.3}$$

$$(J_{LS} + J_D)\ddot{\theta}_{LS} = -3F_{LS}r_{LS} + T_{LS} \tag{4.4}$$

$$J_C\ddot{\theta}_C = 3F_{IP}(r_{SS} + r_{IP}) - 3F_{OP}(r_{OP} + r_{IP}) + 3F_{LS}(r_{LS} + r_{OP}) - 3F_R(r_{LS} + r_{OP}) + T_C \tag{4.5}$$

$$\left(J_R + J_{fd1} + \frac{J_{fd2}}{i_f^2}\right)\ddot{\theta}_R = 3F_R r_R - \frac{T_V}{i_f} \tag{4.6}$$

The rigid model can be further simplified. Firstly, remove the internal force from the planetary gear dynamic equations by algebraic operations as follows

$$\left[\frac{Eq.(4.1)}{r_{SS}} - \frac{Eq.(4.2)}{r_{IP}} + \frac{Eq.(4.3)}{r_{OP}} - \frac{Eq.(4.4)}{r_{LS}} + \frac{Eq.(4.6)}{r_R}\right] r_R \tag{4.7}$$

$$Eq.(4.1) + Eq.(4.2) + Eq.(4.3) + Eq.(4.4) + Eq.(4.5) + Eq.(4.6)\frac{r_{LS} + 2r_{OP}}{r_R} \tag{4.8}$$

According to the algebraic operations from Eq. (4.7) and Eq. (4.8), the rigid body model can be simplified as followings

$$J_{M+SS}\ddot{\theta}_M i_{SS} - 3J_{IP}\ddot{\theta}_{IP} i_{IP} + 3J_{OP}\ddot{\theta}_{OP} i_{OP} - (J_{LS} + J_D)\ddot{\theta}_{LS} i_{LS} + J_{ER}\ddot{\theta}_R = i_{SS}T_M - i_{LS}T_{LS} - T_{ef} \tag{4.9}$$

$$J_{M+SS}\ddot{\theta}_M + 3J_{IP}\ddot{\theta}_{IP} + 3J_{OP}\ddot{\theta}_{OP} + (J_{LS} + J_D)\ddot{\theta}_{LS} + J_C\ddot{\theta}_C + J_{ER}\ddot{\theta}_R\left(\frac{1}{i_{LS}} + \frac{2}{i_{OP}}\right) = T_M + T_{LS} + T_C - T_{ef}\left(\frac{1}{i_{LS}} + \frac{2}{i_{OP}}\right) \tag{4.10}$$

Where $i_{SS} = \frac{r_R}{r_{SS}}$, $i_{IP} = \frac{r_R}{r_{IP}}$, $i_{OP} = \frac{r_R}{r_{OP}}$, $i_{LS} = \frac{r_R}{r_{LS}}$, $J_{M+SS} = J_M + J_{SS}$, $J_{ER} = \frac{i_f^2 J_R + i_f^2 J_{fd} + J_{fd}}{i_f^2}$, $T_{ef} = \frac{T_V}{i_f}$.

According to Eqs. (3.5)-(3.8), the angular accelerations of C, IP, OP, and R can be expressed as angular accelerations of SS and LS as follows

$$\ddot{\theta}_C = a_1\ddot{\theta}_{SS} + a_2\ddot{\theta}_{LS} \tag{4.11}$$

$$\ddot{\theta}_{IP} = b_1\ddot{\theta}_{SS} + b_2\ddot{\theta}_{LS} \tag{4.12}$$

$$\ddot{\theta}_{OP} = c_1\ddot{\theta}_{SS} + c_2\ddot{\theta}_{LS} \tag{4.13}$$

$$\ddot{\theta}_R = d_1\ddot{\theta}_{SS} + d_2\ddot{\theta}_{LS} \tag{4.14}$$

where $a_1 = \frac{r_{SS}}{(r_{SS}+r_{OP})\left(1-\frac{\sin c}{\sin e}\right)+r_{IP}+r_{SS}}$, $a_2 = \frac{r_{LS}}{(r_{LS}+r_{OP})\left(1-\frac{\sin}{\sin}\right)+r_{IP}+r_{SS}}$, $b_1 = \frac{a_1(r_{SS}+r_{IP})-r_{SS}}{r_{IP}}$, $b_2 = \frac{a_2(r_{SS}+r_{IP})}{r_{IP}}$, $c_1 = \frac{a_1(r_{LS}+r_{OP})}{r_{IP}}$, $c_2 = \frac{a_1(r_{LS}+r_{OP})-r_{LS}}{r_{IP}}$, $d_1 = \frac{a_1(r_{LS}+r_{OP})+c_1 r_{OP}}{r_R}$,$d_2 = \frac{a_2(r_{LS}+r_{OP})+c_2 r_{OP}}{r_R}$.

Then, substituting Eqs. (4.11)-(4.14) into Eqs. (4.9) and (4.10), the simplified model will be re-arranged by Eq. (4.15) and Eq. (4.16).

$$\ddot{\theta}_{SS} = g_1 T_M + g_2 T_{LS} + g_3 T_C + g_4 T_{ef} \tag{4.15}$$

$$\ddot{\theta}_{LS} = m_1 T_M + m_2 T_{LS} + m_3 T_C + m_4 T_{ef} \tag{4.16}$$

where $g_1 = \frac{f_2 i_1 - e_2}{f_2 e_1 - f_1 e_2}$, $g_2 = \frac{-f_2 i_4 - e_2}{f_2 e_1 - f_1 e_2}$, $g_3 = \frac{-e_2}{f_2 e_1 - f_1 e_2}$, $g_4 = \frac{e_2(\frac{1}{i_4}+\frac{2}{i_3})-f_2}{f_2 e_1 - f_1 e_2}$, $m_1 = \frac{f_1 i_1 - e_1}{f_1 e_2 - f_2 e_1}$, $m_2 = \frac{-f_1 i_4 - e_1}{f_1 e_2 - f_2 e_1}$, $m_3 = \frac{-e_1}{f_1 e_2 - f_2 e_1}$, $m_4 = \frac{e_1(\frac{1}{i_4}+\frac{2}{i_3})-f_1}{f_2 e_1 - f_1 e_2}$, $e_1 = (J_M + J_{SS})i_1 - 3J_{IP}b_1 i_2 + 3J_{OP}c_1 i_3 + (J_R + \frac{J_V}{i_f})d_1$, $e_2 = -3J_{IP}b_2 i_2 + 3J_{OP}c_2 i_3 - J_{LS}i_4 + (J_R + \frac{J_V}{i_f})d_2$, $f_1 = J_C a_1 +$

$(J_M + J_{SS}) + 3J_{IP}b_1 + 3J_{OP}c_1 + (\frac{1}{i_4} + \frac{2}{i_3})(J_R + \frac{J_V}{i_f})d_1$, $f_2 = J_C a_2 + 3J_{IP}b_2 + 3J_{OP}c_2 + J_{LS} + (\frac{1}{i_4} + \frac{2}{i_3})(J_R + \frac{J_V}{i_f})d_2$.

4.3 THE POWER-ON UPSHIFT STRATEGIES

In the following sections, three different upshift control strategies will be designed to achieve the power-on upshift for the proposed two-speed gearbox. The power-on downshift process is the reverse process of power-on upshift [33]. Therefore, the power-on downshift strategies will be not explored in this chapter.

4.3.1 The constant input torque gearshift strategy (CITGS)

This control strategy is comprised of motor torque control and LS torque control. In this strategy, the motor torque is maintained constant in both the torque phase and the inertia phase.

During the torque phase, $\dot{\theta}_C = 0$ and $\ddot{\theta}_C = 0$, so Eq. (4.1) will be expressed as Eq. (4.17).

$$\ddot{\theta}_{LS} = -\frac{a_1}{a_2}\ddot{\theta}_{SS} \tag{4.17}$$

So, the simplified powertrain model can be regarded as a single degree of freedom system. According to Eq. (4.11), Eq. (4.18) can be obtained by solving Eq. (4.15) and Eq. (4.16).

$$0 = n_0\dot{T}_M + n_1\dot{T}_{LS} + n_2\dot{T}_C + n_3\dot{T}_f \tag{4.18}$$

where $n_0 = a_1 g_1 + a_2 m_1$, $n_1 = a_1 g_2 + a_2 m_2$, $n_2 = a_1 g_3 + a_2 m_3$, $n_0 = a_1 g_4 + a_2 m_4$.

The motor torque is controlled to maintain a constant in the CITGS, so the torque control law of the motor can be expressed as the following

$$\dot{T}_M = 0 \tag{4.19}$$

When the gear shift occurs in the constant power region of the motor with 100% depressed pedal, Eq. (4.19) will fail in the torque phase. Because the maximum available motor torque will change according to the current motor speed, as shown in Figure 3-5.

In the gearshift process, the vehicle resistance torque is often considered unchanged [20, 35, 36, 39], so the assumption can be expressed as

$$\dot{T}_{ef} = 0 \tag{4.20}$$

So, Eq. (4.21) can be obtained by substituting Eqs. (4.19) and (4.20)into Eq. (4.18)

$$\dot{T}_{LS} = -\frac{n_2}{n_1}\dot{T}_C \tag{4.21}$$

Here, T_{LS} is controlled by Eq. (4.22)

$$T_{LS} = \int_{t_0}^{t_1} -\frac{n_2}{n_1}\dot{T}_C \, dt \tag{4.22}$$

Here, $\dot{T}_C = constant < 0$.

T_{LS} inversely related to T_C will increase gradually. When $T_C = 0$, the torque phase is over.

In the inertia phase, the control aim is to make $\dot{\theta}_{LS} = 0$. A polynomial change curve of $\dot{\theta}_{LS} = 0$ is designed as the speed reference trajectory [21]. The difference between reference speed and actual speed is taken as the input of a closed-loop PID controller. The output of the closed-loop controller is the force applied to LS band brake. The brake force can be adjusted to track the curve change. The curve can be expressed as

$$\dot{\theta}_{LS}(t) = 2\frac{\dot{\theta}_{LS0}}{(t_2 - t_1)^3}(t - t_1)^3 - 3\frac{\dot{\theta}_{LS0}}{(t_2 - t_1)^2}(t - t_1)^2 + \dot{\theta}_{LS0} \tag{4.23}$$

Where t_0 is the start time of the torque phase, t_1 is the start time of the inertia phase, t_2 is the end time of the inertia phase and $t_1 \leq t \leq t_2$. $\dot{\theta}_{LS}$ is the initial speed of LS in the inertia phase and $\ddot{\theta}_{LS}(t_1) = \ddot{\theta}_{LS}(t_2) = 0$.When $\dot{\theta}_{LS} = 0$, the inertia phase ends.

The schematic of this strategy is reported theoretically in Figure 4-1.

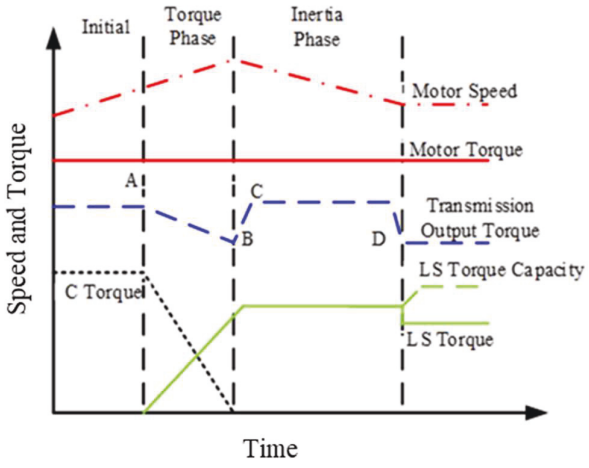

Figure 4-1： The diagram of CITGS

4.3.2 The semi-constant output torque gearshift strategy (SCOTGS)

In this strategy, the gearshift control objective is keeping the output torque of the transmission remain almost unchanged in the inertia phase, which can be achieved by reducing the motor output torque. And the control strategy of torque phase is the same as CITGS. During the torque phase, T_M and T_{LS} are controlled according to Eq. (4.19) and Eq. (4.22), the same as to CITGS.

In the inertia phase, in order to keep the output torque of the transmission constant in the inertia phase, $\ddot{\theta}_R$ is considered as unchanged.

Firstly, substituting Eqs. (4.15) and (4.16) into Eq. (4.14), Eq. (4.24) can be obtained.

$$\ddot{\theta}_R = (d_1 g_1 + d_2 m_1) T_M + (d_1 g_2 + d_2 m_2) T_{LS} + (d_1 g_4 + d_2 m_4) T_{ef} \tag{4.24}$$

Assume $\ddot{\theta}_R = constant$, then

$$n_4 \dot{T}_M + n_5 \dot{T}_{LS} = 0 \tag{4.25}$$

where $n_4 = d_1 g_1 + d_2 m_1$, $n_5 = d_1 g_2 + d_2 m_2$.

Therefore, it is necessary to ensure the motor torque follows Eq. (4.26).

$$T_M = T_{Me} - \int_{t_1}^{t_2} -\frac{n_5}{n_4} \dot{T}_C \, dt \tag{4.26}$$

where T_{Me} is the motor torque at the end timing of torque phase.

According to the change curve of Eq. (4.23), the LS torque can be controlled through the same closed-loop controller designed in Section 4.3. The process for SCOTGS is shown in schematically in Figure 4-2.

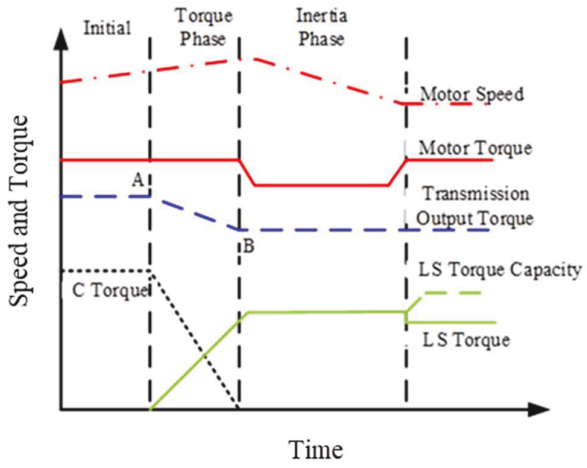

Figure 4-2: The diagram of SCOTGS

4.3.3 The constant output torque gearshift strategy (COTGS)

The control objective of this strategy is to maintain the output torque of the transmission unchanged in the whole gearshift process.

In the torque phase, firstly, assume $\ddot{\theta}_R = 0$ and $\dot{T}_{ef}$. Then, substituting Eqs. (4.15) and (4.16) into Eqs. (4.11) and (4.14) respectively, Eqs. (4.27) and (4.28) can be obtained:

$$(a_1 g_1 + a_2 m_1)\dot{T}_M + (a_1 g_2 + a_2 m_2)\dot{T}_{LS} + (a_1 g_3 + a_2 m_3)\dot{T}_C = 0 \qquad (4.27)$$

$$(d_1 g_1 + d_2 m_1)\dot{T}_M + (d_1 g_2 + d_2 m_2)\dot{T}_{LS} + (d_1 g_3 + d_2 m_3)\dot{T}_C = 0 \qquad (4.28)$$

By solving Eqs. (4.27) and (4.28), T_{LS} and T_M control equations can be presented by Eqs. (4.29) and (4.30).

$$\dot{T}_{LS} = h_2 \dot{T}_C \tag{4.29}$$

$$\dot{T}_M = h_3 \dot{T}_C \tag{4.30}$$

where $h_2 = -\frac{(d_1 g_1 + d_2 m_1)(a_1 g_3 + a_2 m_3) - (d_1 g_3 + d_2 m_3)(a_1 g_1 + a_2 m_1)}{(d_1 g_1 + d_2 m_1)(a_1 g_2 + a_2 m_2) - (d_1 g_2 + d_2 m_2)(a_1 g_1 + a_2 m_1)}$,

$h_3 = -\frac{(a_1 g_3 + a_2 m_3)(d_1 g_2 + d_2 m_2) - (a_1 g_2 + a_2 m_2)(d_1 g_3 + d_2 m_3)}{(a_1 g_1 + a_2 m_1)(d_1 g_2 + d_2 m_2) - (a_1 g_2 + a_2 m_2)(d_1 g_1 + d_2 m_1)}$.

During the torque phase of this tactic, the motor torque has to be restricted by the natural characteristics of the electric motors. The motor torque T_M must vary within the scope.

$$-T_{Mmax} \leq T_M \leq T_{Mmax} \tag{4.31}$$

where T_{Mmax} is the maximum torque of the motor according to its current speed.

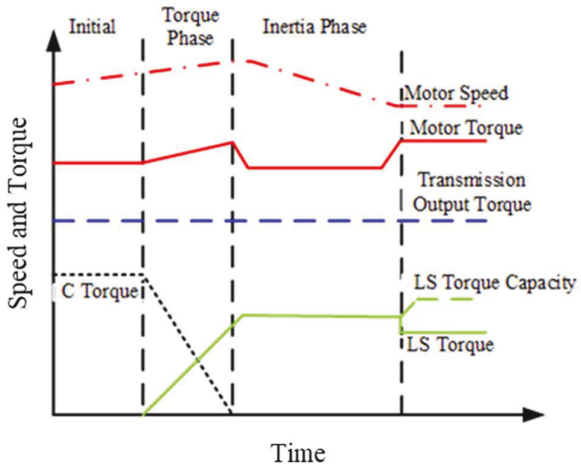

Figure 4-3: The diagram of COTGS

In the inertia phase, the control strategy is the same as that of SCOTGS. The schematic of this strategy is reported in Figure 4-3.

4.4 RESULTS AND DISCUSSION

4.4.1 Power-on upshift results

To investigate the effectiveness of the proposed power-on upshift strategies, different gearshift points are used for all three strategies in simulation, which eliminates the affection of varying shift points. As well known, gearshift duration, vehicle jerk, and friction work are often used to evaluate the shifting quality. Quality shifting requires short duration, in the meanwhile, minimal vehicle jerk and friction loss. Since the shifting duration influences the vehicle jerk and friction loss, the gearshift duration is as 450ms in all strategies to provide a fair platform to evaluate them in terms of vehicle jerk and friction loss. Specifically, the torque phase accounts for 150ms, and the inertia phase takes the rest.

The vehicle jerk presents a measure of the driver observed rate change of longitudinal acceleration of the vehicle in the gearshift process. Transmissions with power-on gearshift ability such as DCTs or ATs are expected to minimize this shifting quality criterion, which will enable the driver and passenger to observe a high-quality gearshift outcome during the power-on gear changing. In Germany, the maximum vehicle jerk during power-on shifting is $|j| \leq 10 m/s^3$ [53]. During the gear shift, the band brake needs to be engaged or released frequently. In consequence, the brake belt will be worn, and the thermal will be generated by the friction work. When the friction surface is over-

heat, the wearing of friction material will be aggravated, which will significantly shorten the service life of the band brake. Therefore, minimizing the friction work is critical.

The first series of results depicted in Figure 4-4, Figure 4-5, and Figure 4-6 stands for the simulated three different kinds of power-on control tactics in the BEV powertrain. These tactics are all triggered at 50% driver demand and 55km/h vehicle speed. These figures present the variation of torque and speed, motor, C, LS, and R representing the transmission output, vehicle acceleration, vehicle jerk, and friction work in the gear shifting respectively. To evaluate the gearshift performance clearly, these simulation results from three different control strategies are summarized in Table 4-1.

It can be obviously seen from Table 4-1 that the same vehicle jerk 11.62m/s^3 in the torque phase is recorded in both CITGS and SCOTGS because their control schedules are the same in this phase, which is maintaining the motor torque constant to achieve the power-on gearshift. In the torque phase, the smallest vehicle jerk 2.51m/s^3 is obtained by COTGS, 9.11m/s^3 smaller than the former two. According to the compared simulation results shown in Table 4-1, COTGS distinctly shows more potential in reducing the vehicle jerk by holding the transmission output torque almost invariant, as shown in Figure 4-6. In the inertia phase, the maximum vehicle jerk of CITGS reaches 8.68m/s^3 which is the largest jerk among three tactics in comparison with 4.10m/s^3 in SCOTGS and 2.10m/s^3 in COTGS. The reason why the largest jerk occurs in CITGS is that the torque transmitted by R increase and then decrease in this phase, which makes the vehicle acceleration change more sharply than the latter two shown in Figure 4-5 and Figure 4-6. It can be found that the vehicle longitude jerk of inertia phase in SCOTGS presents a bigger value than that in COTSGS, though the same control tactics are adopted in the inertia phase of

these two tactics. The reason is that COTSGS and COTSGS apply two different kinds of control tactics in torque phase. Abrupt change of transmission output torque in torque phase will impact the transmission output torque in the inertia phase and then influences the observed jerk.

According to the vehicle jerk comparison at shift point of 50% driver demand and 55km/h vehicle speed, COTGS is proved to have the capacity to provide the best gearshift comfortableness because of almost no output torque hole appearing in the whole gear changing process.

The friction work dissipated by the friction elements in the gearshift process is also presented in Figure 4-4, Figure 4-5, and Figure 4-6. As shown in Table 4-1, SCOTGS generates the least friction work 4.258 kJ which is 0.654 kJ less than of the first one. The most of friction work is consumed in COTGS which dissipates 2.875 kJ and 3.527 kJ more energy than those of the first and second tactics. This because the largest braking torque is exerted on the large sun gear, together with the torque increase of the motor in COTGS, which makes the dissipated energy and the wearing of friction elements increase prominently, consequently shortening the service life of the band brake.

It can be found that COTGS assists the vehicle to attain more acceleration improvement in the gearshift process when compared to the former two, which means that this strategy further improves the dynamic performance of the vehicle by shortening the vehicle acceleration duration.

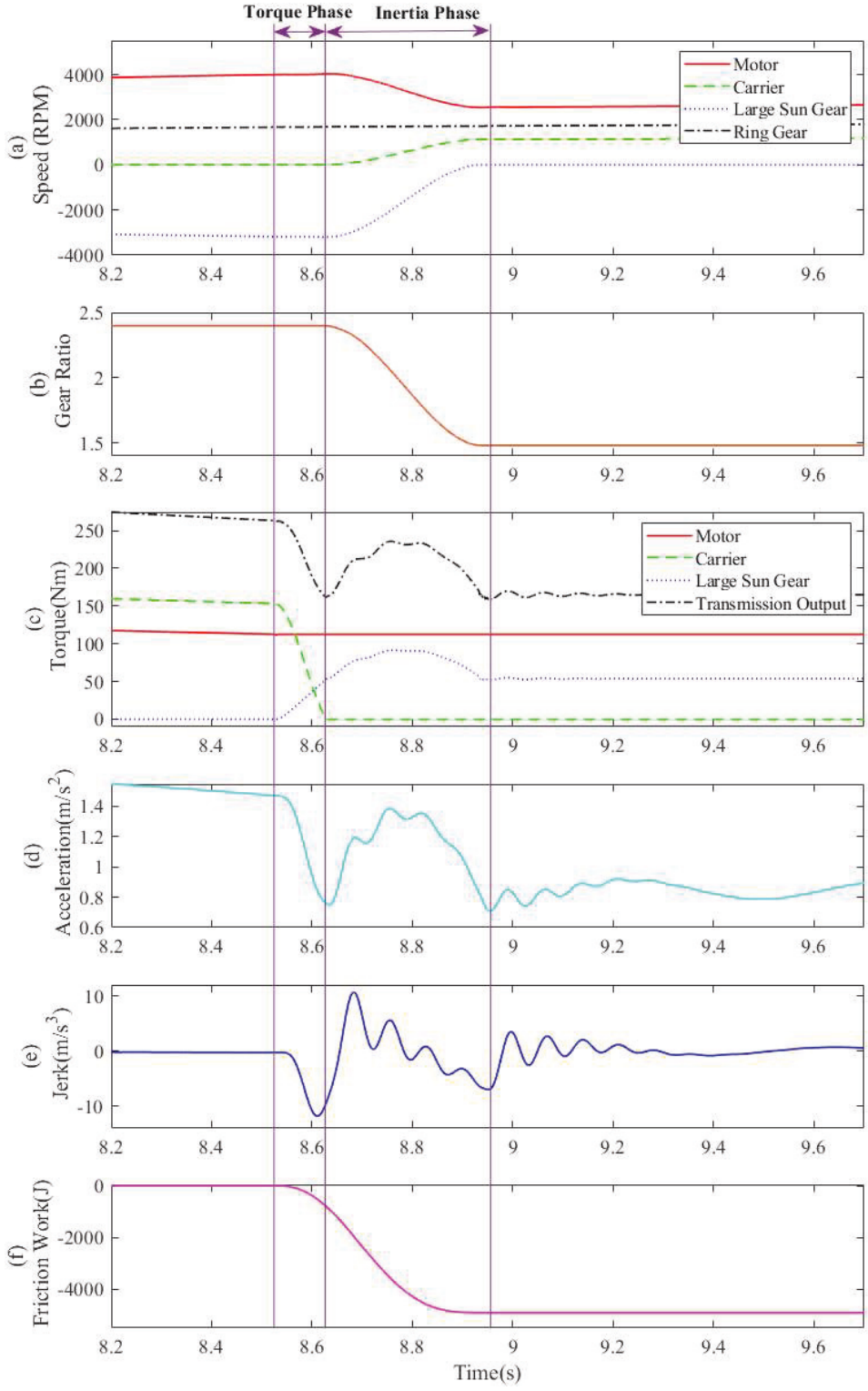

Figure 4-4: Results of CITGS at 50% driver's demand and 50km/h vehicle speed

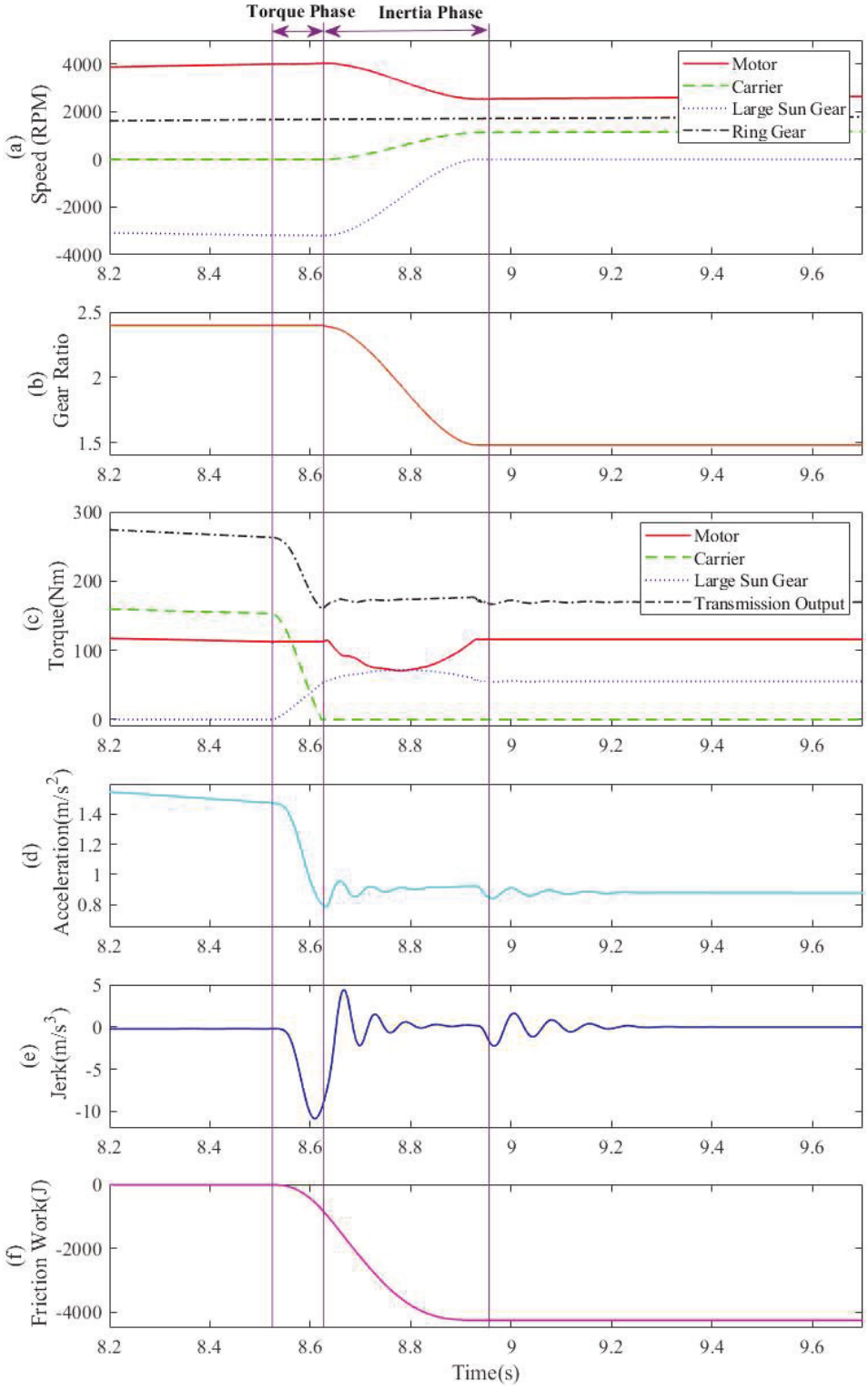

Figure 4-5: Results of SCOTGS at 50% driver's demand and 50km/h vehicle speed

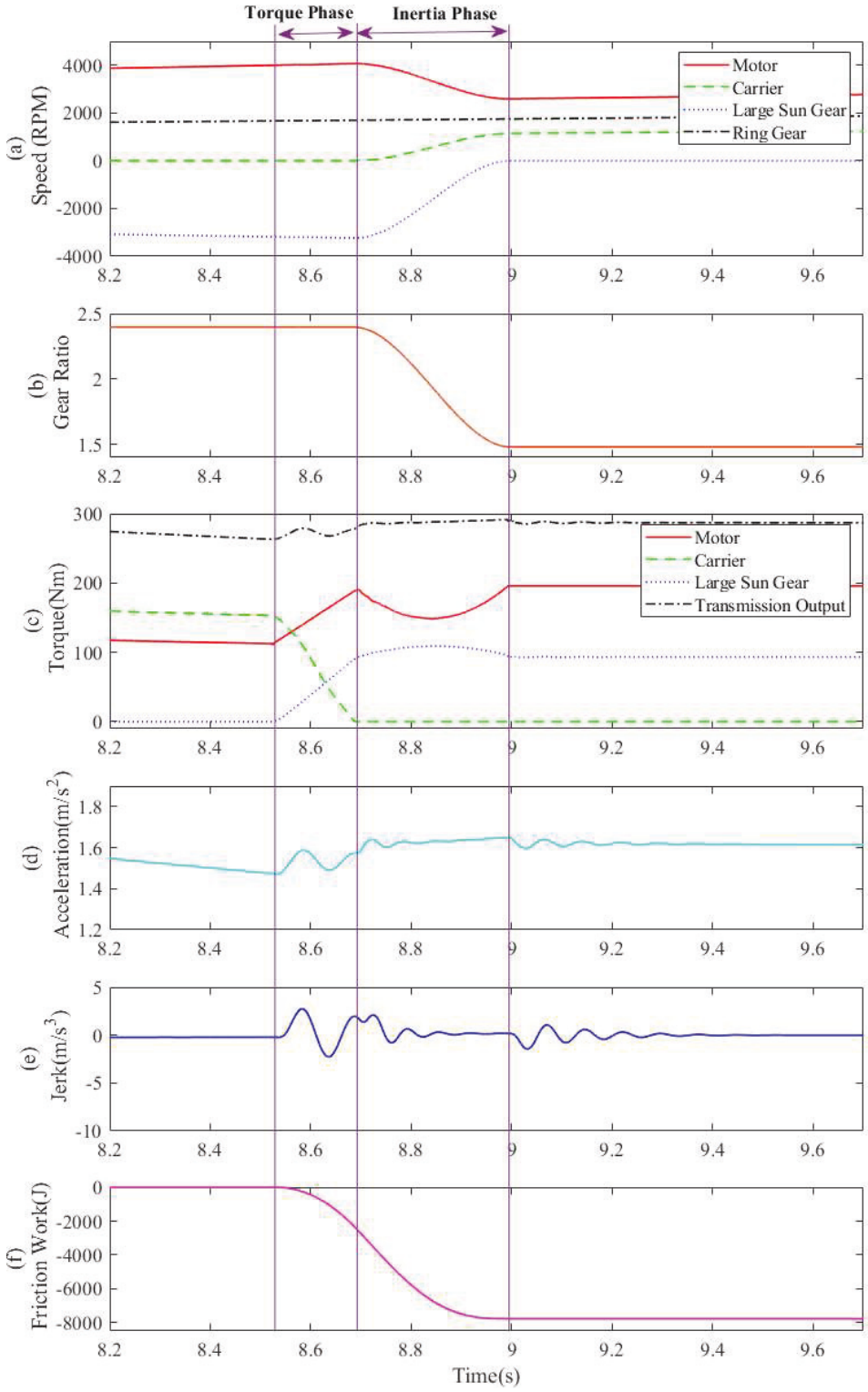

Figure 4-6: Results of COTGS at 50% driver's demand and 50km/h vehicle speed

Table 4-1: Results at 50% driver's demand

	|Jerk| (m/s^3)		**|Friction work| (kJ)**
	Torque phase	**Inertia phase**	
CITGS	11.62	8.68	4.912
SCOTGS	11.62	4.10	4.258
COTGS	2.51	2.10	7.785

Figure 4-7, Figure 4-8, and Figure 4-9 illustrate the shift characteristics of three different tactics at the shift point of 75% driver's command and 65km/h vehicle speed. Table 4-2 depicts the simulation results in detail. It can be found that the vehicle experiences the largest jerk 15.01m/s^3 by adopting COTGS and SCOTGS in the torque phase, which is over Germany index 10m/s^3 and will make the driver and the passenger experience the significant longitudinal shock. However, 12.92m/s^3 vehicle jerk is triggered by COTGS, which is also over 10m/s^3. The reason why the large jerk is attained by COTGS will be explained in the following.

Regarding the first series of simulation results, Figure 4-6 is taken as the benchmark to evaluate the gearshift performance of COTGS under a mild driving condition. In terms of this tactic, the electric motor needs to increase its torque to compensate R torque reduction due to the torque ratio reduction during the torque phase. In this simulation condition, due to the relatively low driver's demand, the desired motor torque is

distributed appropriately within the range defined by the peak torque of the motor, which enables the output torque to be kept invariantly. When shifting to the inertia phase, the output torque is continuously well controlled since LS still slips under the controlled LS torque, in which the motor torque will be reduced to enable the motor speed decrease to synchronize with LS speed. Due to the control flexibility of electric motors, the duration of the gear changing can be shortened in the inertia phase.

However, the shifting dynamics in aggressive driving conditions are different from those under mild driving conditions for COTGS. Figure 4-9 illustrates the characteristics of power-on upshift with the driver demand at 75%. During the torque phase, the torque requirement of the motor becomes comparatively high and exceeds the maximum torque bound restricted by the nature of the motor. Consequently, the motor torque cannot be regulated to increase persistently, only maintained at the maximum torque value according to the current motor speed, which will make the designed control tactic failure in the torque phase and cause the transmission output torque to decrease suddenly. Ultimately, the large longitudinal shock presented by the vehicle jerk impairs the vehicle smoothness in the gearshift process. It is not the aim of the original design intention of the power-on gearshift strategy. Then, during the inertia phase, the output torque is kept unchanged since LS drum still slips under the controlled pressure. Meanwhile, the motor torque is also controlled to promote the motor speed to reduce to the second gear level, which avoids severe friction wear of the band brake. Due to the coordination control of the motor and the band brake during the inertia phase, in COTGS, the jerk is better controlled compared to that of CITGS. Figure 4-6 and Figure 4-9 together demonstrate

that COTGS will damage the gearshift quality when gearshift events occur under aggressive driving conditions.

It is worth noting that the jerk of the first two tactics at 75% driver demand is larger in the torque phase than that at 50% driver demand. This is because the reduction rate of the transmission output torque is bigger. During the inertia phase, Figure 4-7 shows that the vehicle jerk reaches 12.86m/s^3 in the CITGS, more than 10m/s^3, which indicates that the fiercer the change rate of the transmission output torque is, the larger the vehicle jerk will be. Regarding the friction work, at 75% driver demand, the friction work in SCOTGS is less than the first one, which is the same trend as that shown in Table 4-1.

Table 4-2: Simulation results at 75% driver's demand

	|Jerk| (m/s^3)		**|Friction work| (kJ)**
	Torque phase	**Inertia phase**	
CITGS	15.01	12.86	7.292
SCOTGS	15.01	5.39	6.341
COTGS	12.92	7.44	8.662

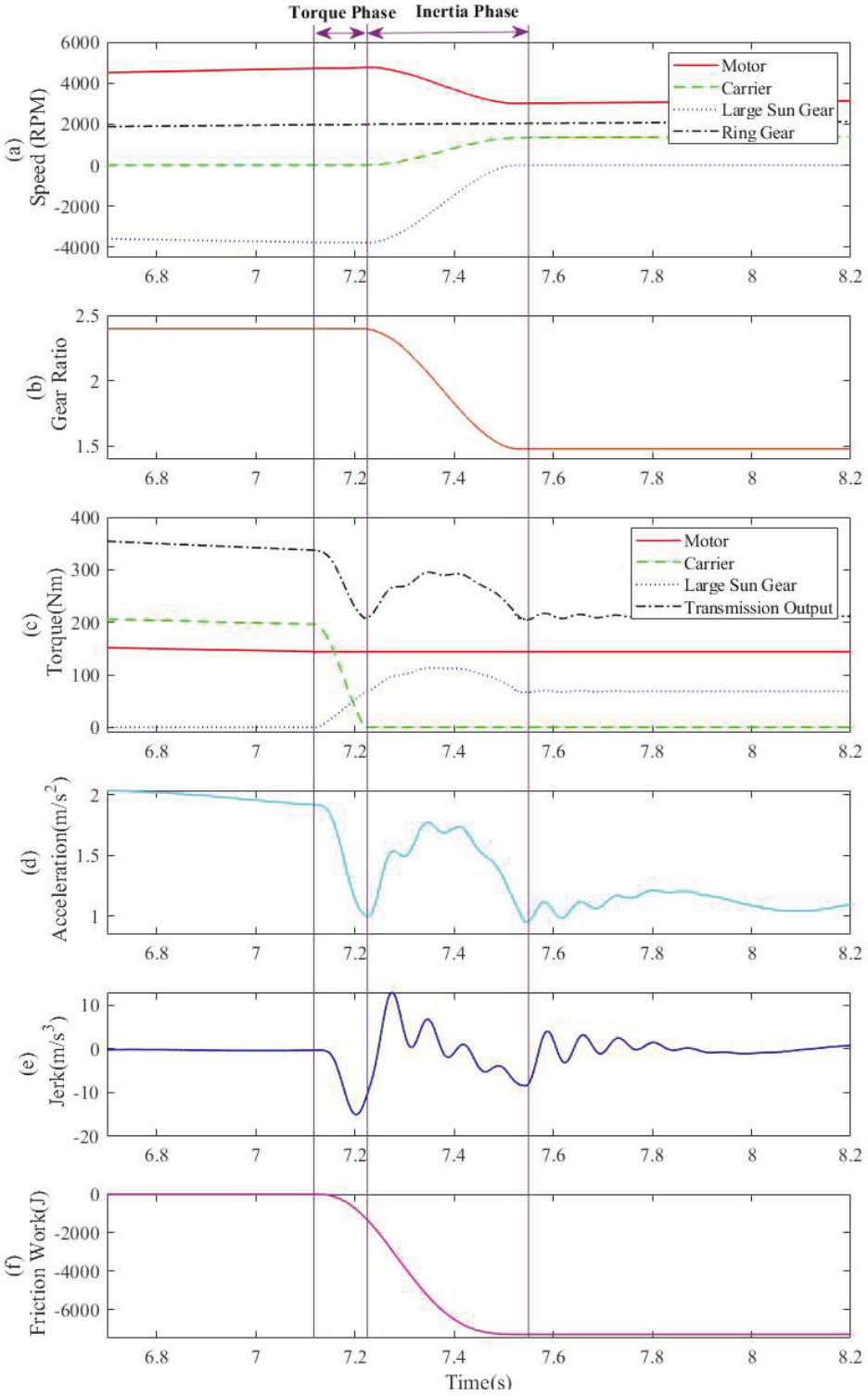

Figure 4-7: Results of CITGS at 75% driver's demand and 65km/h vehicle speed

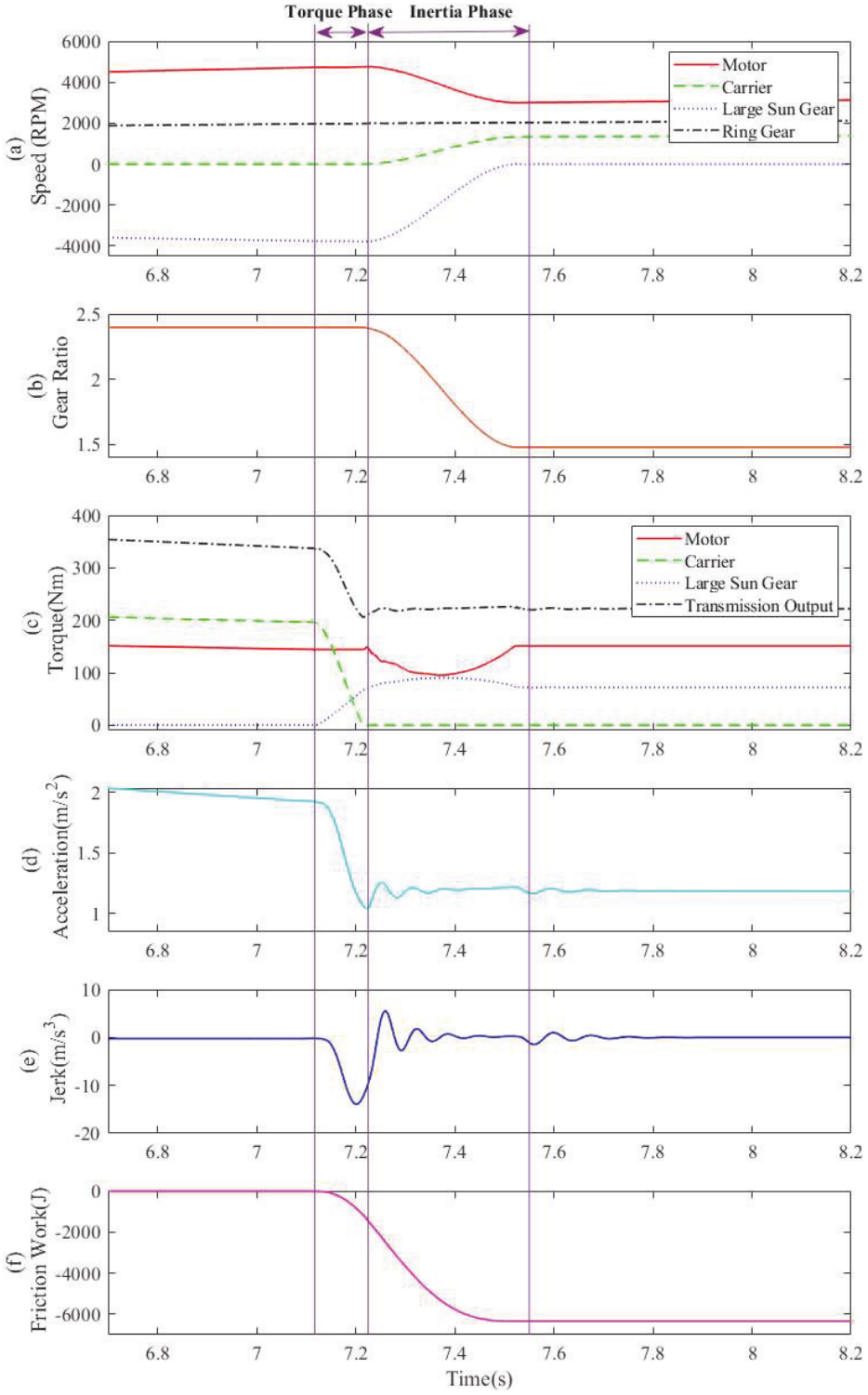

Figure 4-8: Results of SCOTGS at 75% driver's demand and 65km/h vehicle speed

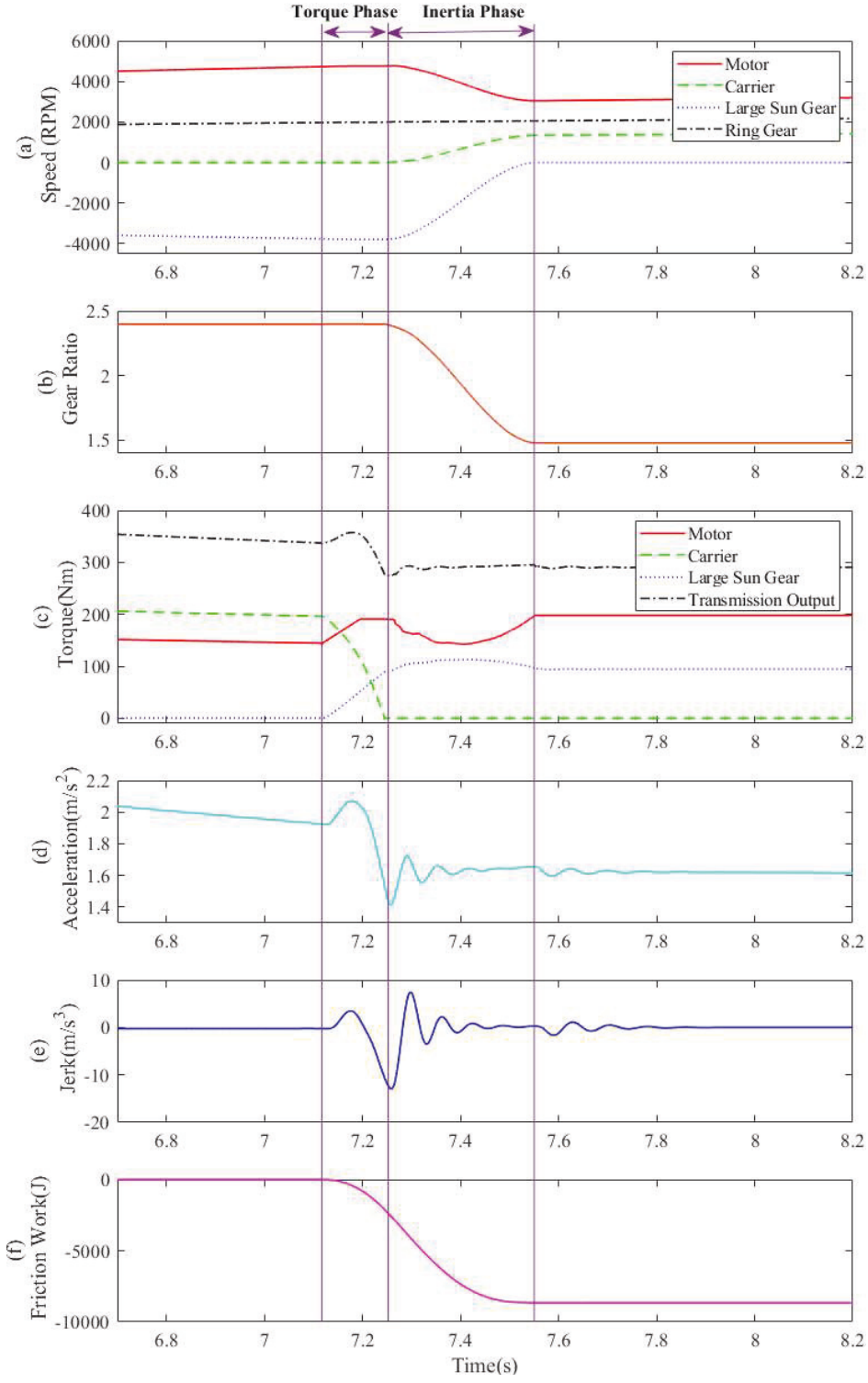

Figure 4-9: Results of COTGS at 75% driver's demand and 65km/h vehicle speed

4.4.2 Power-on downshift results

To compare the gearshift effectiveness of the proposed power-on downshift strategies, (50% driver demand and 45km/h vehicle speed) and (70% driver demand and 50km/h vehicle speed) regarded as different gearshift points are used for all three strategies in simulation. The gearshift duration is as 450ms in all strategies to provide a fair platform to evaluate them in terms of vehicle jerk and friction loss. Specifically, the inertia phase takes 300ms, and the torque phase does the rest.

Figure 4-10, Figure 4-11, and Figure 4-12 show the simulation results from three different kinds of power-on downshift control strategies. Gearshift events start at 50% driver demand and 45km/h vehicle speed. Table 4-3 summarizes these simulation results from three different control strategies. Table 4-3 indicates that the same vehicle jerk 1.49m/s^3 in the inertia phase is recorded in both SCOTGS and COTGS due to their same control tactic in this phase. In the torque phase, COTGS achieves the smallest vehicle jerk 0.79m/s^3. According to the compared simulation results shown in Table 4-3, COTGS distinctly shows more potential in reducing the vehicle jerk by holding the transmission output torque almost unchanged. As shown in Table 4-3, CITGS generates the least friction work, which is a different trend compared to power-on upshift results because there is smaller torque are exerted on LS than SCOTGS and COTGS.

Figure 4-13, Figure 4-14, and Figure 4-15 illustrate the downshift simulation results of three different tactics at the shift point of 75% driver's command and 50km/h vehicle speed. As displayed in Table 4-4, the largest jerk 10.56m/s^3 by adopting CITGS in the inertia phase. However, 5.66m/s^3 vehicle jerk is also triggered by SCOTGS and COTGS.

The reason why the large jerk is attained by SCOTGS and COTGS is that the motor torque cannot be regulated to increase persistently in the inertia phase, only maintained at the maximum torque value according to the current motor speed.

Table 4-3: Simulation results at 50% driver's demand

	|Jerk| (m/s^3)		**|Friction work| (kJ)**
	Inertia phase	**Torque phase**	
CITGS	9.36	12.62	2.993
SCOTGS	1.49	11.86	3.521
COTGS	1.49	0.79	3.752

Table 4-4: Simulation results at 75% driver's demand

	|Jerk| (m/s^3)		**|Friction work| (kJ)**
	Inertia phase	**Torque phase**	
CITGS	10.56	13.54	5.634
SCOTGS	5.66	13.54	6.148
COTGS	5.66	6.02	6.399

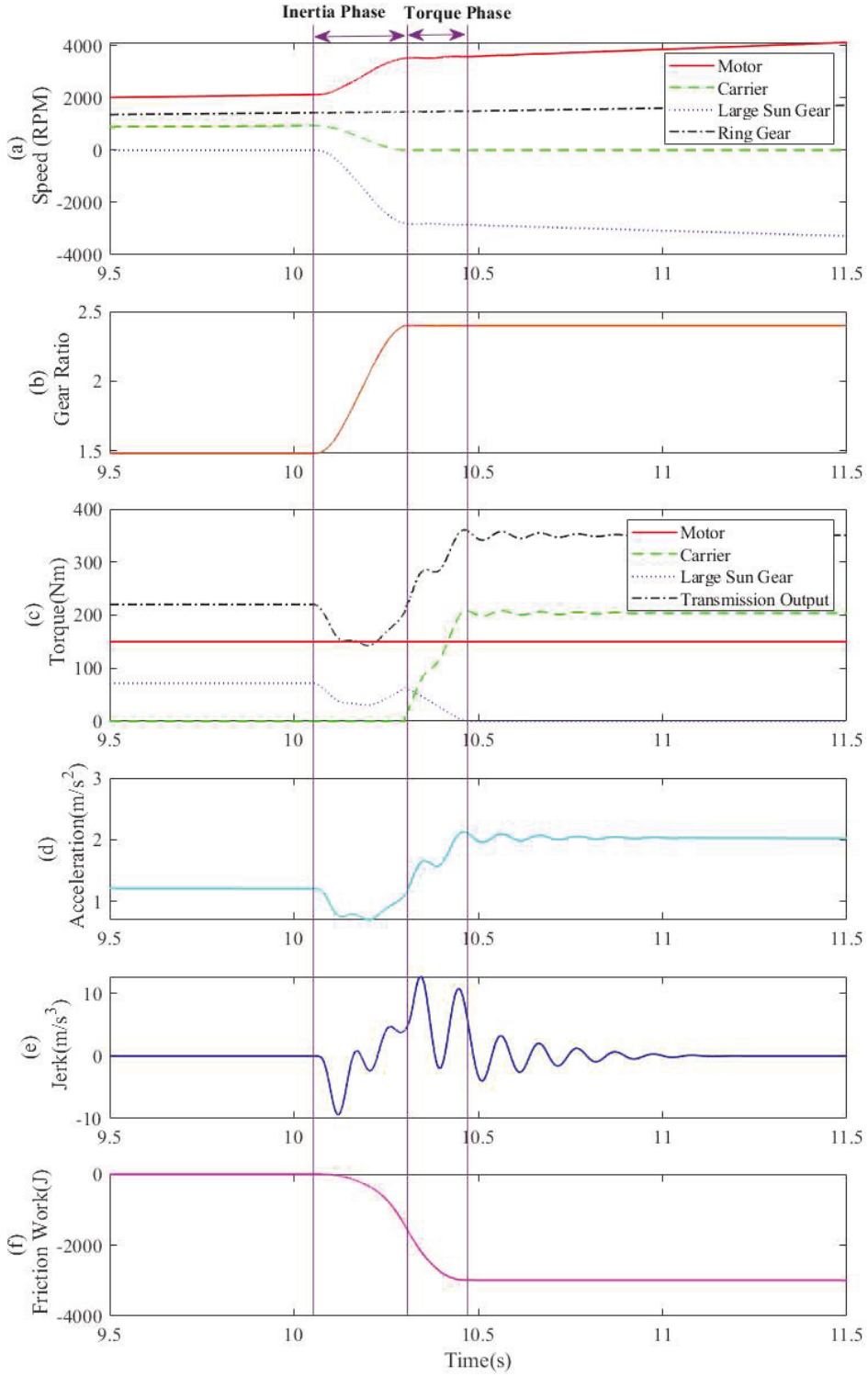

Figure 4-10: Results of CITGS at 50% driver's demand and 45km/h vehicle speed

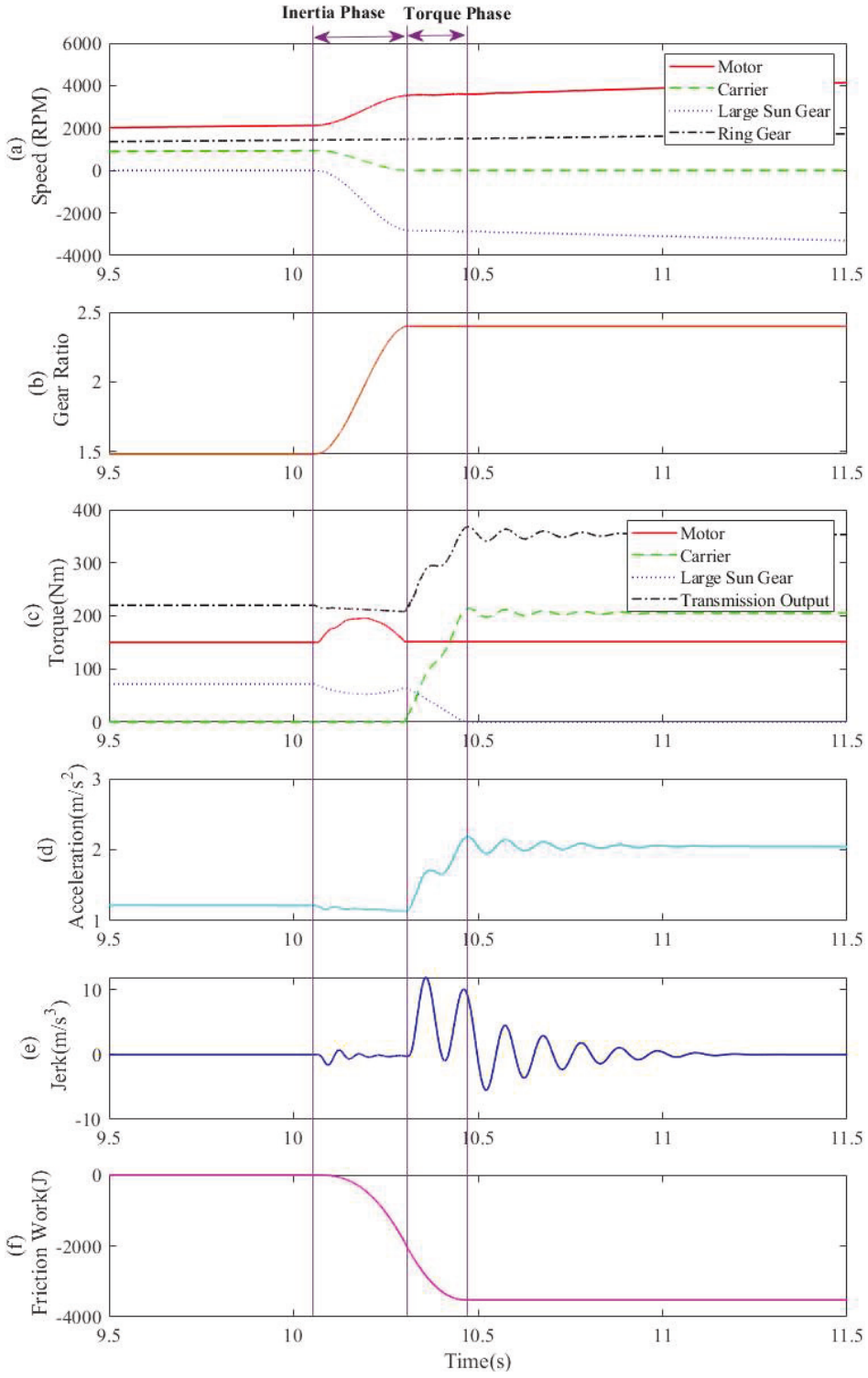

Figure 4-11: Results of SCOTGS at 50% driver's demand and 45km/h vehicle speed

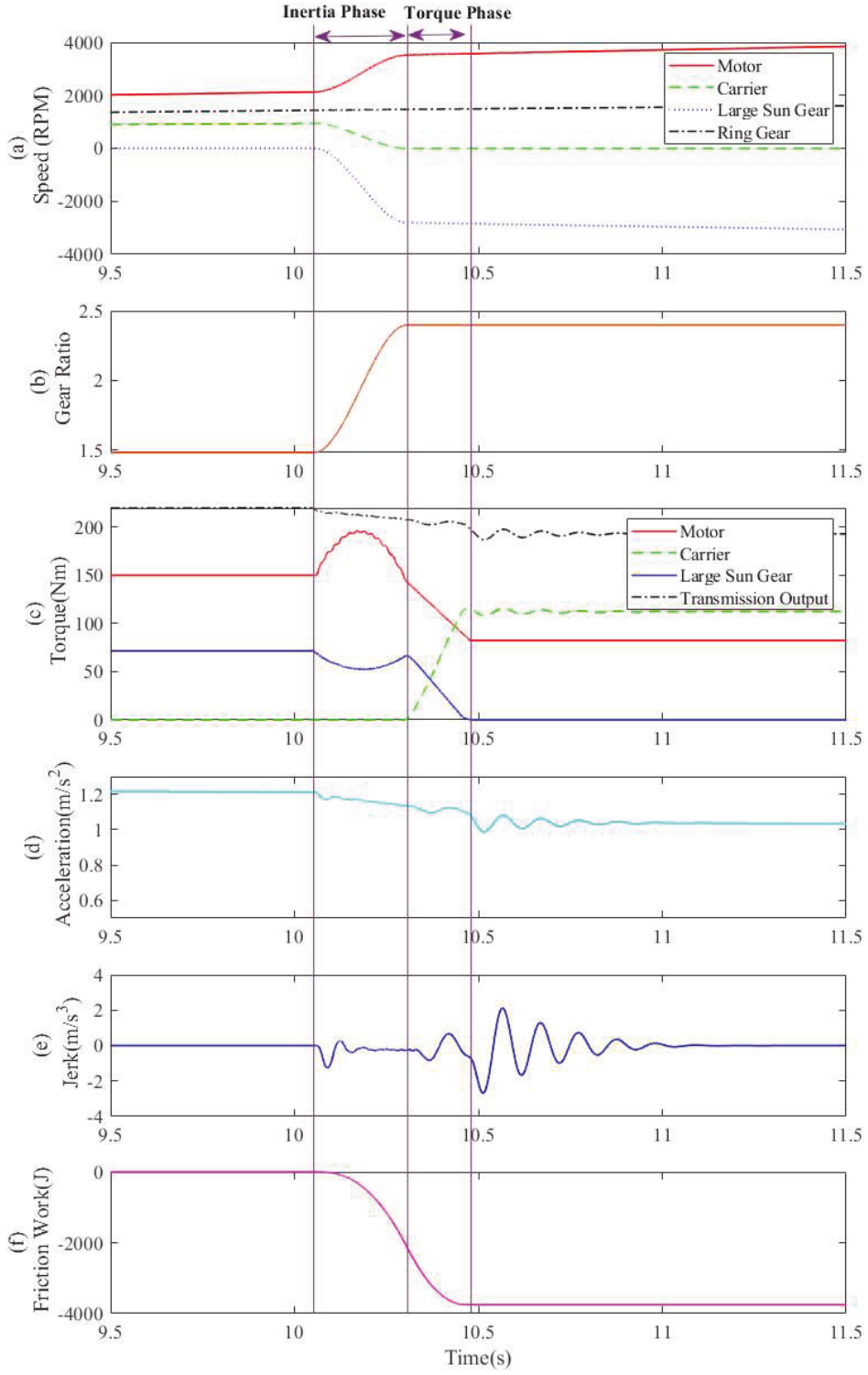

Figure 4-12: Results of COTGS at 50% driver's demand and 45km/h vehicle speed

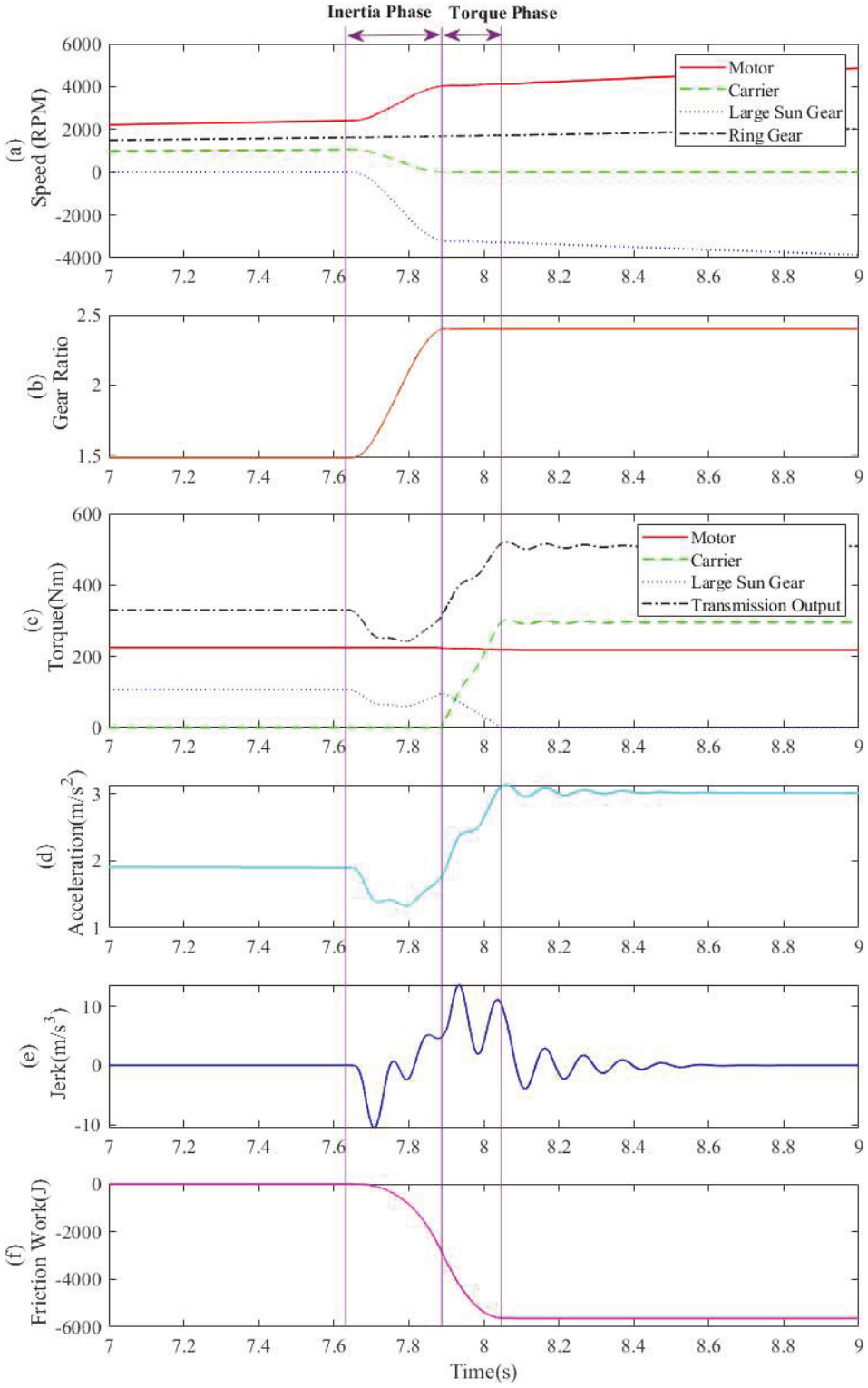

Figure 4-13: Results of CITGS at 75% driver's demand and 50km/h vehicle speed

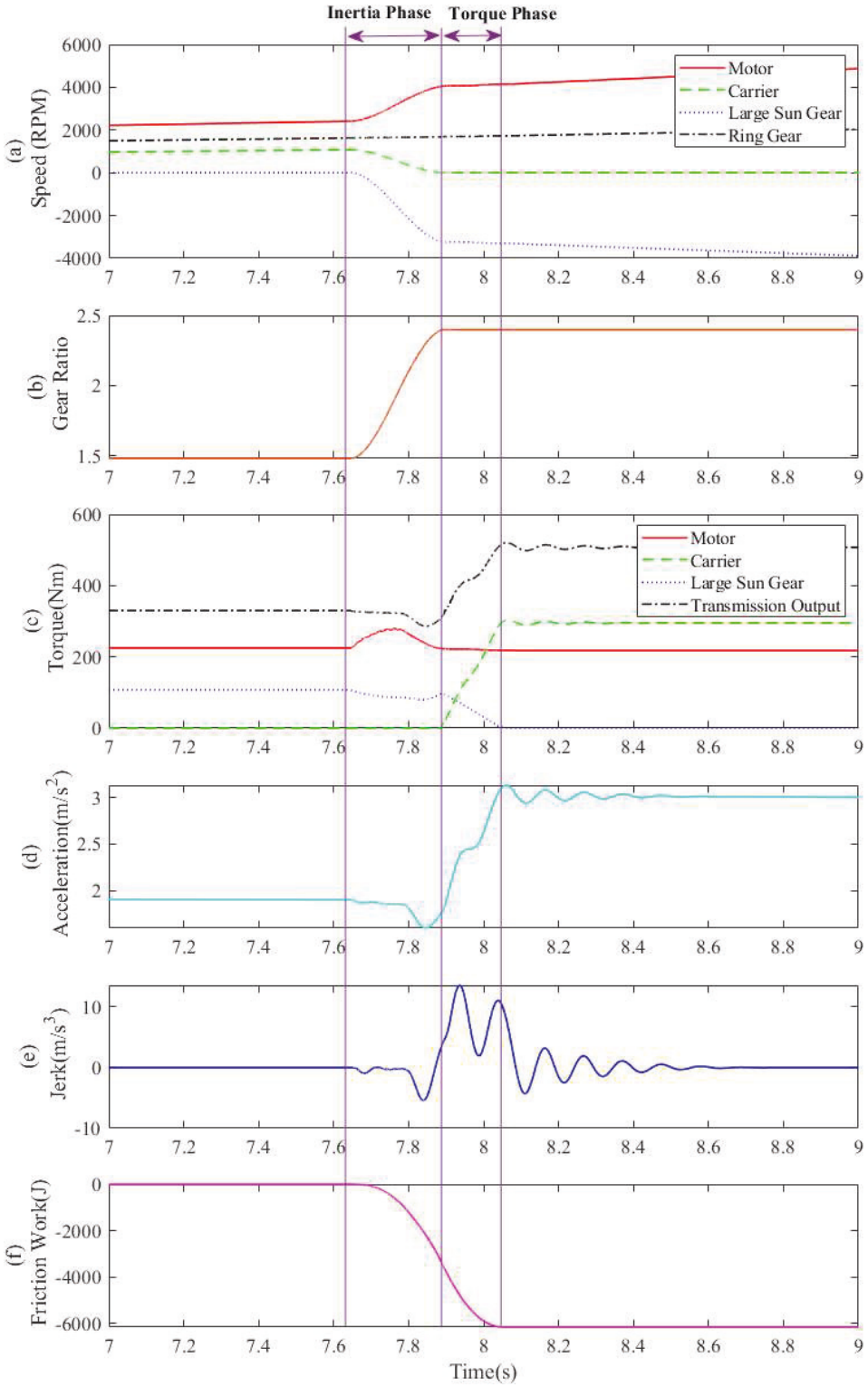

Figure 4-14: Results of SCOTGS at 75% driver's demand and 50km/h vehicle speed

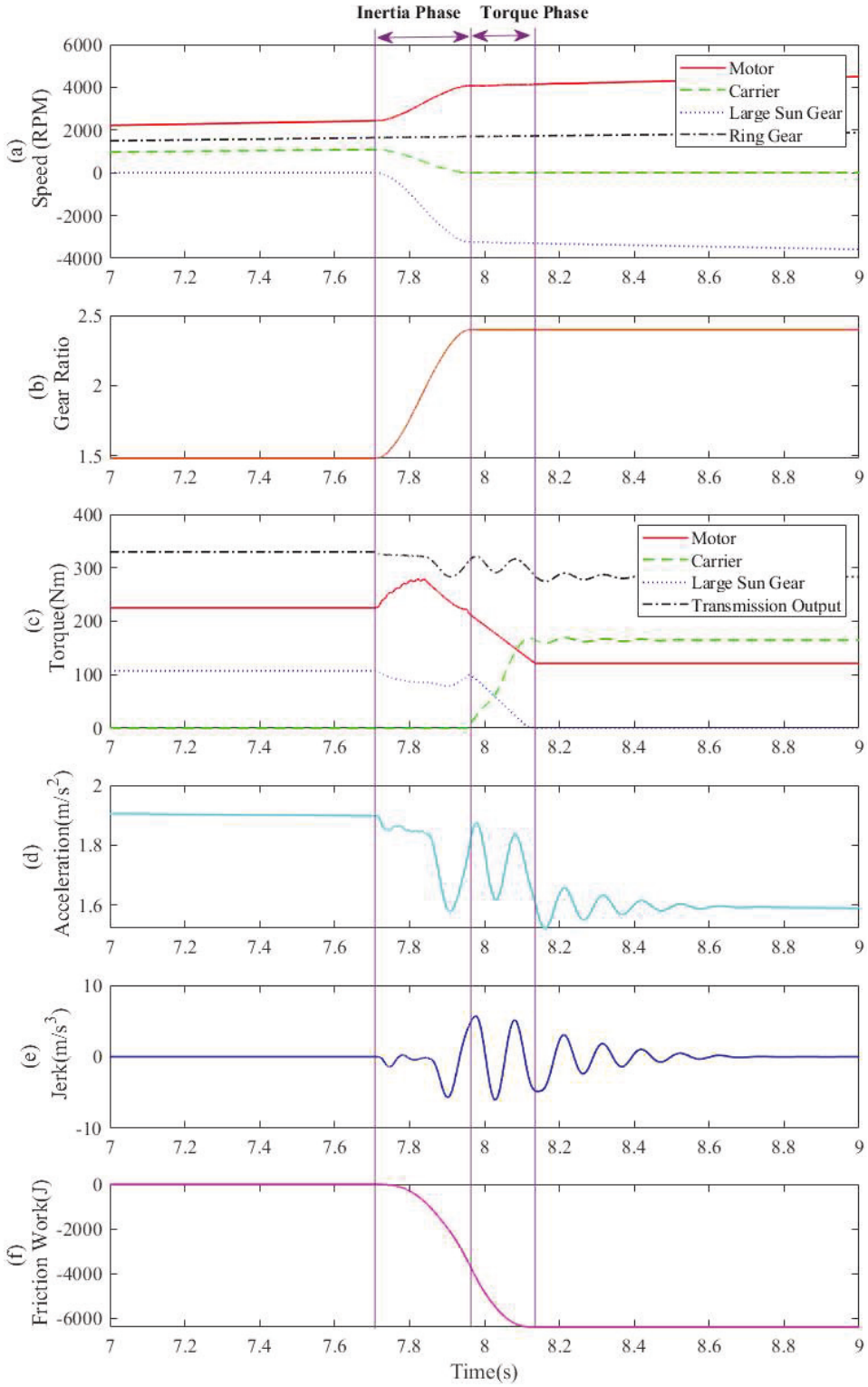

Figure 4-15: Results of COTGS at 75% driver's demand and 50km/h vehicle speed

4.5 CHAPTER CONCLUSIONS

In this chapter, three model-based power-on gearshift control strategies are proposed for the novel two-speed UPAT, termed as CITGS, SCOTGS, and COTGS. In CITGS, the motor torque is maintained constant, which is an easy control method but without taking advantage of the superior controllability of the electric motor. The simulation results of CITGS show that the largest vehicle jerk is attained during the inertia phase. Compared to CITGS, the motor torque is controlled according to the torque ratio of LS brake during the inertia phase in SCOTGS, in consequence, the smaller jerk is achieved by this tactic and it also generates less friction work. COTGS takes advantage of the control flexibility of the electric motor to realize the torque coordination control with the LS brake in both the torque phase and the inertia phase. Simulation results at 50% driver demand demonstrate that the smallest jerk is attained in COTGS. However, due to the increase of the motor torque in the torque phase, the most friction is generated by COTGS. It is worth noting that, in the aggressive driving condition, COTGS is ineffective to an extent in the torque phase due to the limitation of the motor torque, which brings the largest jerk. Both the disadvantages and advantages of these strategies are clearly demonstrated, which provides beneficial knowledge and reference to the researchers undertaking the development of the transmission controller.

CHAPTER 5 : DEVELOPMENT OF TWO-SPEED UPAT TESTING RIG AND EXPERIMENTAL RESULTS ANALYSIS

5.1 INTRODUCTION

The two-speed UPAT testing bench consists of high voltage power, BLDC motor and controller, two-speed UPAT and gearshift control system, torque sensors, speed sensors, dynamometer, and corresponding couplings and shafts to connect BLDC motor, transmission, and eddy current brake. The eddy current brake is used to supply load for the electrified powertrain testing system. Figure 5-1 and Figure 5-2 demonstrate the structure and components of the developed powertrain-testing rig.

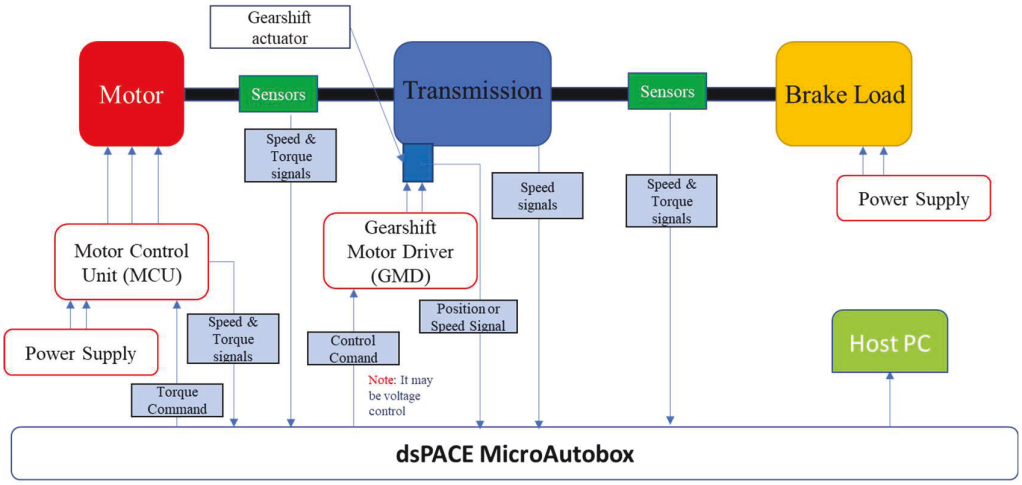

Figure 5-1: Diagram of mechanical and control systems of the testing rig

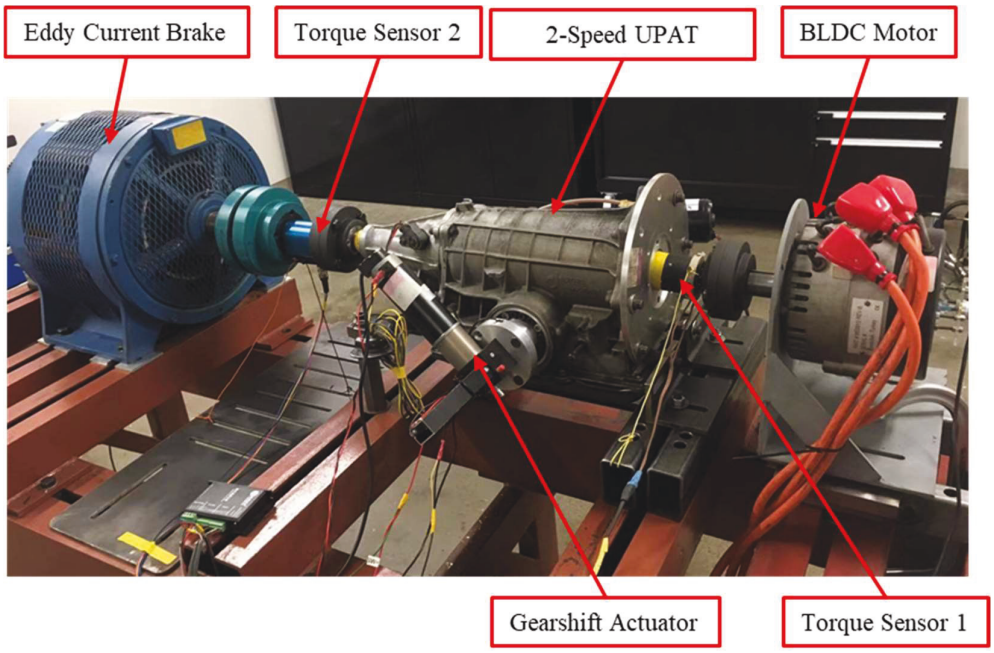

Figure 5-2: Two-speed UPAT prototype test rig

5.2 TORQUE SENSOR CALIBRATION FOR TESTING SYSTEM

The BLDC motor in this test rig can not feedback on its output torque signals to the gearshift control system. Therefore, one wireless torque sensor is installed on the input shaft of the transmission to capture its input torque as the feedback signal for the gearshift control unit. ATi 2000 series is used in this test rig to transmit data from the rotating shaft to a stationary receiver by using telemetry transmitters. A miniature strain gage is adhered to the shaft to transmit shaft torque, as shown in Figure 5-3. A Strain gauge is a sensor whose resistance varies with applied force; It converts force, pressure, tension, weight, etc., into a change in electrical resistance which can then be measured. When external forces are applied to a stationary object, stress and strain are the results. Stress is defined

as the object's internal resisting forces, and strain is defined as the displacement and deformation that occur.

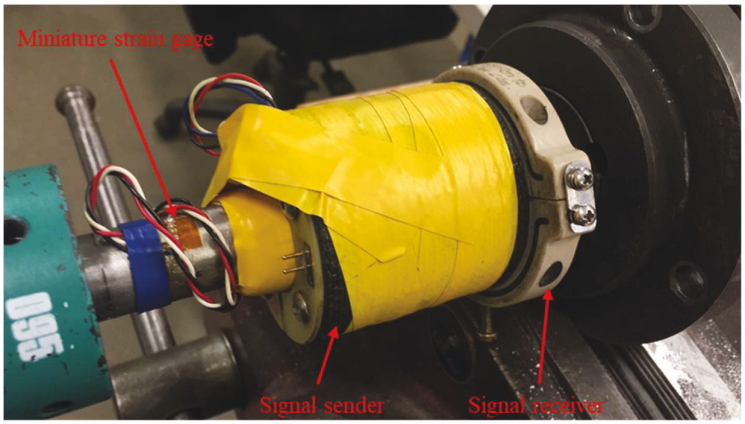

Figure 5-3: ATi 2000 series wireless torque sensor

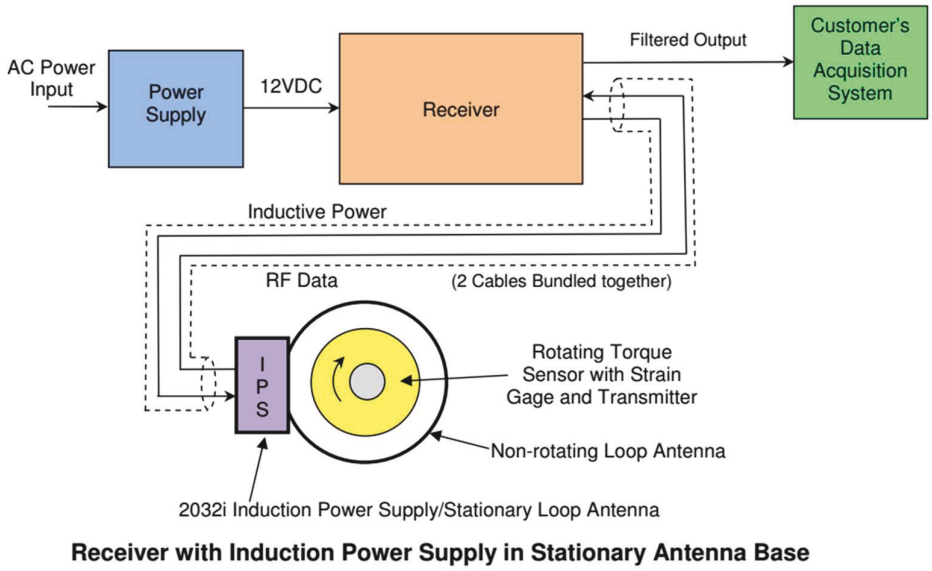

Figure 5-4: Block diagrams of system connections of ATi2000 series

Figure 5-4 shows the block diagrams of system connections of ATi2000 series. The specifications of the torque sensor are shown in Appendix Table A1. Power is supplied

to the transmitter by the induction power supply (IPS). The 2000 series digital receiver supplies DC power to 2032i IPS via a multi-conductor cable. The IPS connects with a stationary loop antenna which radiates 500 kHz power to the rotating loop antenna. This pair of antenna also serves to transmit the sensor signal back to the IPS through a coaxial cable. The signal is then fed from the IPS to the digital receiver via a coaxial cable.

Due to the torque information shown in terms of the analog voltage signal, the mathematical relationship between torque and voltage should be derived and calibrated before actual torque measured. As shown in Figure 5-5, torque is applied to the input shaft of transmission through a bar. One side of the bar is connected to the input shaft by a clamp and the other side is applied torque by adding different weights through a hook. And, the input shaft of the transmission is grounded by a vise clamp.

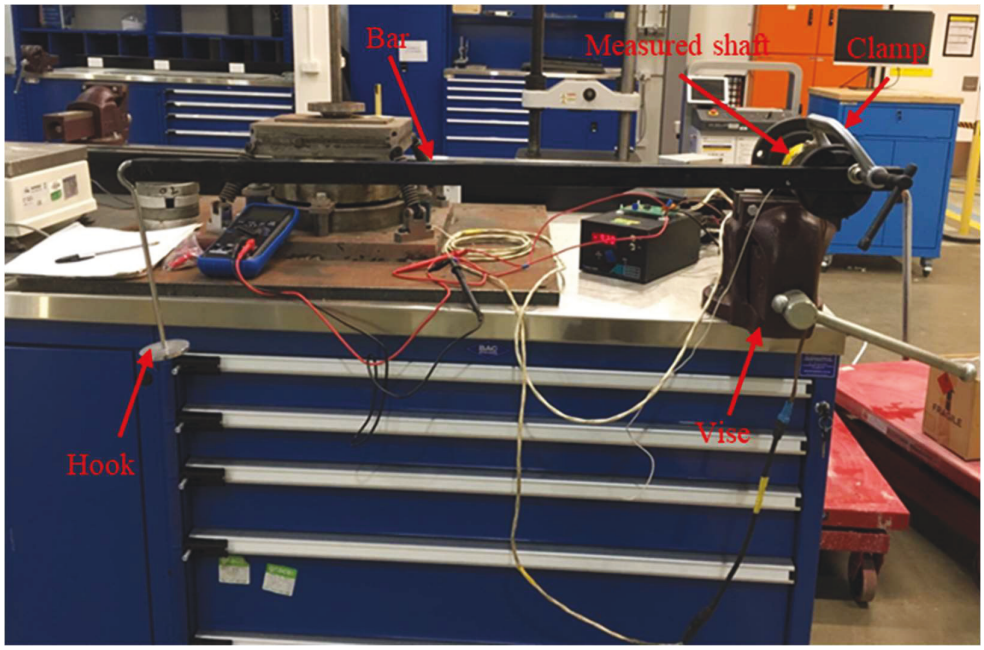

Figure 5-5: Torque sensor calibration

The calibration data of the transmission input shaft torque sensor are presented in Appendix Table A2. The relationships of display voltage and torque measured by sensors are shown in Figure 5-6.

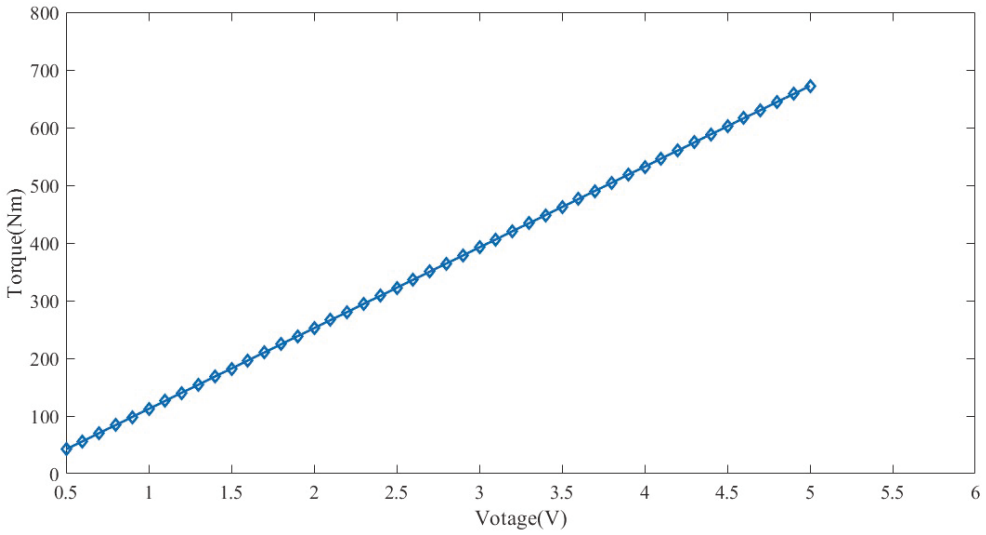

Figure 5-6: Real torque on the input shaft VS sensor display voltage

5.3 CONTROL SYSTEM

The whole control system of BEV powertrain is based on dSPACE MicroAutobox. dSPACE MicroAutoBox is a prototyping solution for numerous gateway and bypassing applications in the field of electronic control unit development/rapid prototyping, and is also able to provide CAN channels required to prototype advanced controls systems for electric/hybrid drives [125]. Rapid Prototyping (RP) technology [126] makes it possible to design products in a virtual environment, shorten the product development cycles, and reduce development costs. Application of RP technology significantly reduces the time to market for new products, and this saves the cost of new product development and

model manufacturing. After the introduction of real-time testing of RP technology, electronic control system design and control algorithms were renamed rapid control prototyping (RCP) technology. Rapid control prototyping is a very efficient method to develop, optimize, and test new control strategies in a real environment quickly without manual programming. For building your own tailored RCP system, dSPACE offers a wide range of software and hardware components, for in-vehicle, laboratory or test bench usage [127].

The block diagrams control system is shown in Figure 5-7. As shown in this figure, an offline tested gearshift control model can be loaded into MicroAutobox by automatic code generation. And, when the rig testing starts, experiment data can be obtained and watched through Control Desk software which is installed in PC. Also, the control variables can be changed by Control Desk software in real-time. MicroAutobox can communicate with BLDC motor controller and gearshift motor controller by CAN Bus

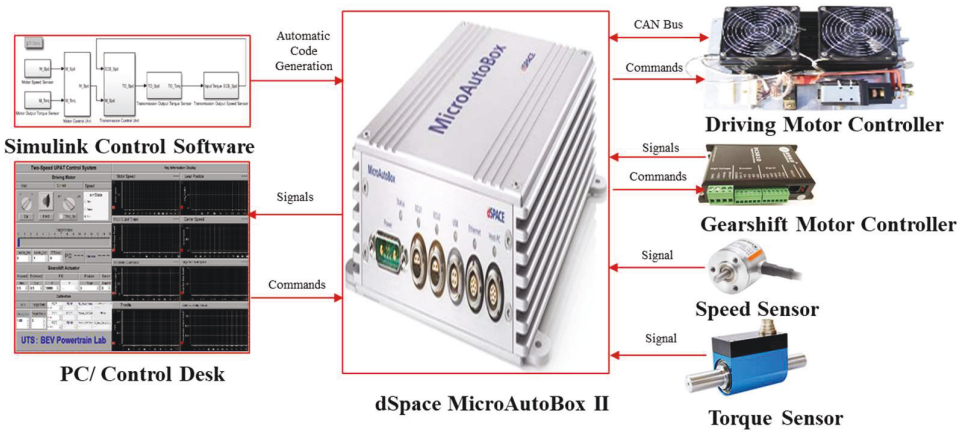

Figure 5-7: Control system of two-speed UPAT

5.4 EXPERIMENTAL RESULTS ANALYSIS

To validate the simulation results of the proposed power-on gearshift strategies, different power-on upshift and downshift experiment is undertaken on two-speed UPAT prototype test rig as shown in Figure 5-2. Since this experiment test rig is just a prototype, the experiment results do not match simulation results based on the whole vehicle model. The first series of results depicted in Figure 5-8, Figure 5-9 and Figure 5-10 present three different kinds of power-on upshift control tactics in this electrified powertrain rig. These tactics are all triggered at 800rpm motor speed. Figure 5-8(a), Figure 5-9(a), and Figure 5-10(a) respectively present the speed variations of the motor, carrier, large sun gear, and transmission output. Figure 5-8(b), Figure 5-9(b), and Figure 5-10(b) show the variation trends of transmission output torque from three different kinds of power-on upshift strategies. According to Figure 5-8(b), Figure 5-9(b) and Figure 5-10(b), it can be found that the torque variation trends is the same to the power-on upshift simulation results in Figure 4-4(c) and Figure 4-7(c), Figure 4-5(c) and Figure 4-8(c), and Figure 4-6(c) and Figure 4-9(c). Therefore, it can be proved that the proposed gearshift strategies are well verified by experimental results and can be applied in practice. Figure 5-11, Figure 5-12, and Figure 5-13 illustrate the shift characteristics of three different tactics at the shift point of 500rpm motor speed. Compared to the simulation results of power-on downshift, the downshift experiment results well validate the simulation results again.

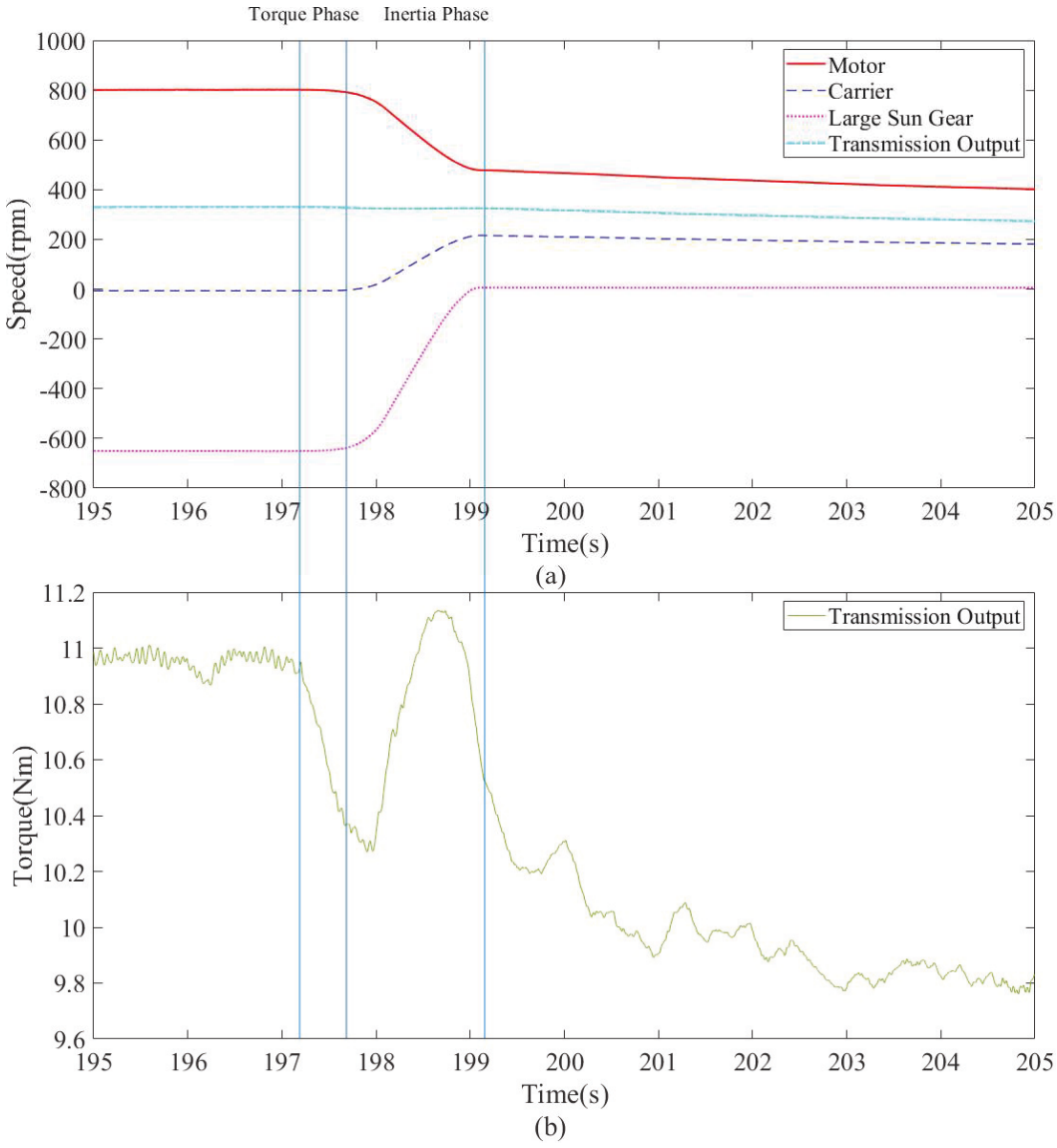

Figure 5-8: Upshift experiment results of CITGS

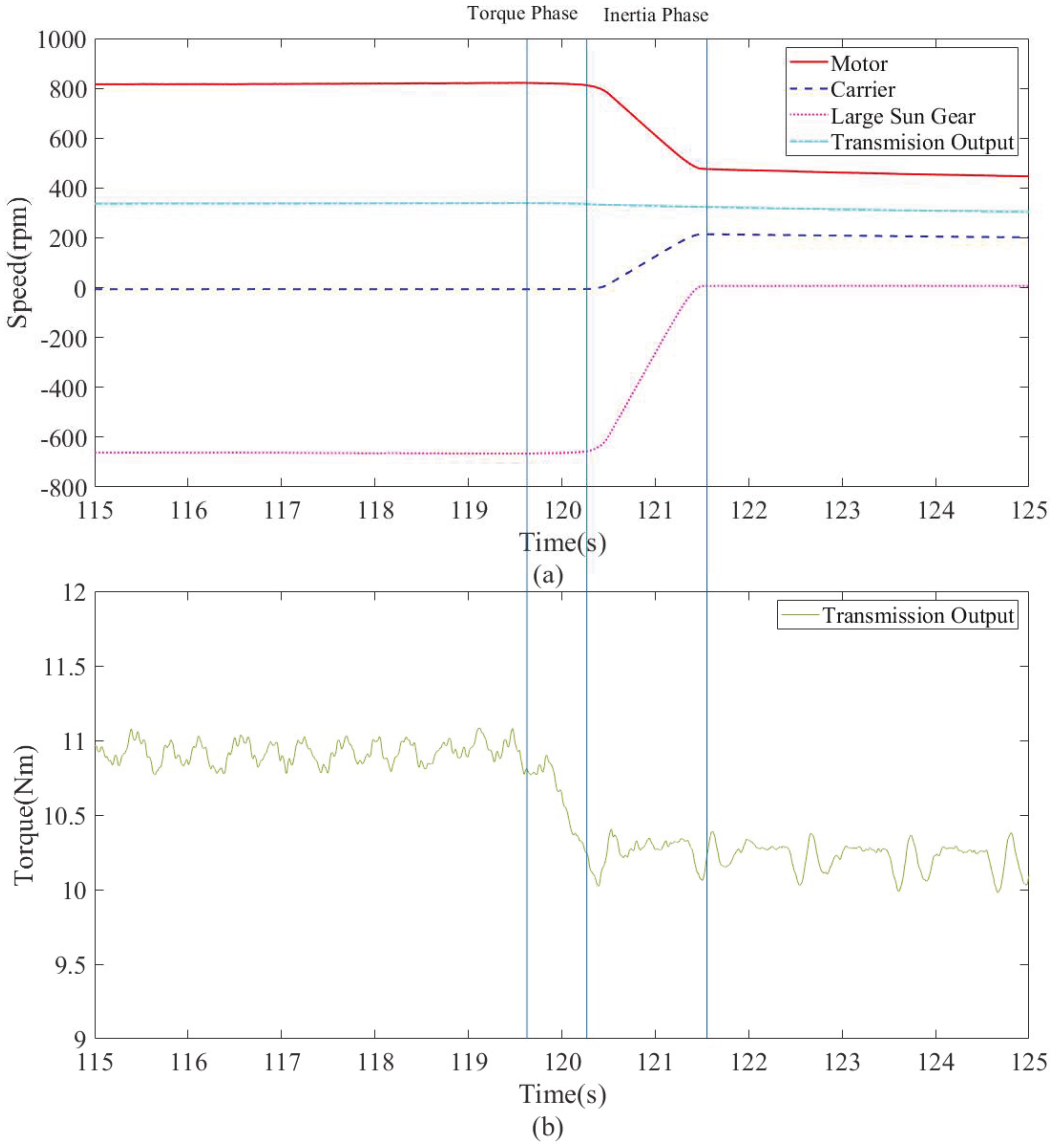

Figure 5-9: Upshift experiment results of SCOTGS

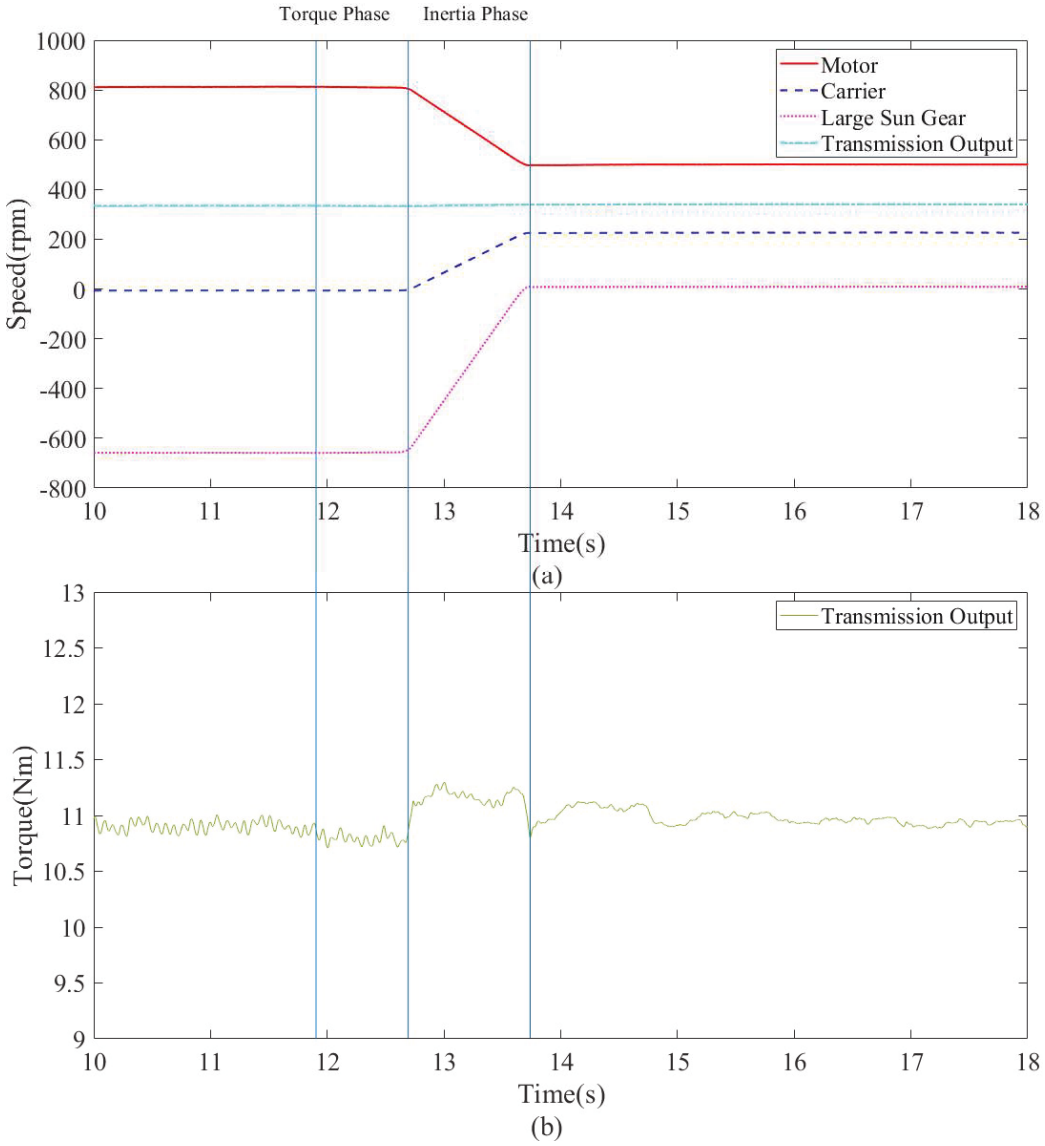

Figure 5-10: Upshift experiment results of COTGS

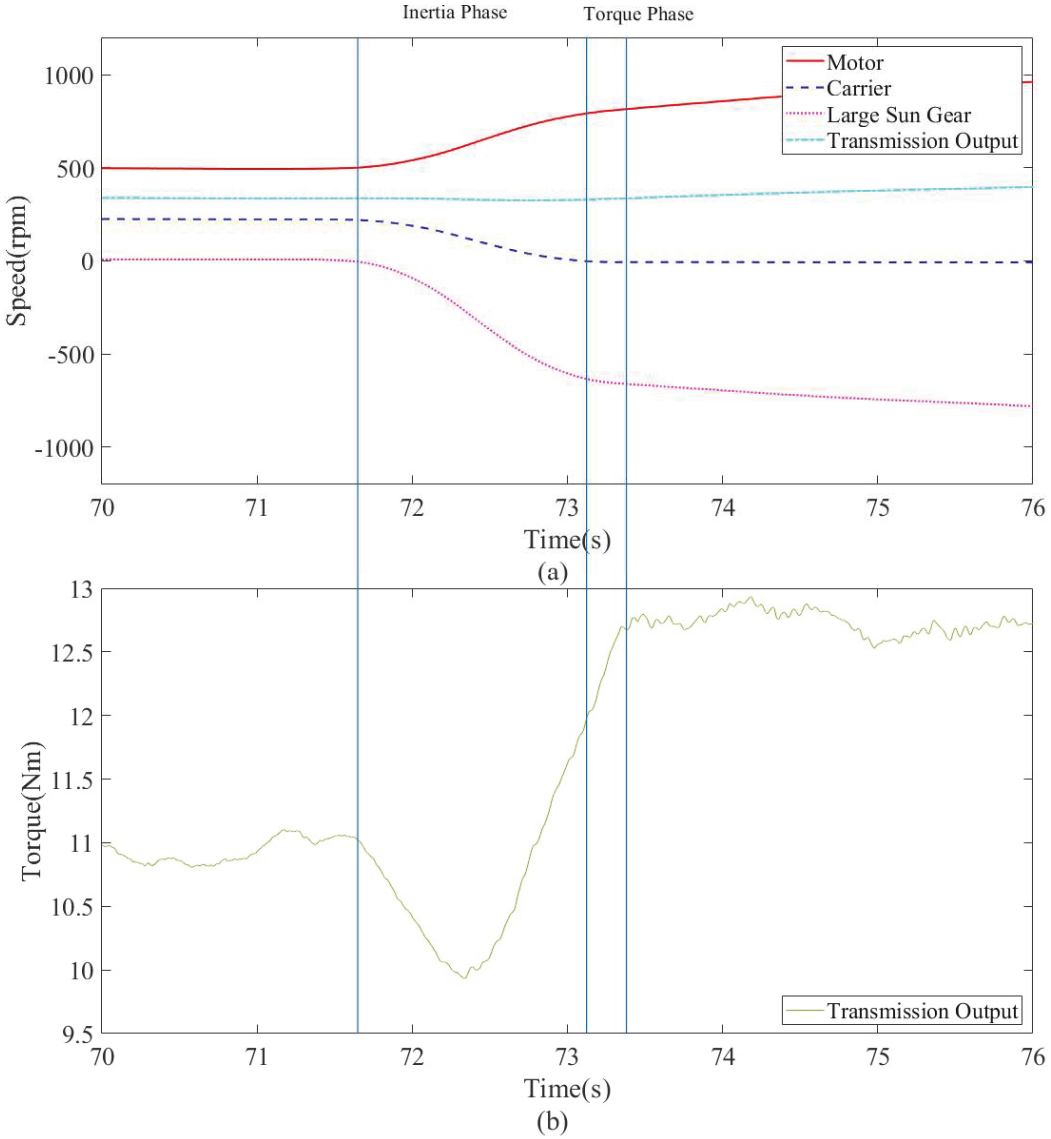

Figure 5-11: Downshift experiment results of CITGS

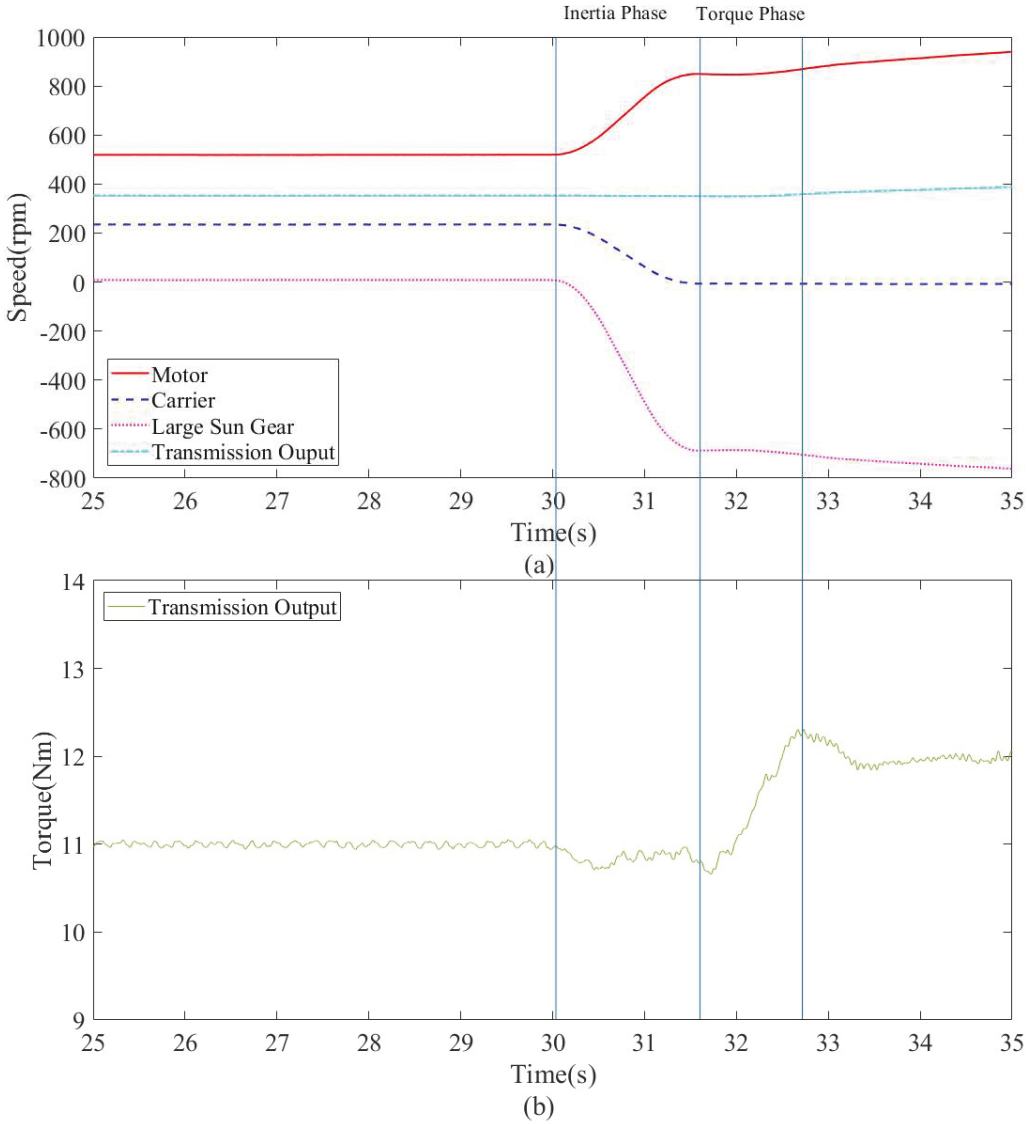

Figure 5-12: Downshift experiment results of SCOTGS

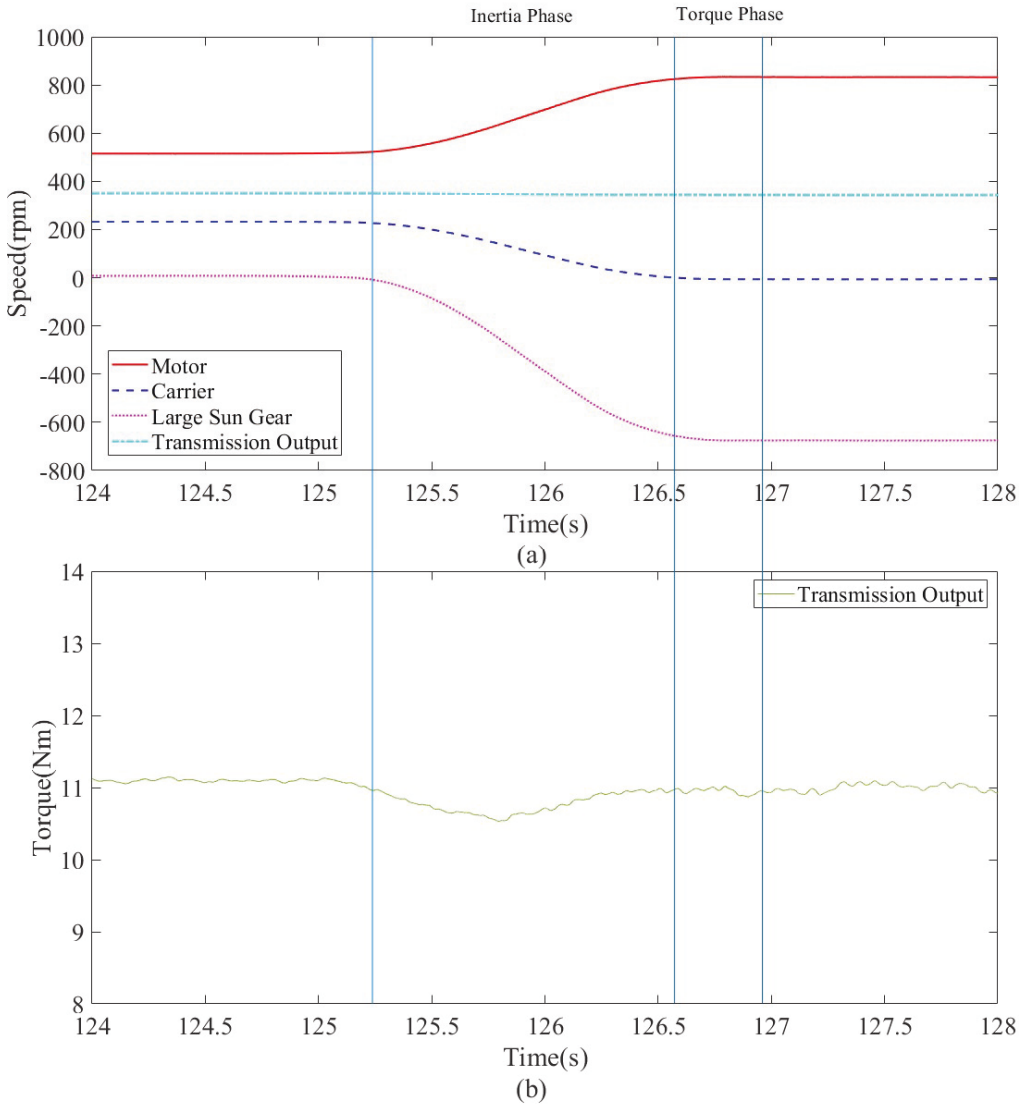

Figure 5-13: Downshift experiment results of COTGS

CHAPTER 6 : OPTIMAL COORDINATING GEARSHIFT CONTROL OF TWO-SPEED UPAT FOR BEVS

6.1 INTRODUCTION

Considering the potential advantages of multispeed transmissions equipped BEVs, this chapter presents an investigation into the optimal coordinating gearshift control of the proposed two-speed UPAT for BEVs. Model-based gearshift tactics are proposed for the torque phase and the inertia phase respectively. In addition, based on available sensor signals, sliding mode observers are employed to estimate unmeasurable torque as feedback information for the optimal controllers in different gear states.

The remainder of this chapter is divided into the following sections: Section 2 shows the comprehensive process of the optimal controller design and optimal results. Section 3 presents the development of sliding mode observers and estimation results. At last, conclusions are presented in Section 4.

6.2 OPTIMAL CONTROLLER DESIGN

6.2.1 Problem statement

With regard to the transmission layout studied in chapter 3, the gear shifting control strategy is usually classified into two different types, namely power-off gearshifts and

power-on gearshifts [77]. The former finishes gear changing without the traction torque transferred to the wheels from the input of the powertrain, which will result in the vehicle acceleration loss and discontinuity and then impact the drivability. Compared to the single-speed version, adopting this gearshift strategy for multiple-speed transmissions will seriously damage the inherent nature of electric vehicles. Therefore, power-on gearshifts should be considered as the most preferred alternative due to there being still torque transmitted from the transmission output shaft to the wheels. As widely acknowledged, the power-on tactic is necessarily categorized into individually two phases. For the power-on upshifts, the first phase is the torque phase which is also vividly interpreted in the so-called torque handover stage, namely the torque transmitted from the off-coming clutch or brake to the on-coming clutch or brake. The following phase is the inertia phase where the speed synchronizing of the on-coming clutch or brake should be smoothly finished. The process of power-on downshifts is the inverse process of the power-on upshifts, namely inertia phase first and then torque phase following.

In this study, the power-on upshift is only regarded as a case to research the gear changing transient response and then derive the optimal gearshift methodology. Aiming to implement the power-on gearshifts, three alternative gearshift strategies are designed and verified in chapter 4. The study results show that the motor torque controlled as a constant value in the torque phase is the most proper strategy for different gearshift conditions. Also, during the inertia phase, the high-quality gearshifts can be obtained through the coordinating control between the electric motor and the gearshift actuator. The coordinating control strategy diagram is presented in Figure 6-1. According to this figure, it can be found that the transmission output torque maintains almost unchanged during

the inertia phase. This will effectively reduce the vehicle jerk to a large extent. In this chapter, this gearshift strategy will be further optimized to promote gearshift performance comprehensively.

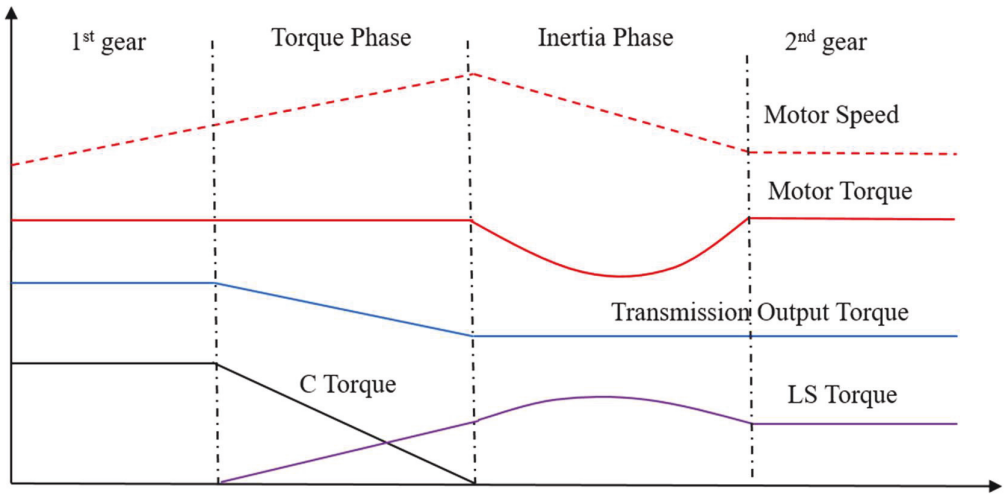

Figure 6-1: The diagram of the power-on upshift strategy

6.2.2 Optimal Control Theory

Modern control theory mainly considers the multi-input and multi-output (MIMO) problems, which are mainly based on a series of differential equations of state variables [128]. Therefore, the system is generally defined by state variables, and the linear time-invariant form is as follows

$$\dot{\boldsymbol{x}}(t) = \boldsymbol{A}\boldsymbol{x}(t) + \boldsymbol{B}\boldsymbol{u}(t) \tag{6.1}$$

$$\boldsymbol{y}(t) = \boldsymbol{C}\boldsymbol{x}(t) + \boldsymbol{D}\boldsymbol{u}(t) \tag{6.2}$$

where $\boldsymbol{x}(t)$, $\boldsymbol{u}(t)$ and $\boldsymbol{y}(t)$ are respectively n, r and m dimensional state, control, and output vectors. $\boldsymbol{A}$ is $n \times n$ state matrix, $\boldsymbol{B}$ is $n \times r$ input matrix, $\boldsymbol{C}$ is $m \times n$ output matrix, $\boldsymbol{C}$ is $m \times n$ transfer matrix.

Analogously, a nonlinear system can be defined as follows

$$\dot{\boldsymbol{x}}(t) = f(\boldsymbol{x}(t), \boldsymbol{u}(t), t) \tag{6.3}$$

$$\boldsymbol{y}(t) = f(\boldsymbol{x}(t), \boldsymbol{u}(t), t) \tag{6.4}$$

Modern control theory shows that all state variables can be fed back with appropriate weight [129]. In a control system, optimization is necessary. The topic of optimization is conceptually based on methods, benefits, signal nature, and phases in various ways to achieve the purpose of optimization. In general, optimization problems can be divided into static optimization and dynamic optimization. Static optimization is to optimize the control system under the condition of stable states. In other words, system variables do not change over time, and control objects can be described by algebraic equations. The solutions used are generally calculus, Lagrange multiplication, linear and nonlinear programming. Dynamic optimization [129] is the optimization of control objects under dynamic conditions. System variables vary over time, and the description of the system includes variations over time. Control objects can be described by differential equations. The solutions are search technique, dynamic programming, variational method, and Pontryagin principle.

The main purpose of optimal control is to optimize the selected performance criteria by determining the control signals to enable the control object to meet some physical

constraints. Description of optimal control problem includes three main parts, i.e. controlled plant, performance index, and boundary conditions, and physical constraints of state quantities and control quantities.

6.2.2.1 Controlled plant

For optimal control, physical control objects are generally described by a series of linear or nonlinear differential equations as shown in Eqs. (6.1)-(6.4).

6.2.2.2 Performance index

In modern control theory, the optimal control problem is to find controlled variables that can make the dynamic system reach a target value or follow a state trajectory and the optimal performance index. Some performance indicators are described in the followings [129]

(1) The performance index of time-optimal control system

The system is expected to reach the specified final state from any initial state in the minimum time, and the corresponding performance index is

$$J = \int_{t_0}^{t_f} dt = t_f - t_0 = t^* \tag{6.5}$$

(2) Fuel optimum control system performance index.

Considering the space shuttle, defined as the thrust of the rocket engine, and assume that the magnitude of the thrust is proportional to the rate of fuel consumption. To minimize total fuel consumption, the performance indicators are set as follows

$$J = \int_{t_0}^{t_f} \sum_{i=1}^{m} R_i |u_i(t)| \, dt \tag{6.6}$$

Where R_i is the weight factor.

(3) Minimum energy control system performance index

To minimize the total energy expenditure, performance indexes are set as follows

$$J = \int_{t_0}^{t_f} \boldsymbol{u}^T \boldsymbol{R} \boldsymbol{u} dt \tag{6.7}$$

Where $\boldsymbol{R}$ is a positive definite symmetric matrix

(4) Terminal control system performance index

Considering the positive and negative of the error and weight factors, the objective function is defined in the following

$$J = \boldsymbol{x}^T(t_f) \boldsymbol{F} \boldsymbol{x}(t_f) \tag{6.8}$$

where $\boldsymbol{F}$ is a semidefinite symmetric matrix.

(5) The performance index of general optimal control system.

Combined with all the above cases, the general form of the optimal control system performance index can be expressed by

$$J = \boldsymbol{x}^T(t_f) \boldsymbol{F} \boldsymbol{x}(t_f) + \int_{t_0}^{t_f} [\boldsymbol{x}^T(t) \boldsymbol{Q} \boldsymbol{x}(t) + \boldsymbol{u}^T \boldsymbol{R} \boldsymbol{u}] dt \tag{6.9}$$

Where $\boldsymbol{R}$ is the positive definite matrix, $\boldsymbol{Q}$ and $\boldsymbol{F}$ is the semi-positive definite matrix., $\boldsymbol{R}$ and $\boldsymbol{Q}$ could be a time-varying matrix. The general form of performance index is called quadratic form.

6.2.2.3 Constraints

The control vectors and the state vectors can be constrained or unconstrained, depending on the physical condition of the control object. The constraints of general control quantities and state quantities are

$$\boldsymbol{u_{min}} \leq \boldsymbol{u}(t) \leq \boldsymbol{u_{max}} \tag{6.10}$$

$$\boldsymbol{x_{min}} \leq \boldsymbol{x}(t) \leq \boldsymbol{x_{max}} \tag{6.11}$$

In the following, the optimal gearshift controller is designed according to the above optimal theory.

6.2.3 Powertrain model

By ignoring the stiffness and damping elements, the powertrain model is considered as a rigid body, which will simplify the derivation process of the optimal controller [20, 35, 36, 39]. Consequently, the powertrain model can be presented as shown in chapter 4. According to Eq. (4.15) and Eq. (4.16), the powertrain model can be expressed by

$$\ddot{\theta}_{SS} = g_1 T_M + g_2 T_{LS} + g_3 T_C + g_4 T_{ef} \tag{6.12}$$

$$\ddot{\theta}_{LS} = m_1 T_M + m_2 T_{LS} + m_3 T_C + m_4 T_{ef} \tag{6.13}$$

where

$g_1 = \frac{f_2 i_1 - e_2}{f_2 e_1 - f_1 e_2}$, $g_2 = \frac{-f_2 i_4 - e_2}{f_2 e_1 - f_1 e_2}$, $g_3 = \frac{-e_2}{f_2 e_1 - f_1 e_2}$, $g_4 = \frac{e_2(\frac{1}{i_4} + \frac{2}{i_3}) - f_2}{f_2 e_1 - f_1 e_2}$, $m_1 = \frac{f_1 i_1 - e_1}{f_1 e_2 - f_2 e_1}$, $m_2 = \frac{-f_1 i_4 - e_1}{f_1 e_2 - f_2 e_1}$, $m_3 = \frac{-e_1}{f_1 e_2 - f_2 e_1}$, $m_4 = \frac{e_1(\frac{1}{i_4} + \frac{2}{i_3}) - f_1}{f_2 e_1 - f_1 e_2}$, $e_1 = (J_M + J_{SS}) i_1 - 3 J_{IP} b_1 i_2 + 3 J_{OP} c_1 i_3 + (J_R + \frac{J_V}{i_f}) d_1$, $e_2 = -3 J_{IP} b_2 i_2 + 3 J_{OP} c_2 i_3 - J_{LS} i_4 + (J_R + \frac{J_V}{i_f}) d_2$, $f_1 = J_C a_1 + (J_M + J_{SS}) + 3 J_{IP} b_1 + 3 J_{OP} c_1 + (\frac{1}{i_4} + \frac{2}{i_3})(J_R + \frac{J_V}{i_f}) d_1$, $f_2 = J_C a_2 + 3 J_{IP} b_2 + 3 J_{OP} c_2 + J_{LS} + (\frac{1}{i_4} + \frac{2}{i_3})(J_R + \frac{J_V}{i_f}) d_2$, $i_1 = \frac{r_R}{r_{SS}}$, $i_2 = \frac{r_R}{r_{IP}}$, $i_3 = \frac{r_R}{r_{OP}}$, $i_4 = \frac{r_R}{r_{LS}}$

6.2.4 Torque phase during power-on upshift

Based on the analysis mentioned above, during this phase, the traction electric motor torque is kept constant to avoid impairing shift smoothness at the aggressive driver torque demand shown in Figure 4-9.

During the torque phase of power-on upshift, $\dot{\theta}_C = 0$ and $\ddot{\theta}_C = 0$. Eq. (6.14) can be obtained as

$$\ddot{\theta}_{LS} = -\frac{a_1}{a_2} \ddot{\theta}_{SS} \tag{6.14}$$

So the simplified powertrain model can be regarded as a single degree of freedom system. According to Eq. (4.18), Eq. (6.15) can be obtained

$$0 = n_0 \dot{T}_M + n_1 \dot{T}_{LS} + n_2 \dot{T}_C + n_3 \dot{T}_{ef} \tag{6.15}$$

where $n_0 = a_1 g_1 + a_2 m_1$, $n_1 = a_1 g_2 + a_2 m_2$, $n_2 = a_1 g_3 + a_2 m_3$, $n_0 = a_1 g_4 + a_2 m_4$

Because the electric motor torque is operated to keep a constant during this phase, $\dot{T}_M = 0$. During the gear shifting process, T_{ef} is often considered as time-invariant, so $\dot{T}_{ef} = 0$. Therefore, according to Eq. (6.15), $\dot{T}_C$ can be expressed by

$$\dot{T}_C = -\frac{n_1}{n_2}\dot{T}_{LS} \tag{6.16}$$

For the control design requirements, the state variables of the control system can be chosen as

$$\boldsymbol{x}_T = [x_{T1}\ x_{T2}\ x_{T3}\ x_{T4}\ x_{T5}]^{\mathrm{T}} = \left[\dot{\theta}_{LS}\ T_M\ T_{LS}\ T_C\ T_{ef}\right]^{\mathrm{T}} \tag{6.17}$$

and the control variable

$$\boldsymbol{u}_T = u_{T11} = \dot{T}_{LS} \tag{6.18}$$

According to Eqs. (6.15)-(6.18), the powertrain model can be re-arranged as follows

$$\dot{x}_{T1} = m_1 x_{T2} + m_2 x_{T3} + m_3 x_{T4} + m_4 x_{T5} \tag{6.19}$$

$$\dot{x}_{T2} = 0 \tag{6.20}$$

$$\dot{x}_{T3} = u_{T11} \tag{6.21}$$

$$\dot{x}_{T4} = -\frac{n_1}{n_2} u_{T11} \tag{6.22}$$

$$\dot{x}_{T5} = 0 \tag{6.23}$$

The more compact form can be expressed as

$$\dot{\boldsymbol{x}}_T = \boldsymbol{A}_T \boldsymbol{x}_T + \boldsymbol{B}_T \boldsymbol{u}_T \tag{6.24}$$

where $\boldsymbol{A}_T = \begin{bmatrix} 0 & m_1 & m_2 & m_3 & m_4 \\ 0 & 0 & 0 & 0 & 0 \\ 0 & 0 & 0 & 0 & 0 \\ 0 & 0 & 0 & 0 & 0 \\ 0 & 0 & 0 & 0 & 0 \end{bmatrix}$, $\boldsymbol{B}_T = \begin{bmatrix} 0 & 0 & 1 & -\frac{n_1}{n_2} & 0 \end{bmatrix}^{\mathrm{T}}$.

The control target during gearshifts is to obtain small vehicle jerk and little friction work in the fixed gearshift duration. Physically, the vehicle jerk can be calculated by Eq. (6.25). The friction work can be modeled by Eq. (6.26).

The vehicle jerk:

$$\begin{aligned} j_T = \frac{da}{dt} = \frac{r_W}{i_f}\frac{d\ddot{\theta}_R}{dt} = \frac{r_W}{i_f}\left(d_1\ddot{\theta}_{SS} + d_2\ddot{\theta}_{LS}\right) \\ = \frac{r_W}{i_f}\left(d_2 - d_1\frac{a_2}{a_1}\right)\left(m_2 - m_3\frac{n_1}{n_2}\right)u_{T11} \end{aligned} \tag{6.25}$$

The friction work:

$$W_T = \int_{t_0}^{t_T} T_{LS}\dot{\theta}_{LS}dt \tag{6.26}$$

where t_0 and t_T are the start time and terminal time of the torque phase.

Based on the above analysis, the optimal gearshift control issue is able to be abstracted as a finite time state regulation problem. In the torque phase of the power-on upshift, the

terminal time is limited by the gearshift actuator capacity, and the terminal states are also constrained restrictedly. So, a limited-time linear-quadratic regulator (LQR) [130] is properly used to address this optimal control issue.

In this phase, the cost function for the LQR design is

$$J_T = \frac{1}{2}\boldsymbol{x}_T^{\mathrm{T}}(t_T)\boldsymbol{F}_T\boldsymbol{x}_T(t_T) = \frac{1}{2}\int_{t_0}^{t_T}(\boldsymbol{x}_T^{\mathrm{T}}\boldsymbol{Q}_T\boldsymbol{x}_T + \boldsymbol{u}_T^{\mathrm{T}}\boldsymbol{R}_T\boldsymbol{u}_T)dt \tag{6.27}$$

where $\boldsymbol{F}_T \in \boldsymbol{R}^{5\times5}$ and $\boldsymbol{Q}_T \in \boldsymbol{R}^{5\times5}$ are symmetric positive semi-definite weighting matrices and $\boldsymbol{R}_T \in \boldsymbol{R}$ is a symmetric positive definite weighting matrix. To be more specific, $\boldsymbol{F}_T$ represents the weighting matrix of the gearshift duration.

In the torque phase of the power-on upshift, the initial states of this system are defined as

$T_M(t_0) = T_{M0}, T_{LS}(t_0) = 0, T_C(t_0) = T_{C0}$

and terminal states

$T_M(t_T) = T_{M0}, T_C(t_T) = 0$

The constraints of system states are

$0 \le T_{LS} \le T_{LS\_Max}, T_{M0} \le T_{M\_Max}$

where T_{M0} and T_{C0} are the initial torque of the motor and OWC during torque phase, T_{LS_Max} is the max torque LS brake can exert and T_{M_Max} is the max motor torque in its current speed state.

By using Hamiltonian approach [130], the control law can be obtained

$$\boldsymbol{u}_T = \boldsymbol{K}_T(t)\boldsymbol{x}_T = -\boldsymbol{R}_T^{-1}\boldsymbol{B}_T^{\mathrm{T}}\boldsymbol{P}_T(t)\boldsymbol{x}_T \tag{6.28}$$

where $\boldsymbol{K}_T(t) \in \boldsymbol{R}^{1\times 5}$ represents the controller gain, $\boldsymbol{P}_T(t) \in \boldsymbol{R}^{1\times 5}$ is the non-negative definite matrix and time-varying matrix, determined by Ricati equation and expressed as following [130]

$$\dot{\boldsymbol{P}}_T(t) = -\boldsymbol{P}_T(t)\boldsymbol{A}_T + \boldsymbol{P}_T(t)\boldsymbol{B}_T\boldsymbol{R}_T^{-1}\boldsymbol{B}_T^{\mathrm{T}}\boldsymbol{P}_T(t) - \boldsymbol{Q}_T - \boldsymbol{A}_T^{\mathrm{T}}\boldsymbol{P}_T(t) \tag{6.29}$$

When $\boldsymbol{P}_T(t_T) = \boldsymbol{F}_T$, the torque phase will be finished. The weighting matrices $\boldsymbol{F}_T$, $\boldsymbol{Q}_T$ and $\boldsymbol{R}_T$ can be adjusted to ensure small friction work and good gearshift performance. Here, symmetric matrices $\boldsymbol{F}_T$, $\boldsymbol{Q}_T$ and $\boldsymbol{R}_T$ are shown as the followings

$$\boldsymbol{F}_T = \begin{bmatrix} 0 & 0 & 0 & 0 & 0 \\ 0 & 0 & 0 & 0 & 0 \\ 0 & 0 & 0 & 0 & 0 \\ 0 & 0 & 0 & f_{T44} & 0 \\ 0 & 0 & 0 & 0 & 0 \end{bmatrix}, \boldsymbol{Q}_T = \begin{bmatrix} q_{T11} & 0 & q_{T13} & 0 & 0 \\ 0 & 0 & 0 & 0 & 0 \\ q_{T3} & 0 & q_{T33} & 0 & 0 \\ 0 & 0 & 0 & q_{T44} & 0 \\ 0 & 0 & 0 & 0 & 0 \end{bmatrix}, \boldsymbol{R}_T = r_{T11}$$

Therefore, the objective function J_T can be rearranged as

$$\begin{aligned} J_T = \underbrace{\frac{1}{2}f_{T44}T_C^2(t_T) + \frac{1}{2}\int_{t_0}^{t_T} q_{T44}T_C^2 dt}_{J_{T1}} + \underbrace{\frac{1}{2}\int_{t_0}^{t_T}\left(q_{T13}T_{LS}\dot{\theta}_{LS} + q_{T31}T_{LS}\dot{\theta}_{LS}\right)dt}_{J_{T2}} \\ + \underbrace{\frac{1}{2}\int_{t_0}^{t_T} r_{T11}\dot{T}_{LS}^2 dt}_{J_{T3}} + \underbrace{\frac{1}{2}\int_{t_0}^{t_T}(q_{T11}\dot{\theta}_{LS}^2 + q_{T33}\dot{T}_{LS}^2)dt}_{J_{T4}} \end{aligned} \tag{6.30}$$

The physical meanings of each part of J_T are represented as follows

J_{T1} forces T_C to converge to zero during the defined torque phase duration. J_{T2} ensures little friction loss generated in this phase. J_{T3} ensures small vehicle jerk. J_{T4} does not

represent physical meanings, but it can adjust q_{T11} and q_{T33} to ensure $\boldsymbol{Q}_T$ symmetric positive semi-definite.

In this chapter, the vehicle jerk shown in all simulation results is obtained by quadratic derivation of the vehicle speed. And, the vehicle acceleration is filtered before derivation by using a low pass filter at 200 Hz, this removes higher transient frequencies from the results but maintains the lower frequency responses. The simulation results of the proposed optimal control strategy during the torque phase of power-on upshift are shown in Figure 6-2. The torque phase of power-on upshift takes about 0.166s from 4.867s to 5.033s. To be more specific, Figure 6-2(a) shows the relationship of torque change rates between C and LS. When LS torque gradually increases, C torque continuously decreases to zero, while the transmission output torque decreases gradually, as shown in Figure 6-2(b). In Figure 6-2(c), the absolute value of the max vehicle jerk in this phase is 8.9m/s^3 which is within. Figure 6-2(d) presents the friction work generated during the torque phase of power-on upshift which is calculated according to Eq. (6.26). The total friction loss in this phase is 1930J.

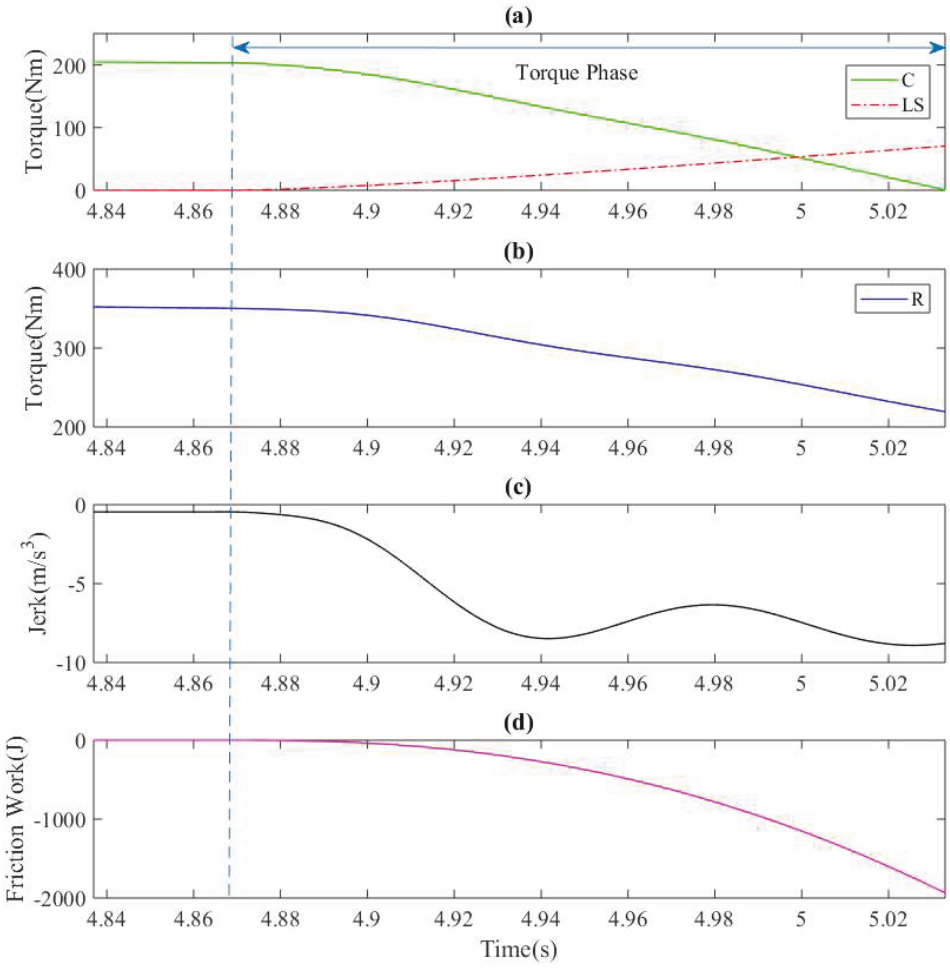

Figure 6-2: Simulation results of the optimal control strategy

To validate the superiority of the optimal control strategy, different types of control strategies existed in current literature are used to conduct the comparisons with the strategy studied in this thesis. Regarding the first strategy used in Refs. [21, 37], T_{LS} is expressed as the form of a linear proportional function, where T_{LS} is inversely related to T_C. According to Eq. (6.16), the torque exerted on the LS can be written as

$$T_{LS} = \int_{t_0}^{t_T} -\frac{n_2}{n_1}\dot{T}_C dt \tag{6.31}$$

where $\dot{T}_C = \text{constant} < 0$

The corresponding simulation results according to Eq. (6.31) are presented in Figure 6-3.

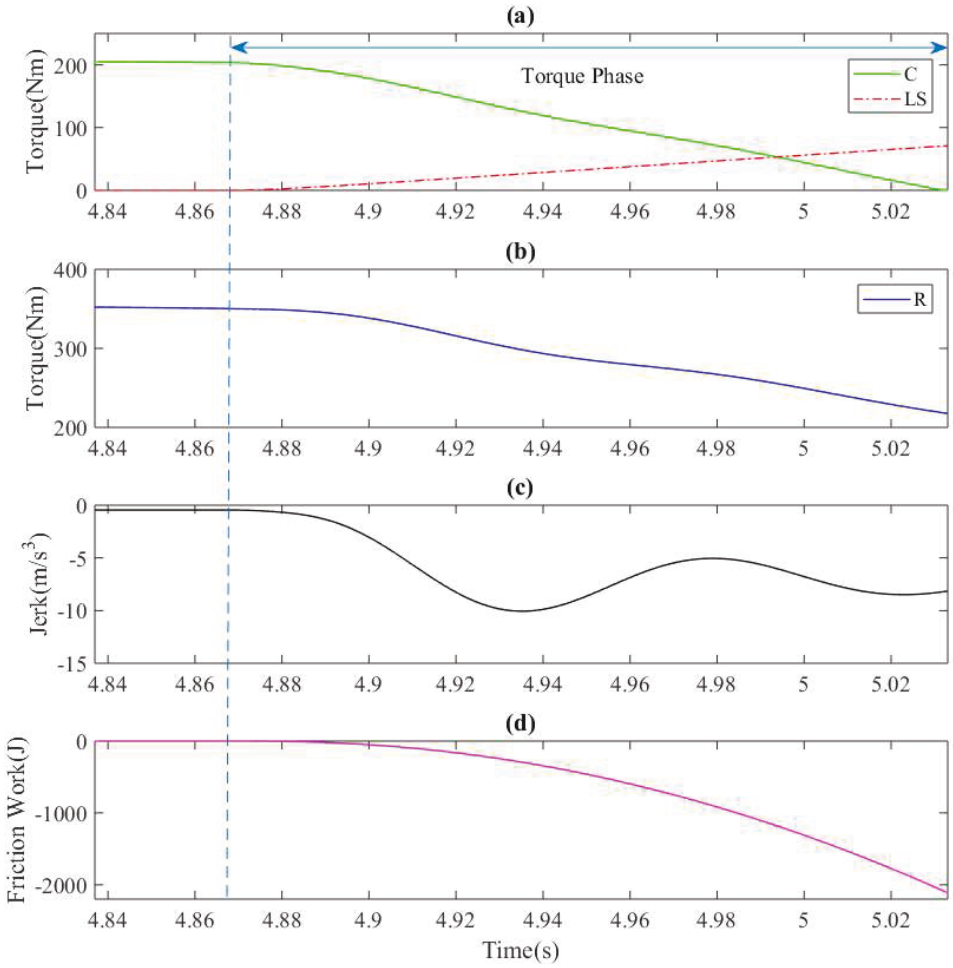

Figure 6-3: Simulation results of the control strategy according to Eq. (6.31)

In Ref. [131], different kinds of polynomials are regarded as the desired reference trajectories for the speed control and torque control. Through the analysis and study, the

authors find that the quantic-polynomial is the optimum desired reference for the gear shifting control among those polynomials. Herein, the quantic-polynomial is used as the second control group to finish the torque transfer during the torque phase, as shown Eq. (6.32). And, the detailed derivation process can refer to the literature [131].

$$T_C = -T_{C0}\left[6\left(\frac{t-t_0}{t_T-t_0}\right)^5 - 15\left(\frac{t-t_0}{t_T-t_0}\right)^4 + 10\left(\frac{t-t_0}{t_T-t_0}\right)^3\right] + T_{C0} \tag{6.32}$$

According to Eqs. (6.16) and (6.32), T_{LS} in the torque phase can be obtained by Eq. (6.33)

$$T_{LS} = \frac{n_2}{n_1}T_{C0}\left[6\left(\frac{t-t_0}{t_T-t_0}\right)^5 - 15\left(\frac{t-t_0}{t_T-t_0}\right)^4 + 10\left(\frac{t-t_0}{t_T-t_0}\right)^3\right] \tag{6.33}$$

According to Eq. (6.33), the corresponding results are displayed in Figure 6-4.

To present the gearshift performance quantitatively, the largest vehicle jerk and the total friction work in the torque phase are shown in Table 6-1 where “1” represents the simulation results of Figure 6-2. while “2” and “3” stand for the results from Figure 6-3. and Figure 6-4, respectively. The largest vehicle jerk (14.3m/s^3) happens in “3”, namely LS torque changing according to Eq. (6.33). The second largest vehicle jerk is 10.1m/s^3 in “2” according to Eq. (6.31). Therefore, it is clearly found that the optimal strategy presented by “1” induces the smallest vehicle jerk (8.9m/s^3), which means that, in comparison with the former two, the proposed strategy improves the vehicle gearshift performance in term of the vehicle jerk. The most friction work (2113J) is generated in “2”. Although the least friction work is 1909J dissipated in “3”, the second least friction work is 1930J which is just 1.09% more than that in “3”. However, in comparison with that in “1”, the friction work dissipated in “2” is 9.48% more. Therefore, the optimal

gearshift control strategy not only reduces the vehicle jerk but also makes the friction loss decrease. Thus, the optimal strategy in the torque phase of power-on upshift promotes the gearshift performance improvement comprehensively.

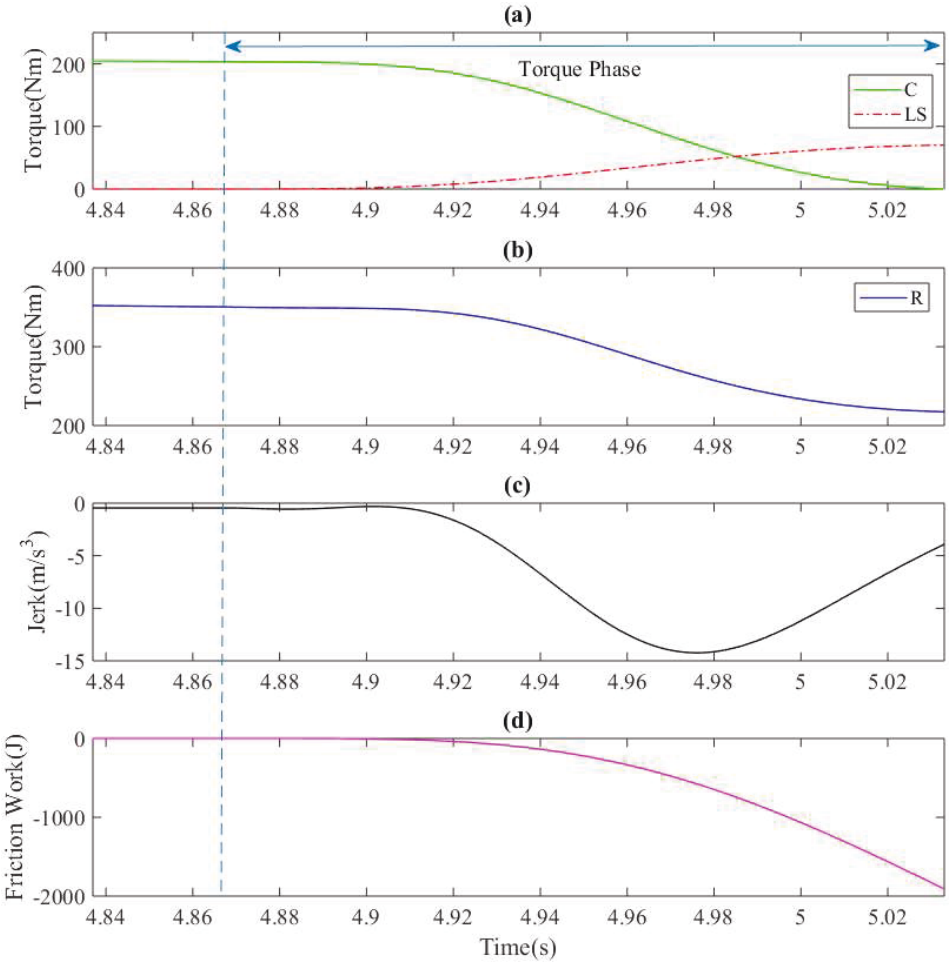

Figure 6-4: Simulation results of the control strategy according to Eq. (6.44)

Table 6-1: Comparison of simulation results

Control Strategy	|Jerk| (m/s^3)	|Friction work| (J)
1	8.9	1930
2	10.1	2113
3	14.3	1909

When the C torque reaches zero, the torque phase is finished terminally. The gearshift procedure should be naturally switched to the inertia phase of power-on upshift. As mentioned above, the dynamics of the powertrain in the inertia phase are entirely different from those in the torque phase. Specifically, the degree of freedom of this transmission comes to change from one in the torque phase to two in the inertia phase. Therefore, the control tactic in the inertia phase of power-on upshift needs to be re-devised to satisfy the gearshift requirements.

6.2.5 Inertia phase during power-on upshift

In this phase, $T_C = 0$. The motion system of this transmission shifts to two degrees of freedom system because $\dot{\theta}_C \neq 0$. To achieve the minimal vehicle jerk during this phase, in advance, the transmission output torque regarded as the control objective is maintained almost unchanged. Hence, $\ddot{\theta}_R$ is considered as unchanged, indicating that the vehicle jerk will almost minimize to zero.

Substituting Eqs. (6.31) and (6.32) into Eq. (6.30), $\ddot{\theta}_R$ can be expressed as

$$\ddot{\theta}_R = (d_1 g_1 + d_2 m_1) T_M + (d_1 g_2 + d_2 m_2) T_{LS} + (d_1 g_4 + d_2 m_4) T_f \tag{6.34}$$

Assume $\dot{\theta}_R = \text{constant}$, then the coordination control laws between the motor and LSB can be described as following

$$0 = n_4 \dot{T}_M + n_5 \dot{T}_{LS} \tag{6.35}$$

where $n_4 = d_1 g_1 + d_2 m_1$, $n_5 = d_1 g_2 + d_2 m_2$

In this phase, the control objective is to make $\dot{\theta}_{LS} = 0$. During the change process of $\dot{\theta}_{LS}$, the optimal control objective only makes the friction loss minimize due to the minimum vehicle jerk guaranteed by Eq. (6.35).

The state variables can be chosen as

$$\boldsymbol{x}_I = [x_{I1}\ x_{I2}\ x_{I3}\ x_{I4}\ x_{I5}]^{\mathrm{T}} = \left[\dot{\theta}_{SS}\ \dot{\theta}_{LS}\ T_M\ T_{LS}\ T_f\right]^{\mathrm{T}} \tag{6.36}$$

And, the control variables as

$$\boldsymbol{u}_I = u_{I11} = \dot{T}_{LS} \tag{6.37}$$

With Eqs. (6.13), (6.14), (6.18) and (6.19), the dynamic powertrain model can be written as followings

$$\dot{x}_{I1} = g_1 x_{I3} + g_2 x_{I4} + g_4 x_{I5} \tag{6.38}$$

$$\dot{x}_{I2} = m_1 x_{I3} + m_2 x_{I4} + m_4 x_{I5} \tag{6.39}$$

$$\dot{x}_{I3} = -\frac{n_5}{n_4} u_{I11} \tag{6.40}$$

$$\dot{x}_{I4} = u_{I11} \tag{6.41}$$

$$\dot{x}_{I5} = 0 \tag{6.42}$$

The more compact form of the linear time-invariant state equations can be expressed as

$$\dot{\boldsymbol{x}}_I = \boldsymbol{A}_I \boldsymbol{x}_I + \boldsymbol{B}_I \boldsymbol{u}_I \tag{6.43}$$

where $\boldsymbol{A}_I = \begin{bmatrix} 0 & 0 & g_1 & g_2 & g_4 \\ 0 & 0 & m_1 & m_2 & m_4 \\ 0 & 0 & 0 & 0 & 0 \\ 0 & 0 & 0 & 0 & 0 \\ 0 & 0 & 0 & 0 & 0 \end{bmatrix}$, $\boldsymbol{B}_T = \begin{bmatrix} 0 & 0 & -\frac{n_5}{n_4} & 1 & 0 \end{bmatrix}^{\mathrm{T}}$

The control aim during this phase is to obtain little friction work. The friction work can be modeled as

$$W_I = \int_{t_T}^{t_I} T_{LS} \dot{\theta}_{LS} dt \tag{6.44}$$

where t_I is the end time of the inertia phase.

The cost function of LQR design is

$$J_I = \frac{1}{2} \boldsymbol{x}_I^{\mathrm{T}}(t_I) \boldsymbol{F}_I \boldsymbol{x}_I(t_I) = \frac{1}{2} \int_{t_T}^{t_I} (\boldsymbol{x}_I^{\mathrm{T}} \boldsymbol{Q}_I \boldsymbol{x}_I + \boldsymbol{u}_I^{\mathrm{T}} \boldsymbol{R}_I \boldsymbol{u}_I) dt \tag{6.45}$$

where $\boldsymbol{F}_I \in \boldsymbol{R}^{5\times5}$ and $\boldsymbol{Q}_I \in \boldsymbol{R}^{5\times5}$ stand for symmetric positive and semi-definite weighting matrices and $\boldsymbol{R}_I \in \boldsymbol{R}$ is a symmetric positive definite weighting matrix.

The state constraint conditions are

$T_M(t_T) = T_{M0}, -T_{M\_Max} \le T_M \le T_{M\_Max}$

$T_{LS}(t_T) = T_{LS0}, 0 \le T_{LS} \le T_{LS\_Max}$

$\dot{\theta}_{LS}(t_T) = \dot{\theta}_{LS0}, \dot{\theta}_{LS}(t_I) = 0$

where T_{M0} and T_{LS0} are the initial torque of the motor and LS brake in the inertia phase and T_{LS_Max} is the max motor torque.

The control law in the inertia phase can be obtained by

$$\boldsymbol{u}_I = \boldsymbol{K}_I(t)\boldsymbol{x}_I = -\boldsymbol{R}_I^{-1}\boldsymbol{B}_I^{\mathrm{T}}\boldsymbol{P}_I(t)\boldsymbol{x}_I \tag{6.46}$$

where $\boldsymbol{K}_I(t) \in \boldsymbol{R}^{1\times 5}$ represents the controller gain and non-negative definite matrix $\boldsymbol{P}_I(t) \in \boldsymbol{R}^{1\times 5}$ is a time-varying matrix and determined by Ricati equation, expressed as following

$$\dot{\boldsymbol{P}}_I(t) = -\boldsymbol{P}_I(t)\boldsymbol{A}_I + \boldsymbol{P}_I(t)\boldsymbol{B}_I\boldsymbol{R}_I^{-1}\boldsymbol{B}_I^{\mathrm{T}}\boldsymbol{P}_I(t) - \boldsymbol{Q}_I - \boldsymbol{A}_I^{\mathrm{T}}\boldsymbol{P}_I(t) \tag{6.47}$$

When $\boldsymbol{P}_I(t_I) = \boldsymbol{F}_I$, the inertia phase finishes. The weighting matrices $\boldsymbol{F}_I$, $\boldsymbol{Q}_I$ and $\boldsymbol{R}_I$ are chosen to ensure small facing wear and good dynamics performance. In this chapter, the symmetric matrices $\boldsymbol{F}_I$, $\boldsymbol{Q}_I$ and $\boldsymbol{R}_I$ are given as the following form

$$\boldsymbol{F}_I = \begin{bmatrix} 0 & 0 & 0 & 0 & 0 \\ 0 & f_{I22} & 0 & 0 & 0 \\ 0 & 0 & 0 & 0 & 0 \\ 0 & 0 & 0 & 0 & 0 \\ 0 & 0 & 0 & 0 & 0 \end{bmatrix}, \boldsymbol{Q}_I = \begin{bmatrix} 0 & 0 & 0 & 0 & 0 \\ 0 & q_{I22} & 0 & q_{I24} & 0 \\ 0 & 0 & 0 & 0 & 0 \\ 0 & q_{I42} & 0 & q_{T44} & 0 \\ 0 & 0 & 0 & 0 & 0 \end{bmatrix}, \boldsymbol{R}_I = r_{I11}$$

The optimal strategy based simulation results in both the torque phase and the inertia phase is entirely presented in Figure 6-5. The inertia phase takes about 0.45s to achieve the terminal gear shifting from 5.033s to 5.486s. According to the optimal strategy for this phase, the motor torque firstly decreases to a low value and then recovers to the initial value of the inertia phase. Contrary to the motor torque, LS torque firstly increases and then decreases to a low value. According to the coordinating control of the electric motor and LSB, R torque almost keeps unchanged, which results in the fairly small vehicle jerk shown in Figure 6-5(d). The reason why there still exits the small jerk is that the design process of this control strategy neglects some dynamic factors of the powertrain, such as the stiffness and the damping.

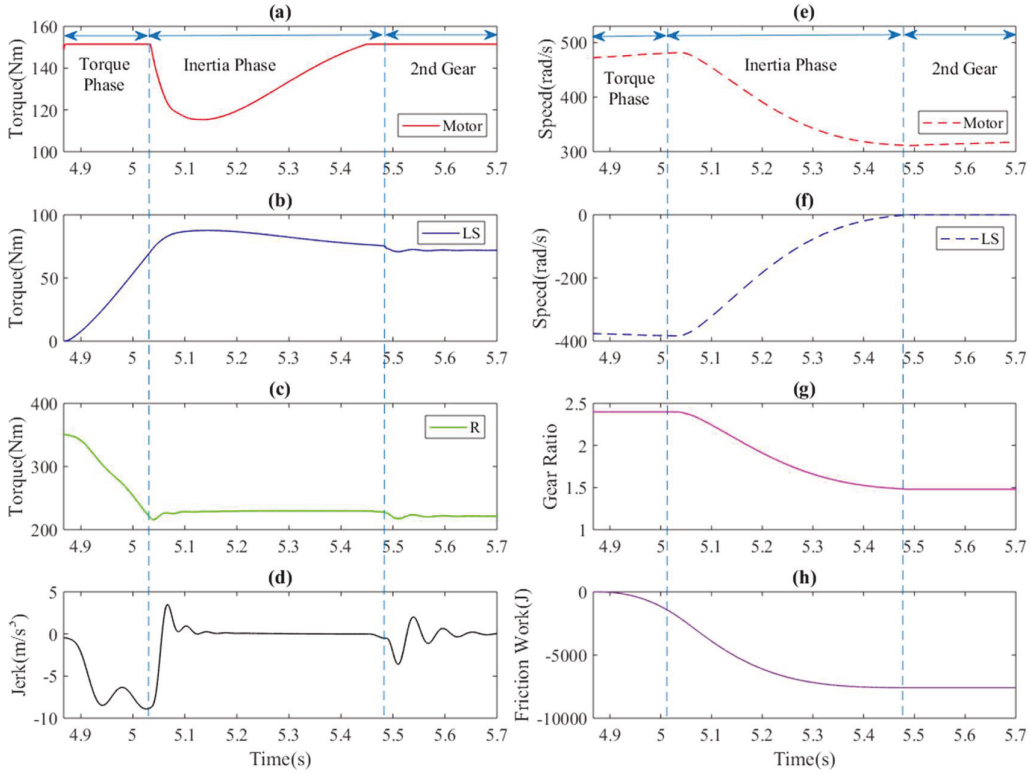

Figure 6-5: Simulation results of the optimal control strategy

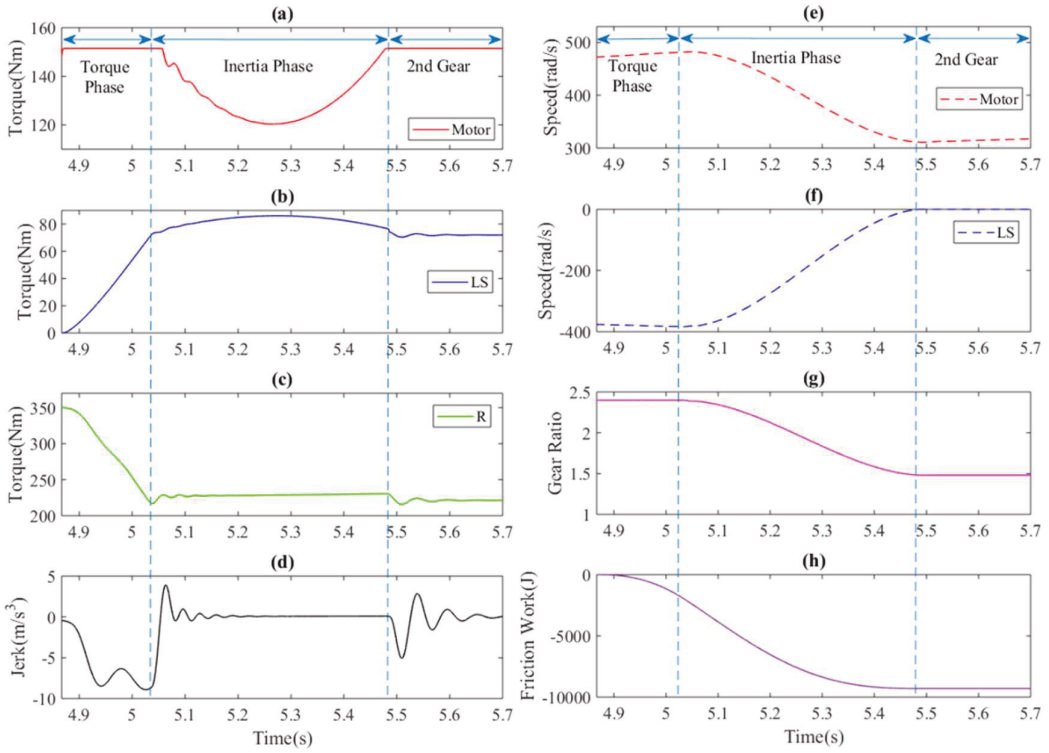

Figure 6-6: Simulation results of the control strategy in Ref. [37]

To verify the preponderance of the optimal strategy, the control strategy of the inertia phase proposed in Ref. [37] is taken as a comparison case, and its corresponding simulation results are displayed in Figure 6-6 where the control tactic in the torque phase is the same as that in Figure 6-5. It can clearly be found that the torque change trends of the motor and LS are similar to those of the optimal strategy due to adopting the same coordinating control strategy. Figure 6-7 shows the simulation results based on the control strategy in Ref. [132], where the control tactic of the torque phase is also the same as that in Figure 6-5. Compared to the control strategy in Ref. [37], the most prominent characteristic of this control strategy is lack of the coordinating control between the motor

torque and LS torque, i.e. the motor torque maintains completely unchanged during the whole gearshift process.

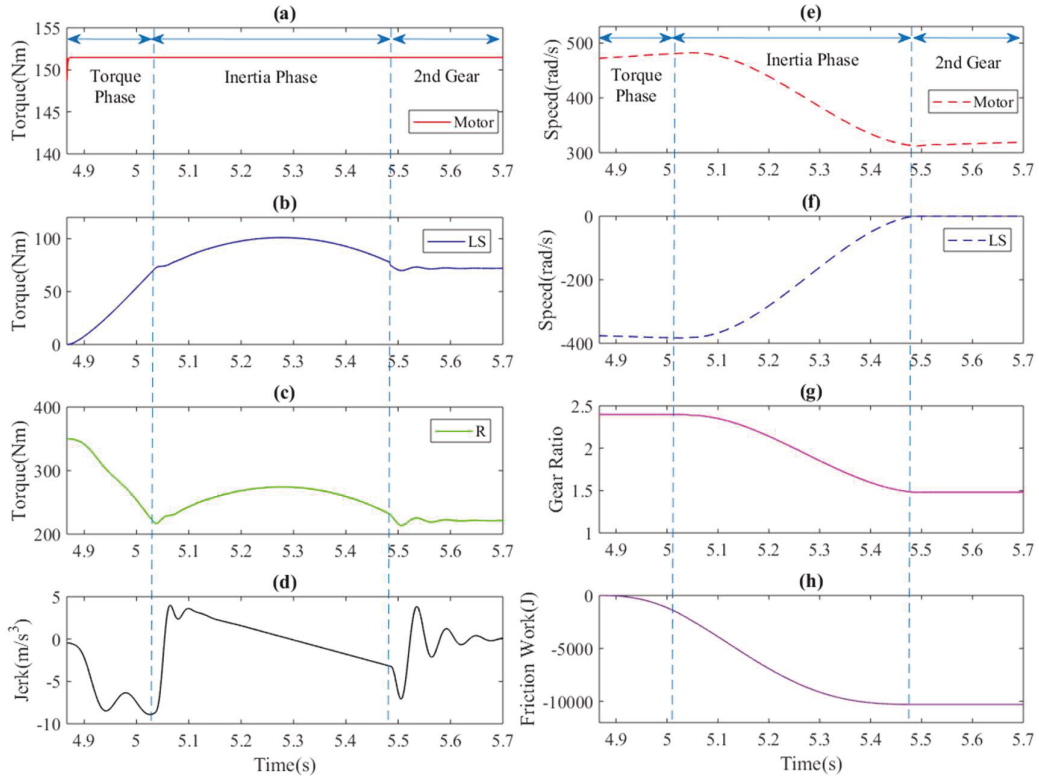

Figure 6-7: Simulation results of the control strategy in Ref. [132]

To compare these strategies in Refs. [37] and [132] with the optimal strategy, the friction work of the inertia phase in Figure 6-5, Figure 6-6, and Figure 6-7 are summarized in Table 6-2: Comparison of simulation results. Herein, “1” stands for the friction work of the inertia phase of Figure 6-5, and “2” and “3” present these simulation results from Figure 6-6 and Figure 6-7. Due to the motor torque maintaining constant in “3”, LS torque in “3” is higher than LS torque in “2”. As shown in Figure 6-6(f) and Figure 6-7(f), change rates of LS speed are the same since their speed reference trajectories are designed by the identical empirical curve. Therefore, according to the change rates of LS torque and speed

in Figure 6-6 and Figure 6-7, the friction work in “3” (8381J) is 16.66% more than that in “2” (7184J). This demonstrates that the coordinating control strategy in Ref. [37] is superior to the strategy without coordinating control between the motor and LS brake in Ref. [132]. In addition, the friction work in “2” is 27.04% more than that in “1” (5655J). This proves that the optimal coordinating control strategy presents the best control performance in comparison with those of Refs. [37] and [132].

Table 6-2: Comparison of simulation results

Control Strategy	**|Friction work| (J)**
1	5655
2	7184
3	8381

6.3 TORQUE OBSERVER DESIGN

6.3.1 Problem Statement

The gearshift controllers developed in Section 6.2 requires some torque information to achieve the feedback control, i.e., the reaction torque on the carrier T_C, the torque exerted on the large sun gear T_{LS} and the motor torque T_M. Generally, production transmission systems are not equipped with torque sensors due to their high cost, inconvenient arrangement, and low durability. T_C needs only be estimated for the first gear and the

torque phase due to the carrier fully disengaged during the inertia phase and the second gear. T_{LS} needs to be estimated by diverse observers for the torque and inertia phases and the second gear since the governing equations are different from each other during the three stages. The sliding mode observer was originally designed by Utkin [133]. This observer guarantees the stability of the estimation error and robustness in the presence of modelling uncertainty for a class of uncertain systems. In the following sections, the sliding mode observers are used to estimate the necessary torque information for the optimal controller.

6.3.2 The first gear

In the first gear, there is only one degree of freedom, $\dot{\theta}_c = 0$, $\ddot{\theta}_c = 0$ and $T_{LS} = 0$. According to Eq. (6.13)-(6.15), the powertrain dynamic model can be rewritten as follows

$$\ddot{\theta}_{ss} = \beta_1 T_M - \beta_2 T_C \tag{6.48}$$

where $\beta_1 = \frac{g_1 m_4 - g_4 m_1}{m_4 + g_4 \frac{a_1}{a_2}}, \beta_2 = \frac{g_4 m_3 - g_3 m_4}{m_4 + g_4 \frac{a_1}{a_2}}$

Herein, it is found in Eq. (6.46) that the vehicle resistance torque T_{ef} is eliminated.

Because the optimal controller described in Section 3 requires the initial value of T_c for gearshift control during torque phase, sliding mode observer should be developed to estimate the torque on the carrier (T_c) in the first gear.

The state equations can be expressed by Eqs. (6.49) and (6.50).

$$\ddot{\theta}_{ss} = \beta_1 T_M - \beta_2 T_C \tag{6.49}$$

$$\dot{T}_C = F_1 \tag{6.50}$$

The torque observer can be designed as

$$\hat{\dot{\theta}}_{ss} = \beta_1 T_M - \beta_2 \hat{T}_C - \beta_2 F_{1smo} \tag{6.51}$$

$$\hat{\dot{T}}_C = \delta_1 F_{1smo} \tag{6.52}$$

The error function is

$$\frac{de_{ss1}}{dt} = -\beta_2 e_{T1} - \beta_2 F_{1smo} \tag{6.53}$$

$$\frac{de_{T1}}{dt} = \delta_1 F_{1smo} - F_1 \tag{6.54}$$

where $e_{ss1} = \hat{\dot{\theta}}_{ss} - \dot{\theta}_{ss}$, $e_{T1} = \hat{T}_C - T_C$

The sliding surface is chosen as $s_1 = \hat{\dot{\theta}}_{ss} - \dot{\theta}_{ss}$ and exponential reaching law [134] is used in this study and described by Eq. (6.55).

$$\frac{ds_1}{dt} = -\kappa_1 sign(s_1) - \lambda_1 s_1 \tag{6.55}$$

where $\kappa_1 > 0$ and $\lambda_1 > 0$ are reaching law parameters.

According to Eqs. (6.51) and (6.53), Eq. (6.56) can be obtained

$$-\beta_2 e_{T1} - \beta_2 F_{1smo} = -\kappa_1 sign(s_1) - \lambda_1 s_1 \tag{6.56}$$

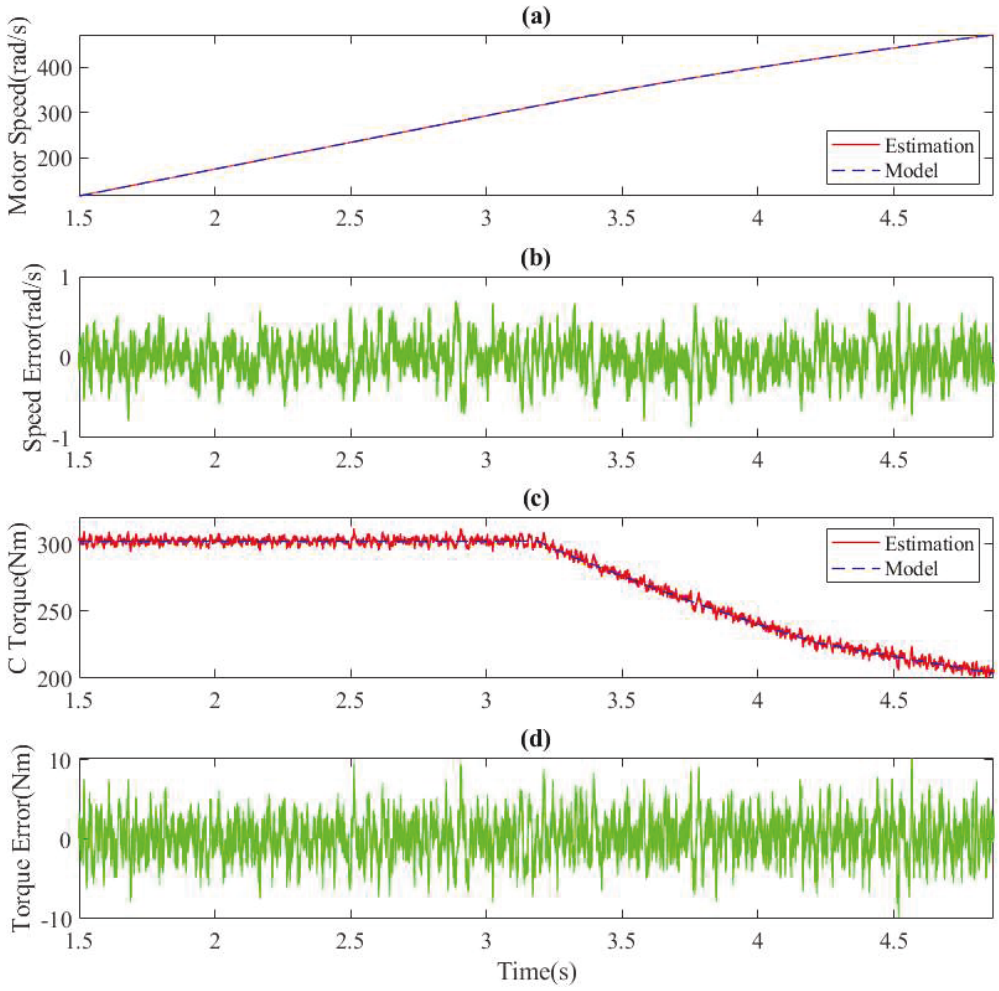

Figure 6-8: Results in the first gear with white noise added to motor torque signal

Thus, the sliding control function F_{1smo} can be designed by Eq. (6.56) with e_{T1} considered as a disturbance of the control function.

$$F_{1smo} = \frac{\kappa_1}{\beta_2} sign(s_1) + \frac{\lambda_1}{\beta_2} s_1 \tag{6.57}$$

To ensure system stability, Eq. (6.58) must be satisfied [134].

$$s_1\dot{s}_1 \leq 0 \tag{6.58}$$

According to Eqs. (6.51)-(6.58), Eq. (6.59) can be expressed as follows

$$\begin{aligned} s_1\dot{s}_1 &= -\beta_2 e_{ss1} e_{T1} - \kappa_1 e_{ss1}\text{sign}(e_{ss1}) - \lambda_1 s_1 e_{SS1}^2 \\ &= \begin{cases} -|e_{ss1}|(\kappa_1 + \beta_2 e_{T1}) - \lambda_1 s_1 e_{SS1}^2, & e_{ss1} > 0 \\ -|e_{ss1}|(\kappa_1 - \beta_2 e_{T1}) - \lambda_1 s_1 e_{SS1}^2, & e_{ss1} < 0 \end{cases} \end{aligned} \tag{6.59}$$

To guarantee $s_1\dot{s}_1 \leq 0$ always holds, κ_1 should satisfy the following inequality

$$\kappa_1 > \beta_2|e_{T1}| \tag{6.60}$$

The simulation results with different types of motor torque error in the first gear are shown in Figure 6-8 and Figure 6-9. Figure 6-8(a) shows the estimated motor speed and the actual motor speed, and Figure 6-8(b) presents the speed error between the estimation and its actual value. According to these two figures, it is found that the motor speed is estimated with good accuracy and the maximum ripple is less than 0.7 rad/s. Consequently, observed C torque well follows that of the model, as shown in Figure 6-8(c) and Figure 6-8(d). Figure 6-9 shows the observed results when 1% bias error is added to the motor torque signal during the first gear. According to these results from Figure 6-9, it can also be found that the designed observer can effectively estimate C torque with a small estimation error. Results from Figure 6-8 and Figure 6-9 prove that the sliding mode observer used in the first gear effectively functions to capture C torque information for the following gearshift control.

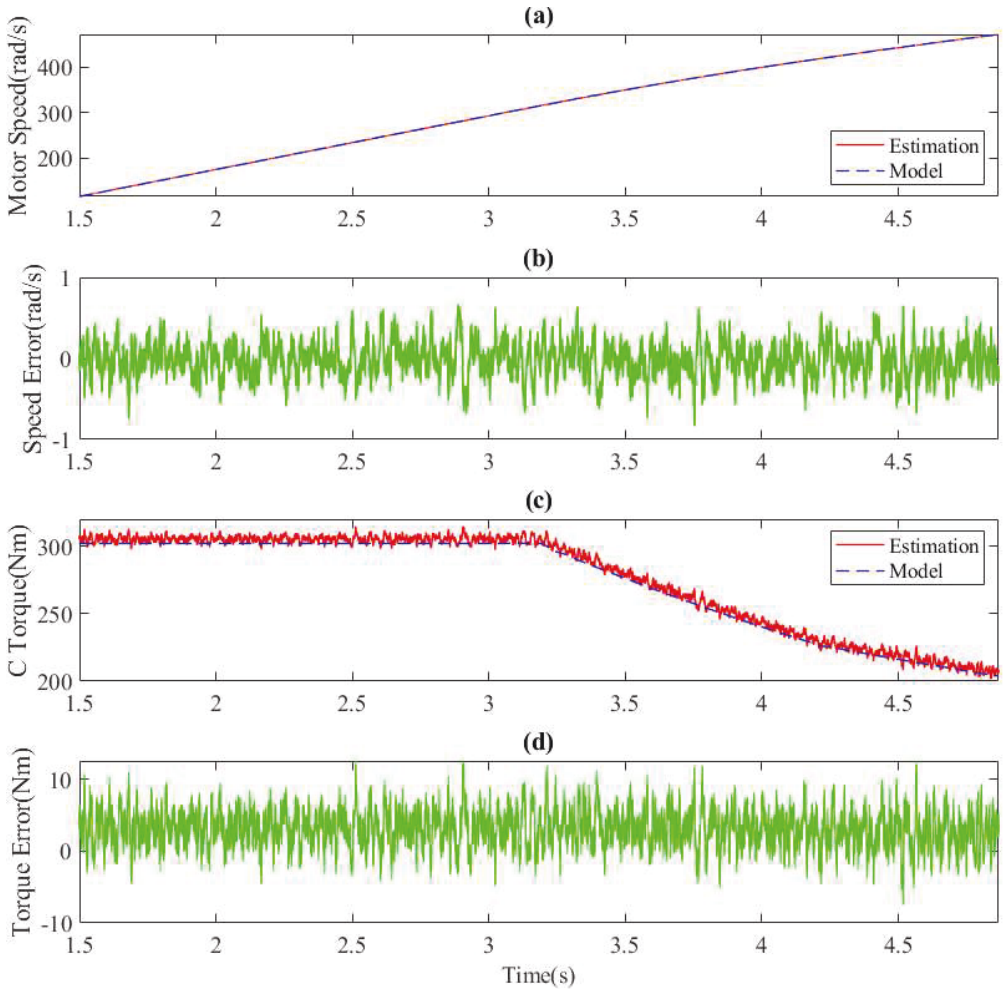

Figure 6-9: Results in the first gear with 1% bias error added to motor torque signal

6.3.3 The torque phase

According to Eqs. (6.12), (6.13) and (6.55), Eq. (6.61) can be obtained

$$\ddot{\theta}_{ss} = \beta_1 T_M - \beta_2 T_C - \beta_3 T_{LS} \tag{6.61}$$

where $\beta_3 = \frac{g_2 m_4 - g_4 m_2}{m_4 + g_4 \frac{a_1}{a_2}}$, $T_M = T_{M0}$.

And,

$$T_C = T_{C0} + \int_{t_0}^{t_T} \dot{T}_C \, dt \tag{6.62}$$

$$T_{LS} = \int_{t_0}^{t_T} \dot{T}_{LS} \, dt \tag{6.63}$$

Substituting Eq. (6.61) into Eq. (6.62), the relationship between T_C and T_{LS} can be expressed as

$$T_C = T_{C0} - \frac{n_1}{n_2} T_{LS} \tag{6.64}$$

Substituting Eq. (6.64) into Eq. (6.61), the re-arranged dynamic equation can be obtained as follows

$$\ddot{\theta}_{ss} = T_{E\_in} - \beta_4 T_{LS} \tag{6.65}$$

where $T_{E\_in} = \beta_1 T_{M0} - \beta_2 T_{C0}, \beta_4 = \left(\beta_3 - \beta_2 \frac{n_1}{n_2}\right)$

The state equations for observer design can be expressed as

$$\ddot{\theta}_{ss} = T_{E\_in} - \beta_4 T_{LS} \tag{6.66}$$

$$\dot{T}_{LS} = F_t \tag{6.67}$$

The torque observer can be designed as

$$\hat{\ddot{\theta}}_{ss} = T_{E\_in} - \beta_4 \hat{T}_{LS} - \beta_4 F_{tsmo} \tag{6.68}$$

$$\hat{\hat{T}}_{LS} = \delta_t F_{tsmo} \tag{6.69}$$

Herein, the sliding control function F_{tsmo} in the torque phase can be designed by (6.70).

$$F_{tsmo} = \frac{\kappa_t}{\beta_4}\text{sign}(s_t) + \frac{\lambda_t}{\beta_4}s_t \tag{6.70}$$

where $\kappa_t > 0$ and $\lambda_t > 0$ are the reaching law parameters of torque phase, and $s_t = \hat{\hat{\theta}}_{ss} - \dot{\theta}_{ss}$.

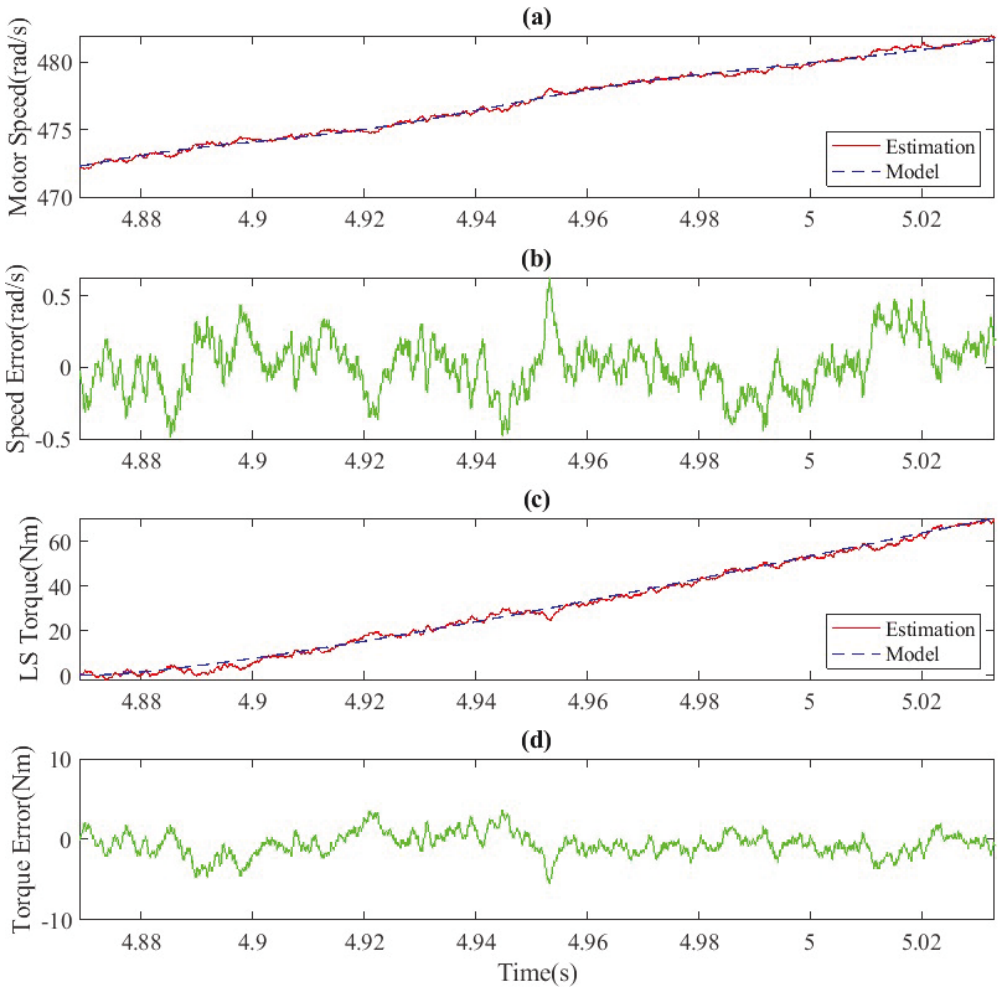

Figure 6-10: Results in the torque phase with white noise added to motor torque signal

Figure 6-10 and Figure 6-11 show observed results with different torque errors added to the motor torque signal in the torque phase. According to the results shown in Figure 6-10 and Figure 6-11, the estimated motor speeds follow the actual speeds well and the maximum estimation error is about 0.5rad/s. And, it is distinctly seen that the LS torque estimation errors are small enough, which proves that this observer algorithm is efficient for the torque estimation during the torque phase despite different disturbance torque errors.

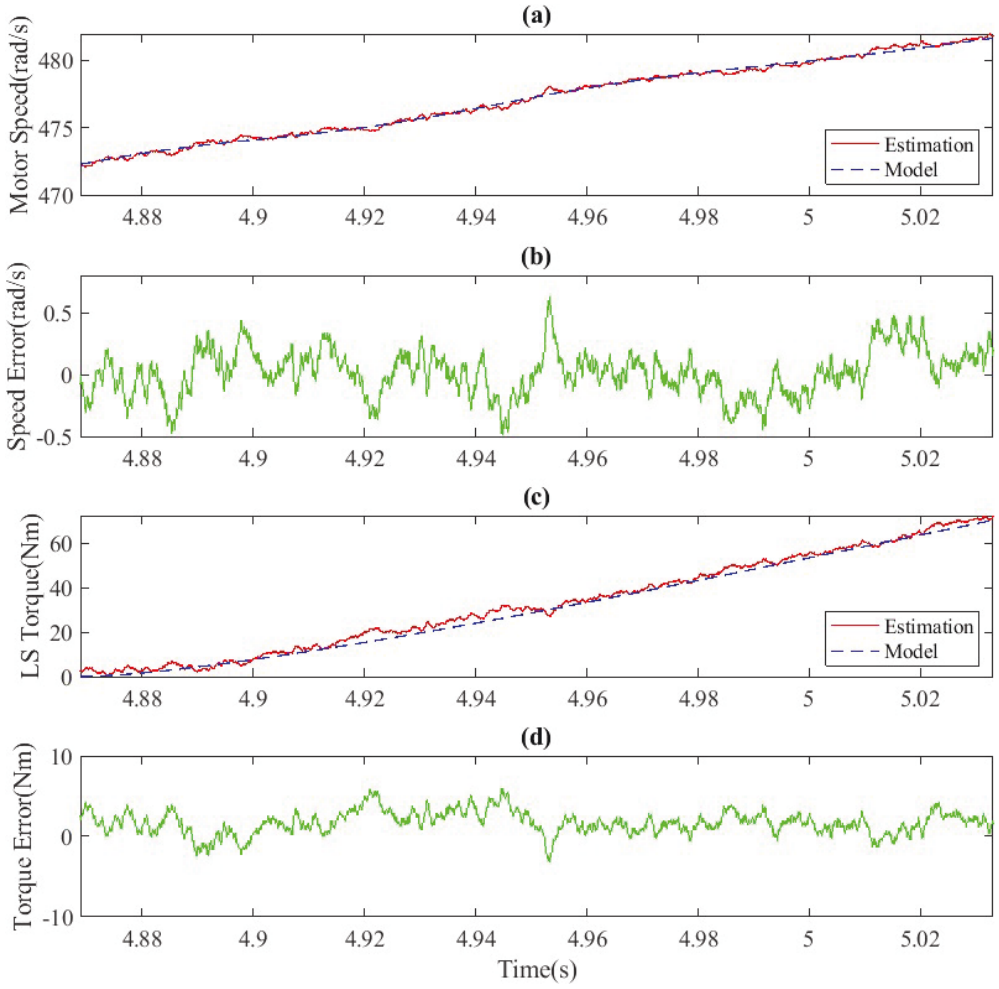

Figure 6-11: Results in the torque phase with 1% bias error added to motor torque signal

6.3.4 The inertia phase and the second gear

According to Eqs. (6.12)-(6.14), $\ddot{\theta}_{ss}$ can be obtained

$$\ddot{\theta}_{ss} = \gamma_1 T_M - \gamma_2 T_{LS} \tag{6.71}$$

where $\gamma_1 = \frac{g_1 m_4 - g_4 m_1}{m_4 + g_4 \frac{d_1}{d_2} - \frac{g_4}{d_2 i_i}}$, $\gamma_2 = -\frac{g_2 m_4 - g_4 m_2}{m_4 + g_4 \frac{d_1}{d_2} - \frac{g_4}{d_2 i_i}}$, $i_i = \frac{\dot{\theta}_{ss}}{\dot{\theta}_R}$

The state equations can be expressed as follows

$$\ddot{\theta}_{ss} = \gamma_1 T_M - \gamma_2 T_{LS} \tag{6.72}$$

$$\dot{T}_{LS} = F_i \tag{6.73}$$

The torque observer can be designed as

$$\hat{\ddot{\theta}}_{ss} = \gamma_1 T_M - \gamma_2 \hat{T}_{LS} - \gamma_2 F_{ismo} \tag{6.74}$$

$$\hat{\dot{T}}_{LS} = \delta_i F_{ismo} \tag{6.75}$$

The sliding control function F_{ismo} in the inertia phase can be designed as

$$F_{ismo} = \frac{\kappa_i}{\gamma_i} sign(s_i) + \frac{\lambda_i}{\gamma_2} s_i \tag{6.76}$$

where $\kappa_i > 0$ and $\lambda_i > 0$ are the reaching law parameters of torque phase, $s_i = \hat{\dot{\theta}}_{ss} - \dot{\theta}_{ss}$.

In the second gear, both the powertrain system model and the torque observer design process is the same as that in the inertia phase. Hence, the observer design procedure is unnecessary to be detailed.

The observed results of the inertia phase and the second gear are shown inFigure 6-12 and Figure 6-13. As shown in these figures, the sliding mode algorithm-based torque observer is capable of estimating LS torque accurately and providing the dependable torque information for feedback control of this two status.

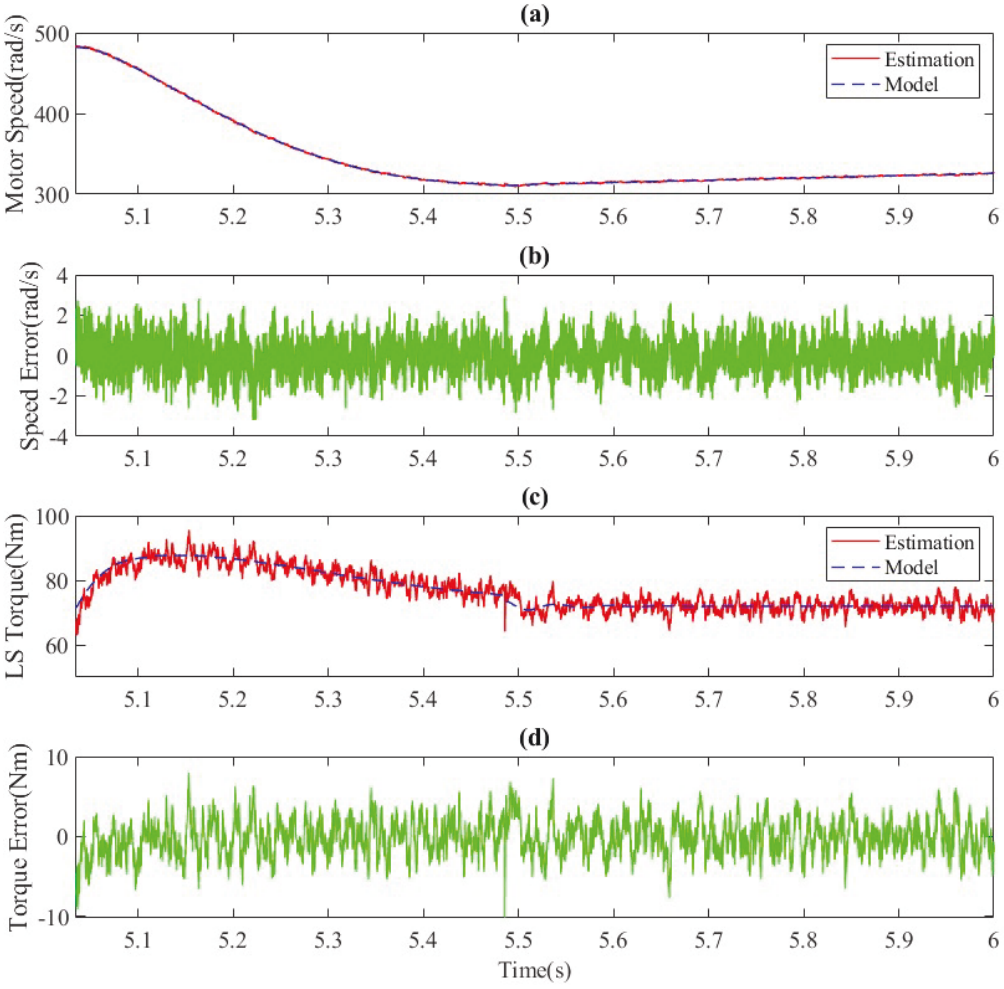

Figure 6-12: Results in the inertia phase and the second gear with white noise

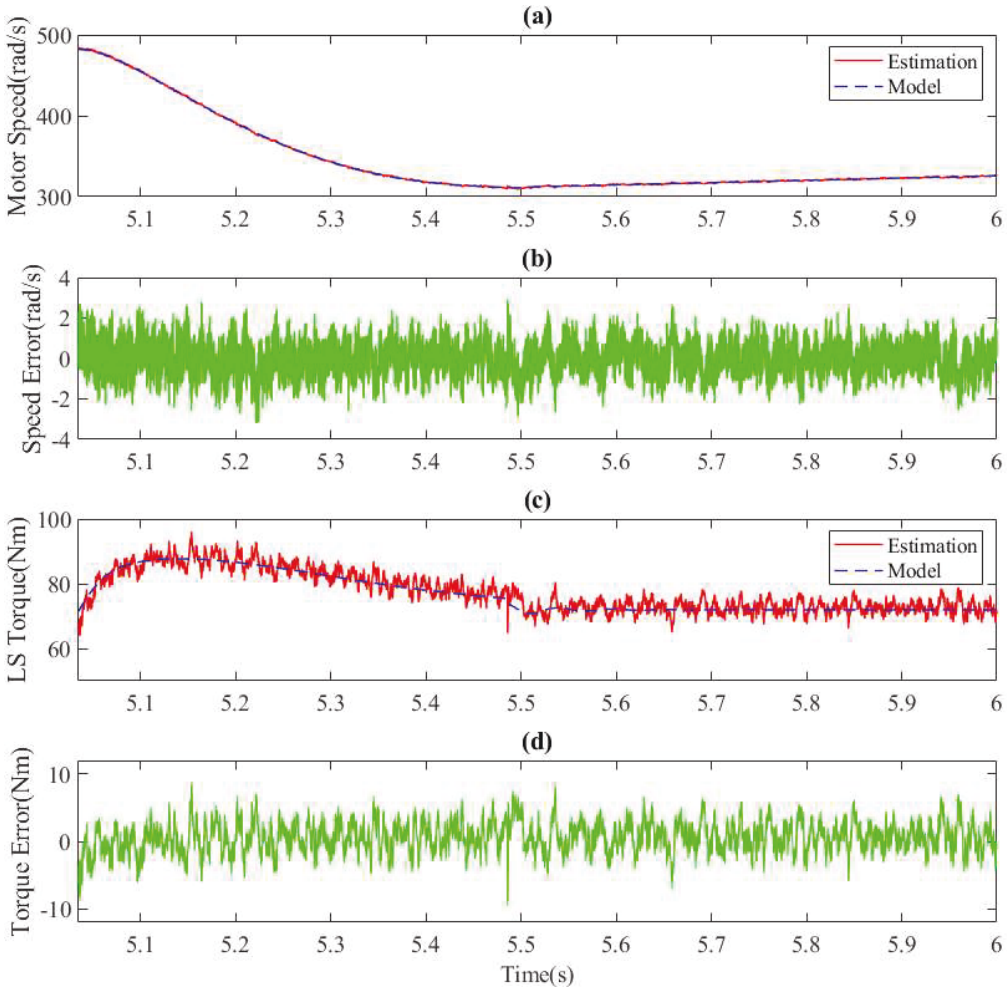

Figure 6-13: Results in the inertia phase and the second gear with constant bias constant

6.4 CHAPTER CONCLUSIONS

This chapter is focused on the gearshift control logic of the proposed two-speed UPAT for BEVs. To comprehensively improve the gearshift quality, optimal gearshift control tactics for the torque phase and the inertia phase are proposed to reduce the vehicle jerk and friction work within the fixed gearshift duration. Model-based optimal gearshift control tactics are developed, and the simulation results demonstrate that the proposed

multi-objective optimal tactic for the torque phase effectively reduces the vehicle jerk and friction work, and the optimal coordinating tactic for the inertia phase decreases the friction work to a high degree. Meanwhile, to provide unmeasurable torque information for executing the proposed optimal strategies, sliding mode theory is employed to design the torque observers which are capable of estimating the torque information sufficiently and accurately.

CHAPTER 7 : MODEL AND GEAR SHIFTING CONTROL OF A NOVEL TWO-SPEED PLANETARY AUTOMATED MANUAL TRANSMISSION FOR BEVS

7.1 INTRODUCTION

In this chapter, a novel two-speed planetary automated manual transmission (PAMT) is proposed. It features a more compact mechanical structure than clutchless automated manual transmission (CLAMT) and easier gear shifting control than power-on transmissions. As illustrated in Figure 7-1, the electrified drivetrain is comprised of an electric machine (EM), a two-speed PAMT, final drive, differential, half shafts, and wheels. To be more specific, the two-speed PAMT consists of a single planetary gear train consisting of a sun gear (S), three planet gears (P), a carrier (C), and a ring gear (R). The input of PAMT is S mechanically connected to an EM via a flexible shaft. C is regarded as the output of PAMT. The gearshift actuator is a synchronizer system which is mainly comprised of gear ring 1 (GR1), spline hub (SH), sleeve (SL), gear ring 2 (GR2), etc. Specifically, GR1 is laid out on the input shaft which is also attached to S, GR2 is fixed on the transmission case and SH is connected to R. SL can be controlled to slide along SH. It is well acknowledged that a single-stage planet gear set exists two degrees of freedom at most. So, this transmission can obtain two different gear ratios. When SL is the neutral position, namely never engaging SH with GR1 nor engaging SH with GR2,

PAMT will work at the neutral gear. When SL is controlled to engaging GR2 with SH, PAMT will be operated at the first gear. The second gear will be obtained through engaging GR1 and SH with SL. Compared to the existing literature, the first contribution of this study is that this thesis proposed a novel planet CLAMT, called PAMT, which features a more compact mechanical layout than CLAMT and easier gear shifting control than power-on transmissions. Secondly, a detailed and original dynamic model of this powertrain is established, and the corresponding gearshift control system is developed. At last, three alternative planning torque trajectories are proposed for the torque reduction and reinstatement of EM.

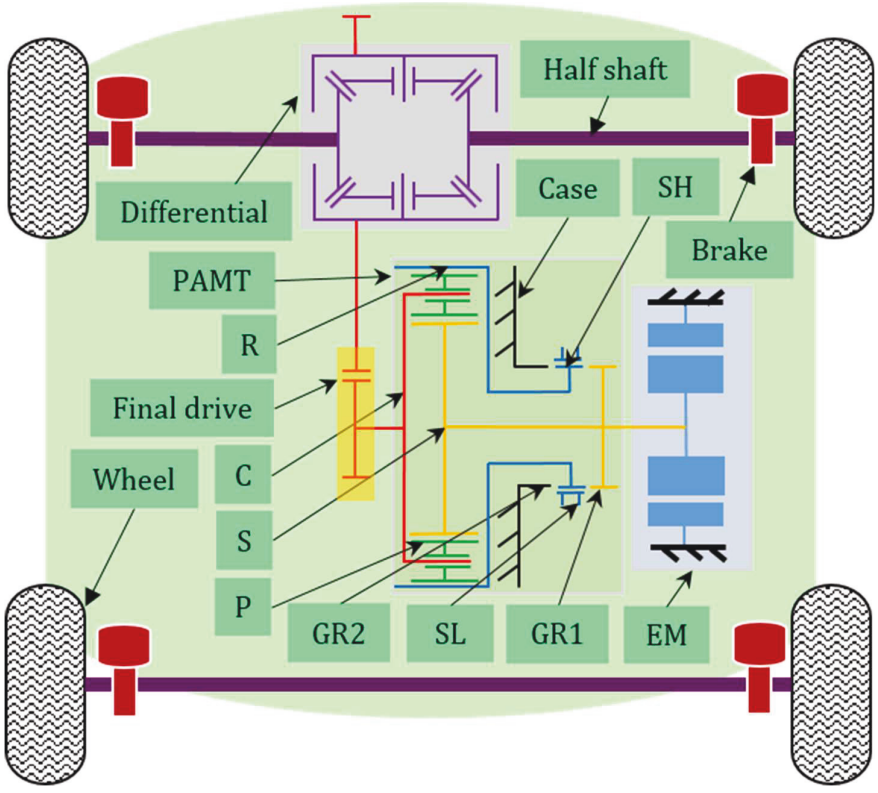

Figure 7-1: Diagram of an electric powertrain adopting 2-speed PAMT

The rest of this study includes the following sections: Section 2 shows the modeling process of the electric-drive system equipped with the two-speed PAMT. Section 3 presents the development process of the gear shifting control system. In Section 4, simulation results and the corresponding analysis are shown in detail. At last, conclusions are presented in Section 5.

7.2 MATHEMATICAL MODEL OF THE ELECTRIFIED POWERTRAIN

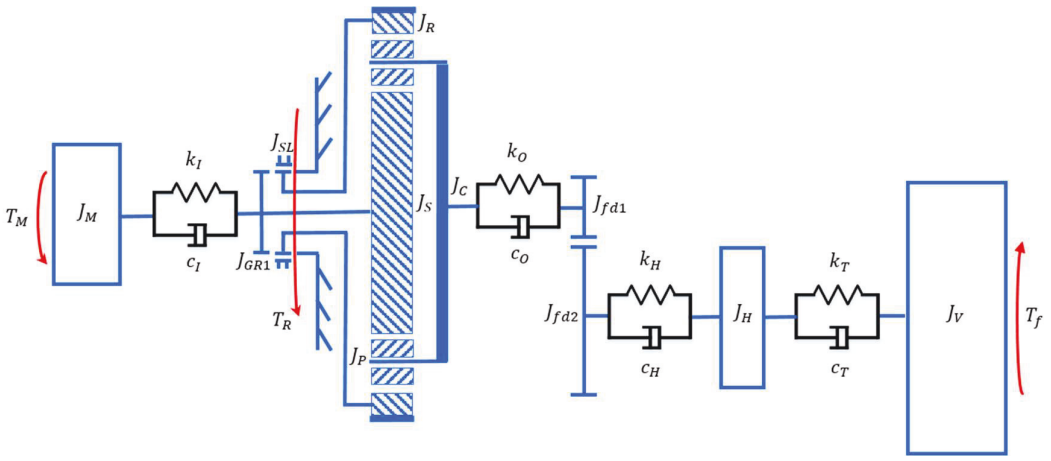

Figure 7-2: Schematic diagram of a Lumped powertrain

The powertrain equipped with the two-speed PAMT is present in Figure 7-2. This system achieves the torque transmitting capability through corresponding shaft components and gear friction contacts. In this study, the key drivetrain components are modeled as lumped inertia elements. This model is mainly comprised of an EM, a two-speed PAMT, the gearshift actuator, main reducer, wheel hub, and vehicle. Herein, some assumptions should be made in advance to simplify the modeling [34, 37, 105]:

a. The rotation elements of the proposed transmission are regarded as a rigid body.

b. There is no backlash during the gear mated process.

c. Stiffness and damping coefficients are linearized.

7.2.1 Electric machine

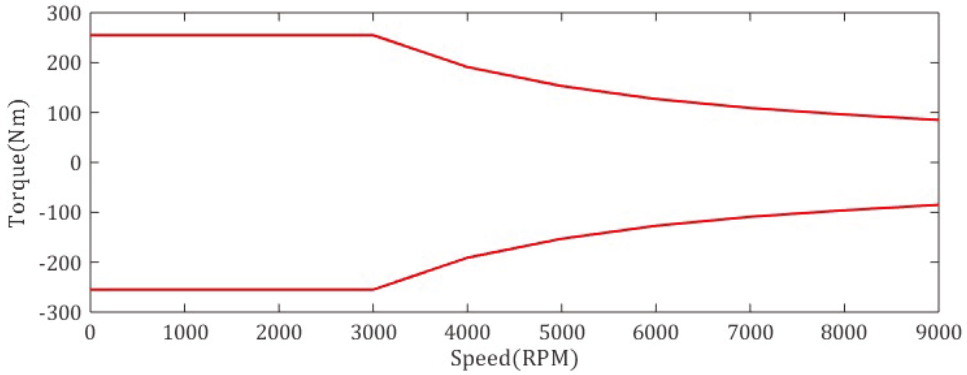

Figure 7-3: Electric machine torque characteristic

As well acknowledged, power electronics of EM feature significantly higher transient response frequency than mechanical components. Therefore, the high-frequency vibrations of power electronics can be ignored, which will simplify EM model. In this study, EM is modeled as rotation inertia J_{EM} and the electromagnetic torque is achieved through a table lookup method. The corresponding EM torque T_M can be expressed by

$$T_M = \alpha_{Pa} f(\dot{\theta}_{EM}) \tag{7.1}$$

where α_{Pa} is the driver's pedal command, $\dot{\theta}_{EM}$ is EM speed and $f(\dot{\theta}_{EM})$ stands for the maximum EM torque at the corresponding $\dot{\theta}_{EM}$, captured from experimental data, shown in Figure 7-3.

The dynamic model of the electric machine is

$$J_{EM}\ddot{\theta}_{EM} = T_{EM} - T_{IN} \tag{7.2}$$

where $\ddot{\theta}_M$ is the angular acceleration of EM and J_M is EM inertia.

The input shaft of PAMT is built as a flexible shaft. So, T_{IN} can be expressed as following

$$T_{IN} = k_I(\theta_M - \theta_S) + c_I(\dot{\theta}_M - \dot{\theta}_S) \tag{7.3}$$

where θ_{EM} is EM torsion angle, θ_S is S torsion angle and $\dot{\theta}_S$ is S rotation speed, k_I is the stiffness coefficient and c_I is the damping factor.

7.2.2 PAMT model

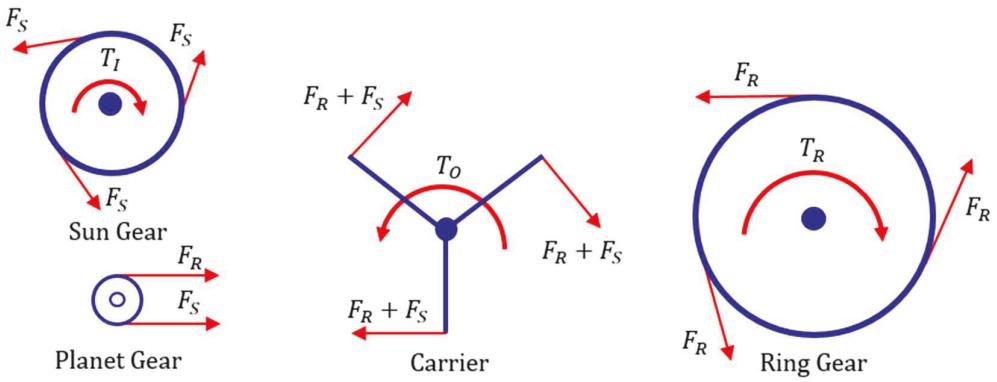

Figure 7-4: Forces and torques added to gear sets

The main mechanical components of PAMT are represented as free individual bodies, displayed in Figure 7-4. Applying the Newtonian mechanics, PAMT model can be developed as followings

$$J_{Eq\_S}\ddot{\theta}_S = T_I - 3F_S r_S \tag{7.4}$$

$$3J_P\ddot{\theta}_P = -3F_S r_P + 3F_R r_P \tag{7.5}$$

$$J_{Eq\_R}\ddot{\theta}_R = -3F_R r_R + T_R \tag{7.6}$$

$$J_C\ddot{\theta}_C = 3(F_R + F_S)r_C - T_O \tag{7.7}$$

where $J_{Eq\_S} = J_{GR1} + J_S$. $J_{Eq\_R} = J_{SL} + J_R, J_{GR1}. J_S, J_{SL}, J_R, J_P$ and J_C are inertias of GR1, S, SL, R, P, and C. F_S and F_R represent the meshing force between S and P, and P and R. r_S, r_P and r_R are the pitch radius of S, P, and R, and the angular accelerations of S, P, R, and C are represented by $\ddot{\theta}_S$, $\ddot{\theta}_P$, $\ddot{\theta}_R$ and $\ddot{\theta}_C$.

Output shaft torque T_O of PAMT is expressed as follows

$$T_O = k_O(\theta_C - \theta_{fd1}) + c_O(\dot{\theta}_C - \dot{\theta}_{fd1}) \tag{7.8}$$

where k_O is the torsion spring coefficient of the output shaft, c_O is the damping coefficient, θ_C and θ_{fd} are torsion angles of C and driving part of the final drive, and $\dot{\theta}_C$ and $\dot{\theta}_{fd1}$ are rotation speeds of C and driving part of the final drive.

Generally, kinematics of a single-stage planet gear set can be expressed as followings [135]

$$\ddot{\theta}_C r_C = \ddot{\theta}_S r_S + \ddot{\theta}_P r_P \tag{7.9}$$

$$\ddot{\theta}_R r_R = \ddot{\theta}_C r_C + \ddot{\theta}_P r_P \tag{7.10}$$

Applying the following mathematical operations, the simplified PAMT model can be obtained by removing some internal forces from Eq. (7.4) to Eq. (7.7).

$$\frac{Eq.(7.4)}{r_S} - \frac{Eq.(7.5)}{r_P} - \frac{Eq.(7.6)}{r_R}$$

$$\frac{J_{Eq\_S}\ddot{\theta}_S}{r_S} - \frac{3J_P\ddot{\theta}_P}{r_P} - \frac{J_{Eq\_R}\ddot{\theta}_R}{r_R} = \frac{T_M}{r_S} - \frac{T_R}{r_R} \tag{7.11}$$

$$\frac{Eq.(7.4)}{r_S} + \frac{Eq.(7.6)}{r_R} + \frac{Eq.(7.7)}{r_C}$$

$$\frac{J_{Eq\_S}\ddot{\theta}_S}{r_S} + \frac{J_{Eq\_R}\ddot{\theta}_R}{r_R} + \frac{J_{Eq\_C}\ddot{\theta}_C}{r_C} = \frac{T_M}{r_S} + \frac{T_R}{r_R} - \frac{T_O}{r_C} \tag{7.12}$$

According to Eq. (7.9) and Eq. (7.10), the following equations can be derived

$$\ddot{\theta}_P = \frac{\ddot{\theta}_C r_C - \ddot{\theta}_S r_S}{\ddot{\theta}_C r_C - \ddot{\theta}_S r_S} \tag{7.13}$$

$$\ddot{\theta}_R = \frac{2\ddot{\theta}_C r_C - \ddot{\theta}_S r_S}{r_R} \tag{7.14}$$

Substituting Eq. (7.13) and Eq. (7.14) into Eq. (7.11) and Eq. (7.12) respectively, the following equations can be obtained

$$a\ddot{\theta}_S - b\ddot{\theta}_C = \frac{T_M}{r_S} - \frac{T_R}{r_R} \tag{7.15}$$

$$c\ddot{\theta}_S + d\ddot{\theta}_C = \frac{T_M}{r_S} + \frac{T_R}{r_R} - \frac{T_O}{r_C} \tag{7.16}$$

where

$$a = \frac{J_{Eq_S}}{r_S} + \frac{3J_P r_S}{r_P^2} + \frac{J_{Eq_S} r_S}{r_R^2}, b = \frac{3J_P r_C}{r_P^2} + \frac{2J_{Eq_R} r_C}{r_R^2}, c = \frac{J_{Eq_S}}{r_S} - \frac{J_{Eq_R} r_S}{r_R^2},$$

$$d = \frac{2J_{Eq_R} r_C}{r_R^2} + \frac{J_{Eq\_C}}{r_C}.$$

Solving Eq. (7.15) and Eq. (7.16), PAMT model is represented as followings

$$\ddot{\theta}_S = \rho_1 T_I + \sigma_1 T_R - \tau_1 T_O \tag{7.17}$$

$$\ddot{\theta}_C = \rho_2 T_I + \sigma_2 T_R - \tau_2 T_O \tag{7.18}$$

Where

$$\rho_1 = \frac{b + d}{(ad + bc) r_S}$$

$$= \frac{\frac{3J_P r_C}{r_P^2} + \frac{4J_{Eq\_R} r_C}{r_R^2} + \frac{J_{Eq\_C}}{r_C}}{\left[\left(\frac{J_{Eq\_S}}{r_S} + \frac{3J_P r_S}{r_P^2} + \frac{J_{Eq\_R} r_S}{r_R^2}\right)\left(\frac{2J_{Eq\_R} r_C}{r_R^2} + \frac{J_{Eq\_C}}{r_C}\right) + \left(\frac{3J_P r_C}{r_P^2} + \frac{2J_{Eq\_R} r_C}{r_R^2}\right)\left(\frac{J_{Eq\_S}}{r_S} - \frac{J_{Eq\_R} r_S}{r_R^2}\right)\right] r_S}$$

$$\sigma_1 = \frac{b-d}{(ad+bc)r_R}$$

$$= \frac{\frac{3J_P r_C}{r_P^2} + \frac{J_{Eq\_C}}{r_C}}{\left[\left(\frac{J_{Eq\_S}}{r_S} + \frac{3J_P r_S}{r_P^2} + \frac{J_{Eq\_R} r_S}{r_R^2}\right)\left(\frac{2J_{Eq\_R} r_C}{r_R^2} + \frac{J_{Eq\_C}}{r_C}\right) + \left(\frac{3J_P r_C}{r_P^2} + \frac{2J_{Eq\_R} r_C}{r_R^2}\right)\left(\frac{J_{Eq\_S}}{r_S} - \frac{J_{Eq\_R} r_S}{r_R^2}\right)\right] r_R}$$

$$\tau_1 = \frac{b}{(ad+bc)r_C}$$

$$= \frac{\frac{3J_P r_C}{r_P^2} + \frac{2J_{Eq\_R} r_C}{r_R^2}}{\left[\left(\frac{J_{Eq\_S}}{r_S} + \frac{3J_P r_S}{r_P^2} + \frac{J_{Eq\_R} r_S}{r_R^2}\right)\left(\frac{2J_{Eq\_R} r_C}{r_R^2} + \frac{J_{Eq\_C}}{r_C}\right) + \left(\frac{3J_P r_C}{r_P^2} + \frac{2J_{Eq\_R} r_C}{r_R^2}\right)\left(\frac{J_{Eq\_S}}{r_S} - \frac{J_{Eq\_R} r_S}{r_R^2}\right)\right] r_C}$$

$$\rho_2 = \frac{(a-c)}{(ad+bc)r_S}$$

$$= \frac{\frac{3J_P r_S}{r_P^2} + \frac{J_{Eq\_R} r_S}{r_R^2} + \frac{J_{Eq\_R} r_S}{r_R^2}}{\left[\left(\frac{J_{Eq\_S}}{r_S} + \frac{3J_P r_S}{r_P^2} + \frac{J_{Eq\_R} r_S}{r_R^2}\right)\left(\frac{2J_{Eq\_R} r_C}{r_R^2} + \frac{J_C}{r_C}\right) + \left(\frac{3J_P r_C}{r_P^2} + \frac{2J_{Eq\_R} r_C}{r_R^2}\right)\left(\frac{J_{Eq\_S}}{r_S} - \frac{J_{Eq\_R} r_S}{r_R^2}\right)\right] r_S}$$

$$\sigma_2 = \frac{(a-c)}{(ad+bc)r_R}$$

$$= \frac{\frac{3J_P r_S}{r_P^2} + \frac{J_{Eq\_R} r_S}{r_R^2} - \frac{J_{Eq\_R} r_S}{r_R^2}}{\left[\left(\frac{J_{Eq\_S}}{r_S} + \frac{3J_P r_S}{r_P^2} + \frac{J_{Eq\_R} r_S}{r_R^2}\right)\left(\frac{2J_{Eq\_R} r_C}{r_R^2} + \frac{J_C}{r_C}\right) + \left(\frac{3J_P r_C}{r_P^2} + \frac{2J_{Eq\_R} r_C}{r_R^2}\right)\left(\frac{J_{Eq\_S}}{r_S} - \frac{J_{Eq\_R} r_S}{r_R^2}\right)\right] r_R}$$

$$\tau_2 = \frac{a}{(ad+bc)r_C}$$

$$= \frac{\frac{J_{Eq\_S}}{r_S} + \frac{3J_P r_S}{r_P^2} + \frac{J_{Eq\_R} r_S}{r_R^2}}{\left[\left(\frac{J_{Eq\_S}}{r_S} + \frac{3J_P r_S}{r_P^2} + \frac{J_{Eq\_R} r_S}{r_R^2}\right)\left(\frac{2J_{Eq\_R} r_C}{r_R^2} + \frac{J_C}{r_C}\right) + \left(\frac{3J_P r_C}{r_P^2} + \frac{2J_{Eq\_R} r_C}{r_R^2}\right)\left(\frac{J_{Eq\_S}}{r_S} - \frac{J_{Eq\_R} r_S}{r_R^2}\right)\right] r_C}$$

According to the different sleeve position, T_R can be derived from Eq. (7.17) and Eq. (7.18). Specifically, T_R can be expressed as four types at different cases:

Case 1: Neutral gear

In this situation, SL is on the neutral position, which means that the synchronizer is open. According to Eq. (7.17) and Eq. (7.18), this transmission system features two degrees of freedom. So, no torque is transmitted by SL. Hence,

$$T_R = 0 \tag{7.19}$$

Case 2: First gear

In this case, the synchronizer mechanism makes ring gear engaged with the transmission case, $\dot{\theta}_R = 0$ and $\ddot{\theta}_S = i_1 \ddot{\theta}_C$. This transmission system will lose one degree of freedom. Solving Eq. (7.17) and Eq. (7.18), T_R can be expressed as following

$$T_R = \frac{(i_1\rho_2 - \rho_1)}{(\sigma_1 - i_1\sigma_2)} T_I + \frac{(\tau_1 - i_1\tau_2)}{(\sigma_1 - i_1\sigma_2)} T_O \tag{7.20}$$

where $i_1 = 2.7$.

According to Eq. (7.20), it can be found that T_R is the reaction torque determined by the input torque and output torque of two-speed PAMT.

Case 3: Second gear

In this situation, R and S are engaged with the synchronizer mechanism. This gearbox is also a single degree of freedom status, i.e., $\ddot{\theta}_S = i_2 \ddot{\theta}_C$. Hence,

$$T_R = \frac{(\rho_2 - \rho_1)}{(\sigma_1 - \sigma_2)} T_I + \frac{(\tau_1 - \tau_2)}{(\sigma_1 - \sigma_2)} T_O \tag{7.21}$$

where $i_2 = 1$.

Case 4: During the gear shifting

As shown in Figure 7-5, typical synchronizer mechanisms are designed to balance loads in the engaging synchronizer process [136]. The engagement of the synchronizer moves through several different stages as the cone clutch is engaged and the sleeve moves forward with the engagement, locking the gear and shaft in preparation for shifting. Many different process descriptions are available with deviations by authors reflecting different research focuses [137, 138]. However, this study mainly focuses on that vehicle jerk and shift duration from the first stage, and the fifth stage is how to be influenced by the alternative change trajectories of motor torque. So, in this chapter, the synchronizer mechanism model is developed by using the Double-Sided Synchronizer block of Simscape/Driveline which is a high-fidelity driveline simulation tool appropriate for modeling and simulating vehicle transmission systems [123]. In the sliding friction process, the synchronizer model is regarded as friction load torque which eliminates the relative rotational motion between the driving part and the driven of the cone clutches [105]. The friction torque is often obtained as following

$$T_R = \frac{\mu_D R_C F_{SL}}{\sin \alpha_C} \tag{7.22}$$

where T_R is the friction torque of the cone clutch, μ_D represents the dynamic friction factor, R_C is the mean value of the cone clutch radius, F_{SL} is the force exerted by the gearshift actuator, and α_C is the cone angle.

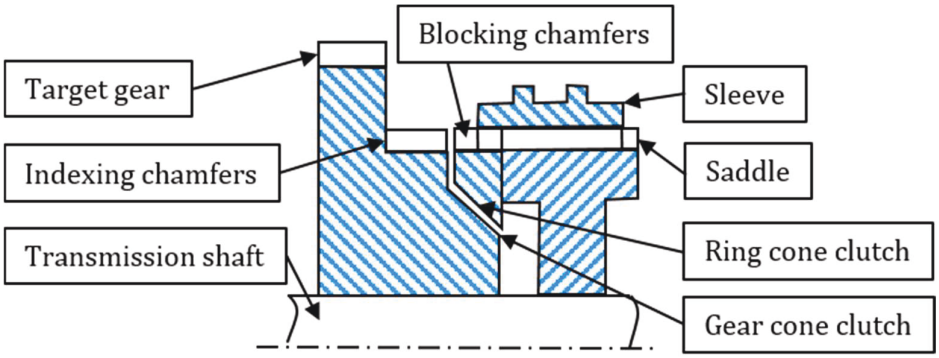

Figure 7-5: Typical synchronizer mechanism

7.2.3 Driveline and vehicle

As shown in Figure 7-3, these sub-models in this section can be expressed as followings

$$\left(J_{fd1}i_{fd}^2 + J_{fd2}\right)\frac{\ddot{\theta}_{fd1}}{i_{fd}} = i_{fd}T_O - k_H\left(\frac{\theta_{fd1}}{i_{fd}} - \theta_H\right) - c_H\left(\frac{\dot{\theta}_{fd1}}{i_{fd}} - \dot{\theta}_H\right) \tag{7.23}$$

$$\begin{aligned} J_H\ddot{\theta}_H = {} & k_H\left(\frac{\theta_{fd1}}{i_{fd}} - \theta_H\right) + c_H\left(\frac{\dot{\theta}_{fd1}}{i_{fd}} - \dot{\theta}_H\right) - k_T(\theta_H - \theta_T) \\ & - c_T\left(\dot{\theta}_H - \dot{\theta}_T\right) \end{aligned} \tag{7.24}$$

$$J_V\ddot{\theta}_T = k_T(\theta_H - \theta_T) + c_T\left(\dot{\theta}_H - \dot{\theta}_T\right) - T_f \tag{7.25}$$

where T_f is the resistance applied to the vehicle.

And, it can be expressed as

$$T_f = \left[mg\sin\alpha + \mu mg\cos\alpha + \frac{1}{2}\rho C_D A_S\left(\dot{\theta}_T r_T\right)^2\right] r_T \tag{7.26}$$

where J_{fd1}, J_{fd2}, J_H and J_V stand for inertias of driving part of differential, driven part of differential, wheel hubs, and whole vehicle; θ, $\dot{\theta}$ and $\ddot{\theta}$ are utilized to represent the angular replacement, speed, and acceleration for the final drive, wheel hubs and tires; torsion stiffness and damping coefficients are depicted as k_H and c_H, and k_T and c_T by the subscripts of corresponding elements; i_{fd} is the gear ratio of final drive; m is the whole vehicle mass; g is gravity acceleration; α is incline angle; μ is rolling resistance factor; ρ is air density; C_D is drag coefficient; r_T is the tire radius; A_S is the vehicle frontal area.

7.3 GEAR SHIFTING CONTROL SYSTEM

In general, the control of the vehicle powertrain system is executed in a hierarchical manner, as shown in Figure 7-6. The driving and braking operations as well as gear shifting are coordinated by the vehicle control unit (VCU) which also monitors driver inputs and vehicle states, e.g. throttle opening, motor torque, speeds, and so on, to determine whether to perform the gear shifting operations. During the driving and braking operations, the gear ratio of the transmission is constant. Therefore, there is no effort required in the transmission control unit (TCU). The driver's torque demands are met by the motor control unit (MCU) which controls the power inverter to achieve driver inputs. When gear change events occur, much higher demand is placed on the TCU and VCU will handle coordination control between MCU and TCU.

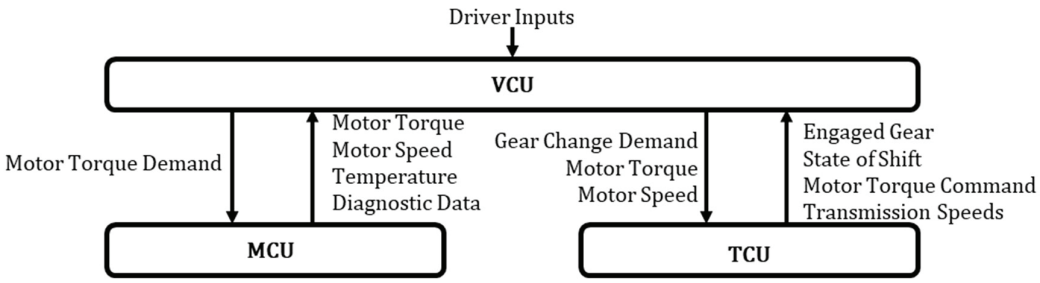

Figure 7-6: Vehicle control hierarchy

In this study, 65km/h vehicle speed and 50% throttle opening, and 50km/h vehicle speed and 50% throttle opening are called as the gear shifting points which are decided by dual-parameter gearshift schedule, and Ref. [19] shows the gearshift schedule design process in detail. Namely, when the vehicle reaches this state, the gear change event will be triggered. And, before the moment of the shift, the VCU will record the throttle value and then send it to TCU. Then, TCU will store it as the initial value for the first stage and the end value for the fifth stage. In the gear shift process, the TCU essentially takes control of the vehicle as it must control both the electric motor and gear shifting actuator to ensure good gear shifting performance. Therefore, the driver's throttle input has been shielded. In this study, TCU controls the motor torque output according to the planning throttle change trajectories in the first stage and the fifth stage of the proposed gear shift strategy.

7.3.1 Control strategy

Gear shifting control of PAMT requires a coordination strategy that can combine displacement control for the synchronizer mechanism and speed and torque controls for EM. Regarding a traditional AMT, the primary clutch should be completely disengaged

before gear shifting. This decouples the ICE from the remainder of the powertrain in the gear change process. Therefore, the load force exerted on the synchronizer will be reduced to a large degree during its disengagement and engagement process. Compared to ICE, EM features the better speed and torque controllability, which can achieve precise speed matching before engaging the target gear. Therefore, the cone friction clutches applied to minimize any relative slip speed between the driving cone clutch and the driven one may ideally be not required for gear shifting [139].

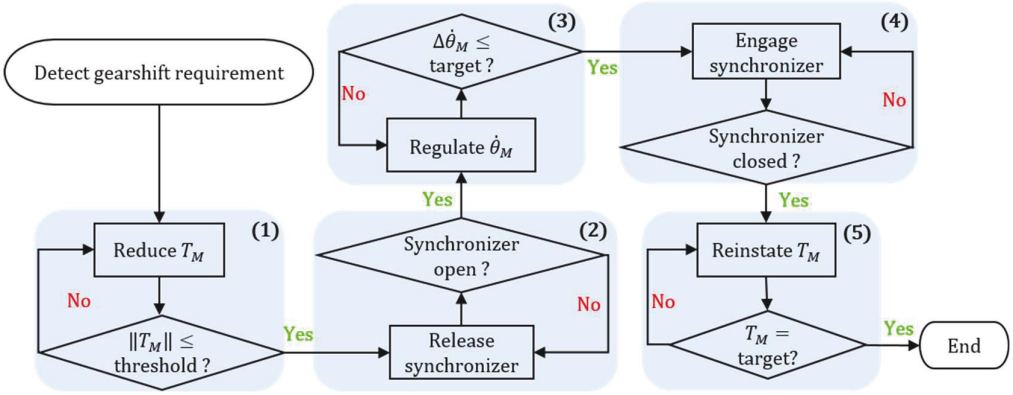

Figure 7-7: Flow chart of gear shifting strategy

Schematically, the shifting coordination control tactic of the gear shifting process is shown in Figure 7-7. This tactic is mainly comprised of five stages, including the torque and speed control of the electric machine and the displacement control of synchronizer mechanisms. Stage 1: Reduce electric machine torque to the threshold value; Stage 2: Release synchronizer to the neutral position; Stage 3: Regulate electric machine speed to the target value; Stage 4: Engage synchronizer mechanism to the target gear; Stage 5: Reinstate electric machine torque to the target value. To be specific, at the first stage, this tactic requires that T_M should be reduced to 0 when this stage finished and the throttle

opening will be controlled to recover the level before the gear shifting. It should be also noted that the control modes of driving electric machine switches according to the different gear shifting stages, as shown in Figure 7-8.

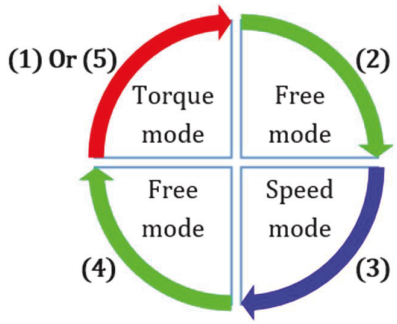

Figure 7-8: EM Control schedules

7.3.2 Evaluation metrics of gear shifting quality

In order to evaluate the gear shifting quality, some metrics should be given. In this study, longitudinal vehicle jerk and shifting time are chosen as the evaluation metrics. Since the relative slip speed difference between the cone clutch driving side and the driven has been adjusted to a small range at the third stage, the friction dissipation energy from the cone clutches is not considered as a metric.

(1) Longitudinal vehicle jerk is rate change of acceleration observed by the driver. Minimising jerk will offer a reference of improving the gear shifting quality, and what factors will impose impacts on gear shifting quality. Ref. [105] demonstrated that the largest level of jerk induced at the first stage and the fifth stage. It should be worth noting that the standard level of jerk in German is $|J| \leq 10\mathrm{m}/s^3$, while in China it is $|J| \leq$

$17.64\mathrm{m}/s^3$ [34, 140]. In this study, the longitudinal vehicle jerk can be calculated as follows

$$J = \frac{da_V}{dt} = \frac{d^2(\dot{\theta}_T r_T)}{dt^2} \tag{7.27}$$

where J is the longitudinal vehicle jerk ($\mathrm{m/s^3}$), and a_V is the longitudinal vehicle acceleration ($\mathrm{m/s^2}$).

(2) Gearshift duration measures the entire period when gearshift happens, and it can be observed by the diver. In this study, it is calculated by the sum of the time consumption in each stage of the shifting process. The entire gear shift time is able to be reduced by minimizing each stage duration. However, this will be at the expense of increased jerk [105].

7.3.3 Gearshift control

According to the description of Section 7.3.1, the gearshift execution components include the driving electric machine and synchronizer mechanisms. In this study, three alternative torque trajectories are proposed to control T_M change rate at the first stage and the fifth stage. And, adopting an on-off manner to control synchronizer mechanisms achieves the gear change by a PID controller.

7.3.3.1 Electric machine torque control

According to PAMT dynamic equations, this transmission is a single degree of freedom system in the first and fifth stages of the gear shifting process. If using the vehicle jerk

and shift durations as optimal objectives in these two stages, the torque control problem of EM can be formulated as a multiple-objective optimization problem. To solve this kind of optimization problem, Pontryagin's minimum principle and dynamic programming [130] are often applied to generate the optimized control variable trajectories. However, these two methods are so computationally intensive that they are unable to be utilized online in real-time, especially in high transient gear shifting operations. To address this issue, this study proposes three alternative empirical polynomials to plan the motor torque change rate at the first stage and the fifth stage. These alternative polynomials are respectively the third-degree polynomial (TDP), the fifth-degree polynomial (FDP), and the seventh-degree polynomial (SDP). They are ideal for real-time applications due to the low amount of computation. The torque control system diagram is shown in Figure 7-9.

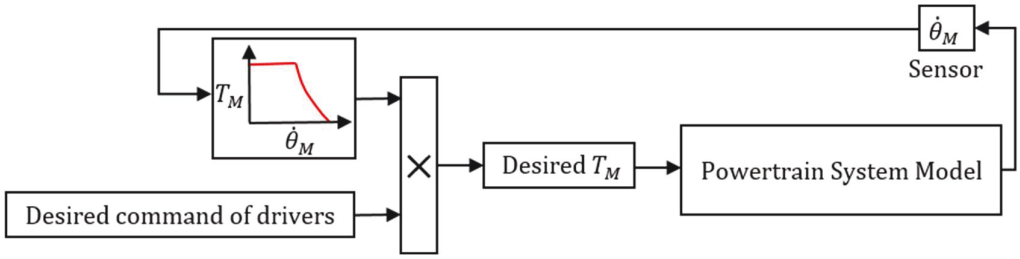

Figure 7-9: Schematic diagram of T_M controller

According to Eq. (7.1), T_{EM} can be determined by α_{Pa} when knowing $\dot{\theta}_{EM}$. Base on control strategies of the first and the fifth stages, these desired candidates α_{Pa} polynomials should meet the following requirements

$$\delta_p(t_0) = \delta_{P_0}, \delta_p(t_f) = \delta_{P_f} \tag{7.28}$$

where δ_p represents the desired α_{Pa} at the first and the fifth stages, t_0 and t_f is the start timing and end timing of actuation operations, δ_{P_0} and δ_{P_f} are respectively the start and end values of pedal opening. At the first stage, $\delta_p(t_0) = \delta_{P_0}$ and $\delta_p(t_f) = 0$. At the fifth stage, $\delta_p(t_0) = 0$ and $\delta_p(t_f) = \delta_{P_f}$.

The design process of three alternative candidate polynomials is shown as followings

#1 TDP

In order to represent the function $\delta_p(t)$, a normal cubic polynomial $\chi(\psi)$ are used as following

$$\chi(\psi) = -2\psi^3 + 3\psi^2 \tag{7.29}$$

Herein, defining $\psi = \frac{t-t_0}{t_f-t_0}$ where $t \in [t_0, t_f]$. So, $0 \leq \psi \leq 1$.

Eq. (7.29) can meet the below conditions

$$0 \leq \chi(\psi) \leq 1 \tag{7.30}$$

And, $\chi(\psi)$ also meets the following initial and end conditions

$$\chi(0) = 0,\ \dot{\chi}(0) = 0,\ \chi(1) = 1,\ \dot{\chi}(1) = 0 \tag{7.31}$$

#2 FDP

The fifth-degree polynomial is displayed as following

$$\chi(\psi) = 6\psi^5 - 15\psi^4 + 10\psi^3 \tag{7.32}$$

This polynomial meets the same initial and end conditions as TDP.

#3 SDP

The seventh-degree polynomial is

$$\chi(\psi) = -20\psi^7 + 70\psi^6 - 84\psi^5 + 35\psi^4 \tag{7.33}$$

According to Eq. (7.29), Eq. (7.32) and Eq. (7.33), the desired throttle opening δ_p can be obtained

$$\delta_p(t) = \Delta\delta_p \chi(\psi) + \delta_p(t_0) \tag{7.34}$$

where $\Delta\delta_p = \delta_{P_f} - \delta_{P_0}$.

Hence, Eq. (7.34) can meet $\delta_p(t_0) = \delta_{P_0}$ and $\dot{\delta}_p(t_0) = 0$, and $\delta_p(t_f) = \delta_{P_f}$ and $\dot{\delta}_p(t_f) = 0$ which makes T_M change smoothly at the initial and end phases. When both t_0 and t_f are known, the polynomial function $\delta_p(t)$ will be defined. Hence, through adjusting $t_f - t_0$, the time consumed at the corresponding stages can be denoted. Therefore, the gear shifting time can be controlled as short as possible. However, to trade off the conflict between the vehicle jerk and the gear shifting time, the shifting time is supposed to be within a reasonable range.

7.3.3.2 Electric machine speed control

In this transmission, driving EM is mechanically connected to S. So, $\dot{\theta}_S$ can be regulated by changing EM speed. This can also regulate $\dot{\theta}_R$ during the gear change according to the following

$$\dot{\theta}_C(r_S + r_R) = \dot{\theta}_R r_R - \dot{\theta}_S r_S \tag{7.35}$$

During the third stage of the gear shifting, the vehicle speed does not change almost due to the large vehicle inertia and the short shift duration. Hence, $\dot{\theta}_C$ will also be almost kept unchanged. Since this transmission system is two degrees of freedom at this stage, $\dot{\theta}_R$ can be changed by regulating $\dot{\theta}_S$.

When shifting from 1st gear to 2nd gear with gear ratio changing from $i_1 = 2.7$ to $i_2 = 1$, the end condition of speed regulation is $\dot{\theta}_S = \dot{\theta}_R$, i.e., $\dot{\theta}_S = \dot{\theta}_R = \dot{\theta}_C$. So, $\dot{\theta}_S$ and $\dot{\theta}_C$ need to be regulated to be the same ideally. When shifting from 2nd gear to 1st gear in which $\dot{\theta}_R$ is required to reach as close to 0 as possible so that R will be engaged with the transmission case through the synchronizer mechanism. When the speed synchronization completed, the next shift stage will be operated. In this section, the desired $\dot{\theta}_M$ trajectory is also devised according to the torque polynomials proposed in Section 7.3.3.1. The speed control system is shown in Figure 7-10. It is worth noting that this transmission is two degrees of freedom system at this stage so that T_M does not have any impact on the vehicle jerk.

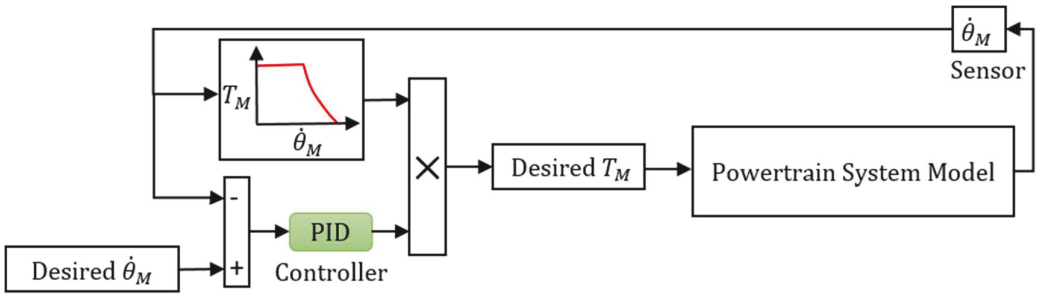

Figure 7-10: Schematic diagram of $\dot{\theta}_M$ controller

7.3.3.3 Synchronizer mechanism displacement control

The displacement closed-loop control system is shown in Figure 7-11. The desired sleeve displacement trajectories are designed according to different gearshift stages, shown in Eq. (7.36) and Eq. (7.37).

Shift from the first gear to the second gear,

$$D_S = \begin{cases} P & Stage\ 1 \\ 0 & Stage\ 2 \\ 0 & Stage\ 3 \\ -P & Stage\ 4 \\ -P & Stage\ 5 \end{cases} \tag{7.36}$$

Shift from the second gear to the first gear,

$$D_S = \begin{cases} -P & Stage\ 1 \\ 0 & Stage\ 2 \\ 0 & Stage\ 3 \\ P & Stage\ 4 \\ P & Stage\ 5 \end{cases} \tag{7.37}$$

where D_S is the desired displacement of the sleeve and $P = 15mm$.

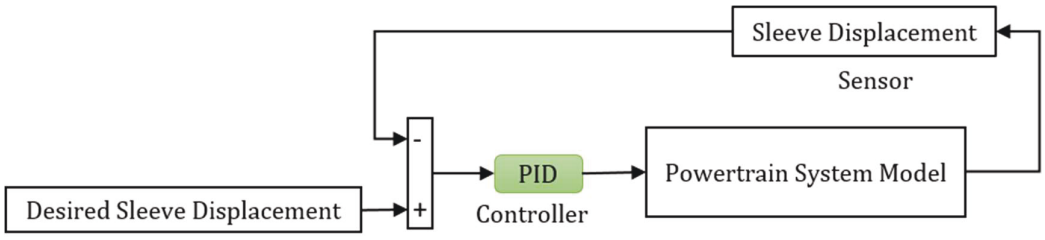

Figure 7-11: Schematic diagram of the displacement controller

7.4 RESULTS AND DISCUSSION

To exploit the transient response of the drivetrain during the gear change, the simulation model is built in MATLAB/Simulink environment. The ode14x solver with 0.1ms fixed-step size is utilized in the simulating process. A series of simulation results of up and downshifts are presented to demonstrate the effectiveness of the proposed alternative T_M trajectories during the first stage and the fifth stage of gearshifts. The key parameters used for the simulations are described in Table 7-7 which is obtained from [34, 37, 105].

7.4.1 Upshift by applying the same shift duration

Figure 7-12, Figure 7-13 and Figure 7-14 show respectively the upshift transient responses according to the inputs of different T_M trajectories devised in Section 7.3.3.1. Each simulation figure is comprised of 6 sub-figures, i.e., (a) shift stages according to the gear shifting strategy is shown in Figure 7-6, and especially stage 0 means this transmission is in the current gear and stage 6 stands for finishing the gear shifting; (b) sleeve displacement responses; (c) rotating speeds of main components where abbreviations of EM, R, and C stand for electric motor, ring gear and carrier (d) electric

motor (EM) torque and transmission output (TO) torque; (e) longitudinal vehicle acceleration and (f) longitudinal vehicle jerk.

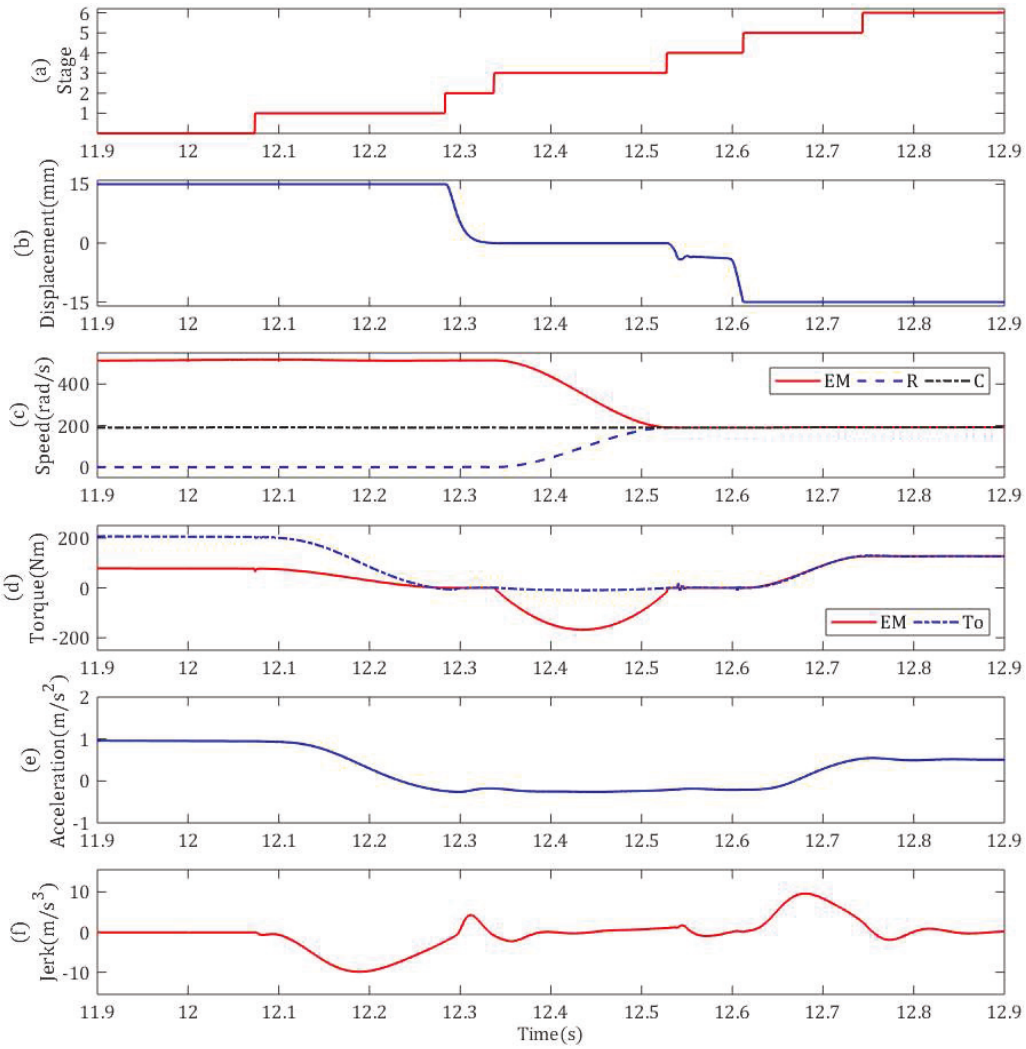

Figure 7-12: Upshift simulation results by applying TDP

The upshift point is set at 50% throttle opening and 65km/h vehicle velocity. To compare the vehicle jerk responses triggered by the alternative T_M trajectory inputs, the shift duration of each stage is strictly set to be the same. The shift duration of each stage is shown in Table 7-1. It can be seen that the total gearshift duration is 669ms. According

to Eq. (7.34), the shift durations of the first and the fifth stages can be regulated by just changing the value of $t_f - t_0$. Through regulating $t_f - t_0$, the longitudinal vehicle jerk can meet the gearshift requirements.

Table 7-1: Shift duration of each shifting stage during upshift

	Stage 1	Stage 2	Stage 3	Stage 4	Stage 5
Shift duration (ms)	209	54	190	84	132

Figure 7-12 shows the upshift simulation results by applying TDP. Firstly, by regulating the value $t_f - t_0$, the longitudinal vehicle jerks of Stage 1 and Stage 5 can be regulate to satisfy less than 10m/s^3. This is regarded as a normal peak jerk to evaluate which polynomial can suppress the longitudinal vehicle jerk response to the highest degree. According to Table 7-1, it is clearly found that Stage 5 (the torque reinstatement stage) takes less time than Stage 1 (the torque release stage) with guaranteeing the almost same peak jerk. The reason is that i_2 is less than i_1 so that, when restoring the pedal opening to the level before gear shifting, the shift duration of the fifth stage is shorter than that of the first stage. Based on the proposed control tactics, the shift durations in the second stage, and the fourth stage are decided by the torque capacity of the gearshift actuator. The shift time of the third stage is decided by the maximum EM torque capacity at the current $\dot{\theta}_M$. Figure 7-12(c) shows the speed dynamic responses of EM, R, and C. In the third stage, it can be clearly seen that $\dot{\theta}_M$ is reduced in order to match $\dot{\theta}_R$. In this process, $\dot{\theta}_C$ changes little due to the large vehicle inertia and the short shift duration. Due to $\dot{\theta}_M$ reduction, the

braking T_M, i.e., $-T_M$, should be exerted to quickly complete this process, as shown in Figure 7-12(d).

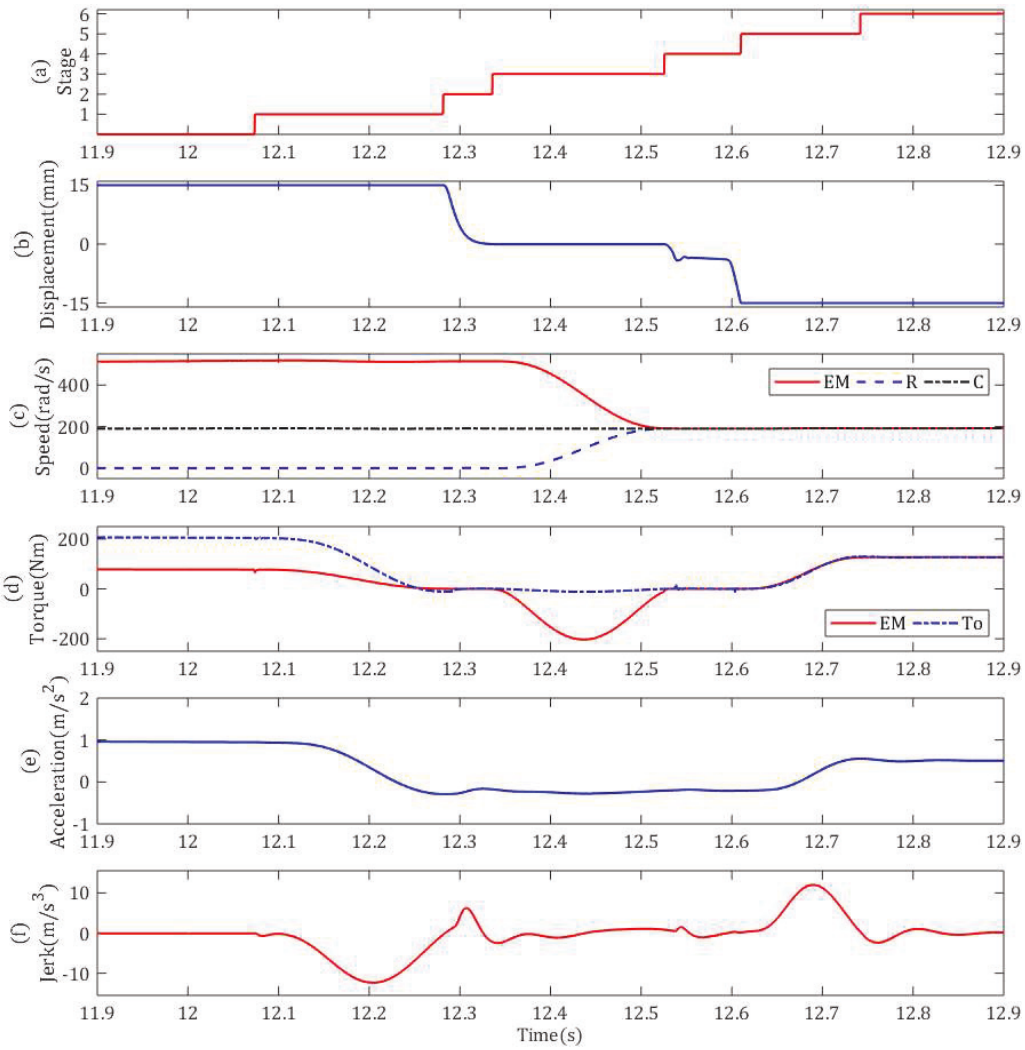

Figure 7-13: Upshift simulation results by applying FDP

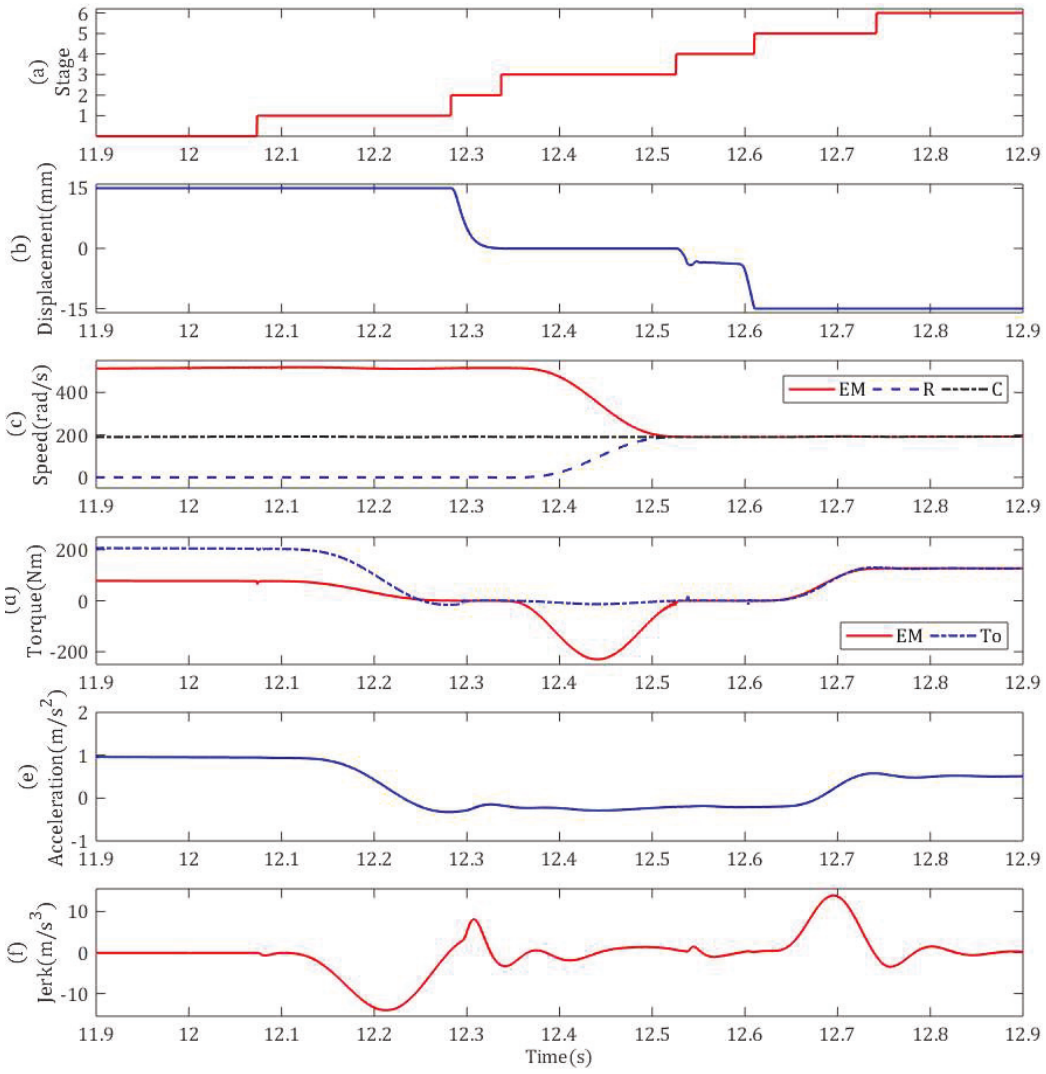

Figure 7-14: Upshift simulation results by applying SDP

Figure 7-12(f), Figure 7-13(f), and Figure 7-14(f) display respectively the transient vehicle jerk responses when adopting the different types of polynomials. From these sub-figures, it can be seen that the largest vehicle jerk occurs in Stage 1 or Stage 5. To perform the clear comparison, the quantitative jerk response results at Stage 1 and Stage 5 are abstracted into Table 7-2. According to Table 7-2, adopting the TDP triggers the least vehicle jerk among these three in these two stages, and the largest jerk is obtained by SDP.

Compared to jerks triggered by TDP, FDP triggers 25.06% and 25.22% larger jerk, and 42.28% and 52.26% larger are done by SDP respectively, which demonstrates that applying TDP can make the upshift achieve the least peak jerk when the same shift duration is set in advance.

Table 7-2: Upshift jerks at the first stage and the fifth stage

	Jerk (m/s^3)	
	Stage 1	Stage 5
TDP	-9.875	9.575
FDP	-12.35	11.99
SDP	-14.05	13.89

7.4.2 Downshift results by applying the same shift duration

Figure 7-15, Figure 7-16 and Figure 7-17 show the downshift simulation results according to three different kinds of T_M trajectories. The downshift point is set at 50% throttle opening and 50km/h vehicle velocity. To compare the vehicle jerk response results under the alternative T_M trajectories, the shift duration of each stage is also set to be the same and the total downshift duration is 670ms, as shown in Table 7-3. Each subfigure of the downshift process presents the orderly corresponding simulation results as that of the upshift process. Herein, the adjustment of shift duration also applies the same approach

as that of the upshift process. However, it is found that the fifth stage takes more time than the first stage with the almost same peak vehicle jerk. This trend is different from that of the upshift process. The reason is that the new gear ratio i_1 is larger than the old one ratio i_2. Due to the downshift process, $\dot{\theta}_M$ should be controlled to increase through exerting the accelerating T_M, as shown in Figure 7-15(d), Figure 7-16d) and Figure 7-17(d). Table 7-4 summaries quantitatively the vehicle jerk responses of the first stage and the fifth stage during downshifting. According to Table 7-4, applying TDP to plan the torque trajectory stimulates the least longitudinal vehicle jerk response during Stage 1 and Stage 2. This demonstrates the conclusion of the upshift simulation again.

Table 7-3: Shift duration of each shifting stage during downshifting

	Stage 1	Stage 2	Stage 3	Stage 4	Stage 5
Shift duration (ms)	131	55	143	78	263

Table 7-4: Downshift jerks at the first stage and the fifth stage

	Jerk (m/s^3)	
	Stage 1	Stage 5
TDP	-9.876	9.84
FDP	-12.24	12.25
SDP	-14.28	14.03

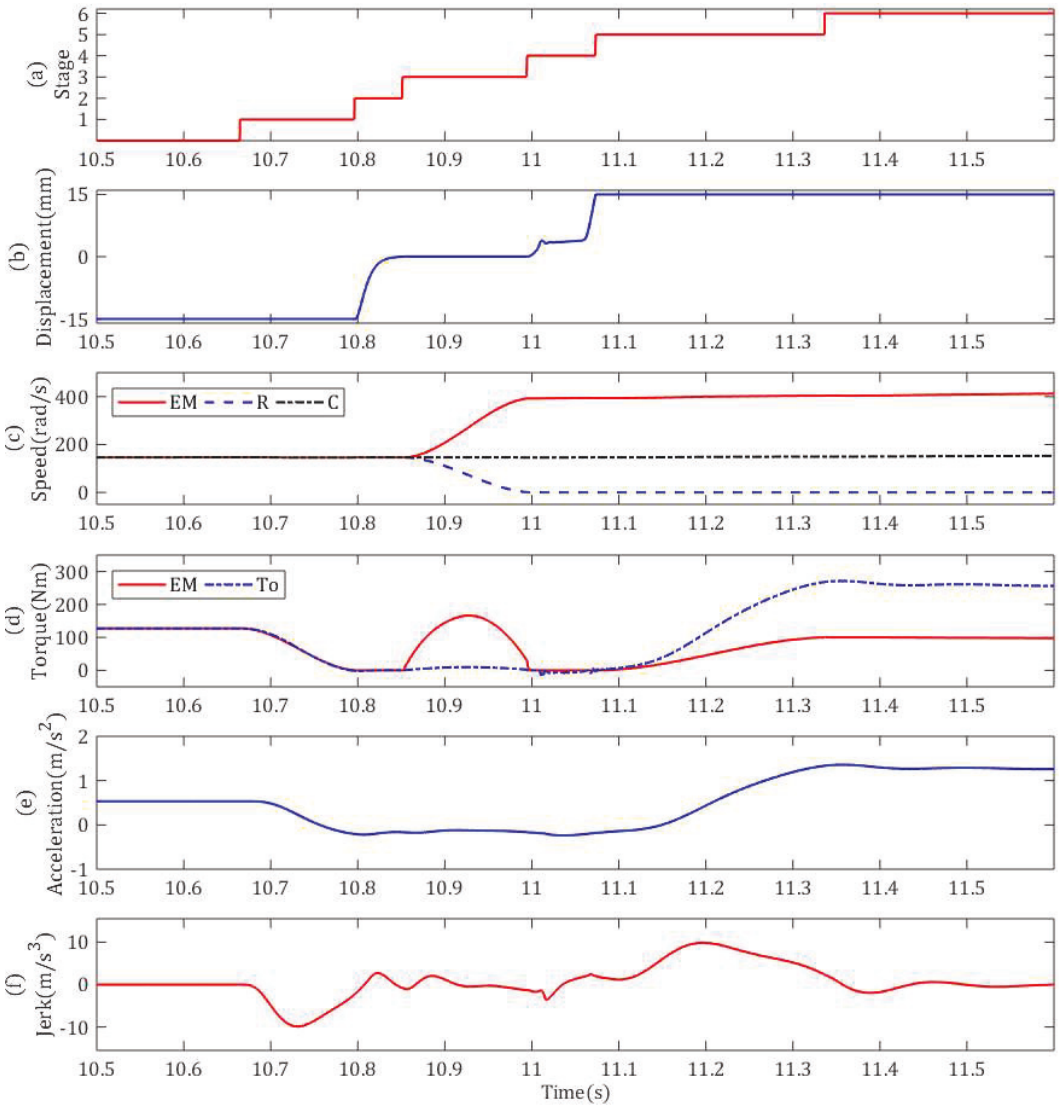

Figure 7-15: Downshift simulation results by applying TDP

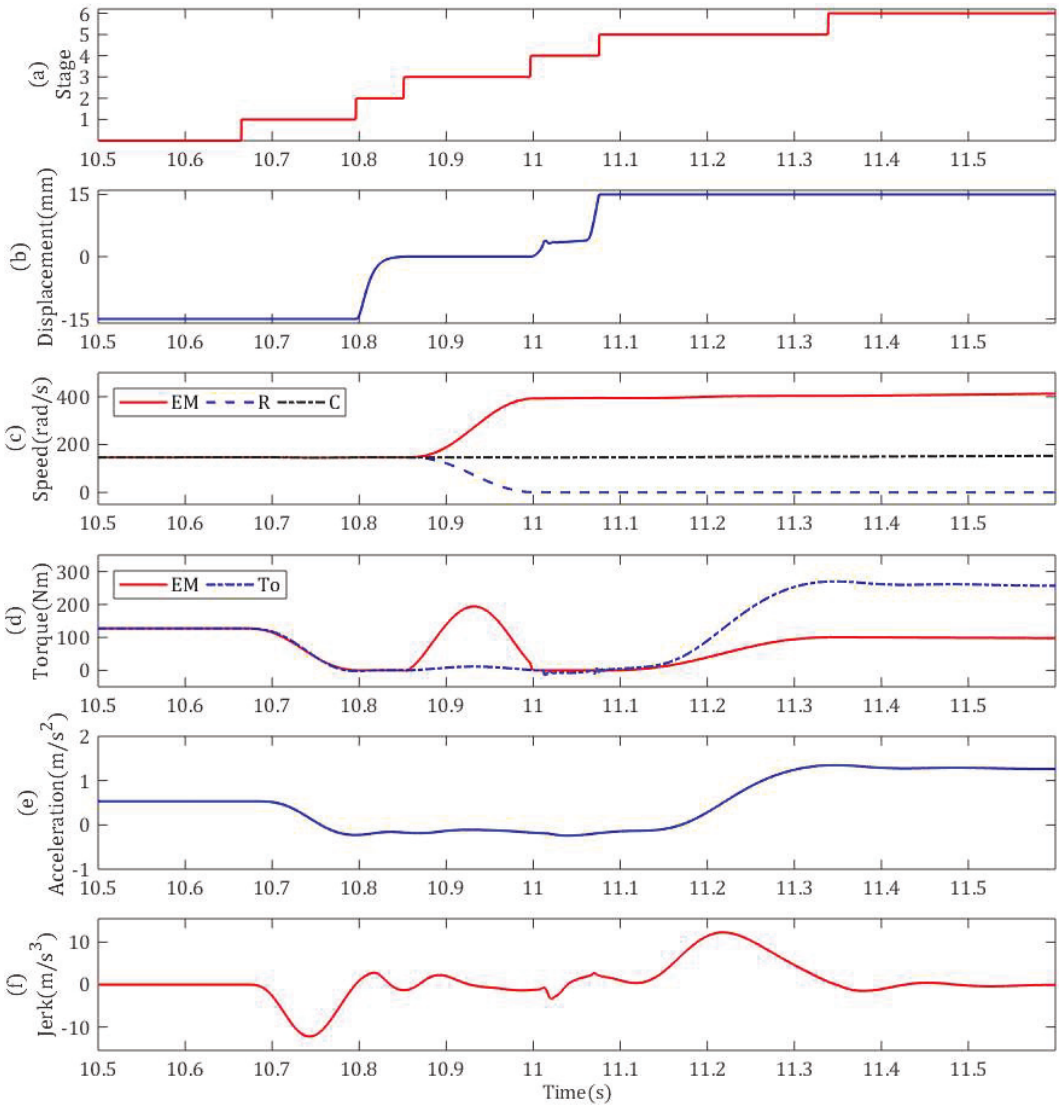

Figure 7-16: Downshift simulation results by applying FDP

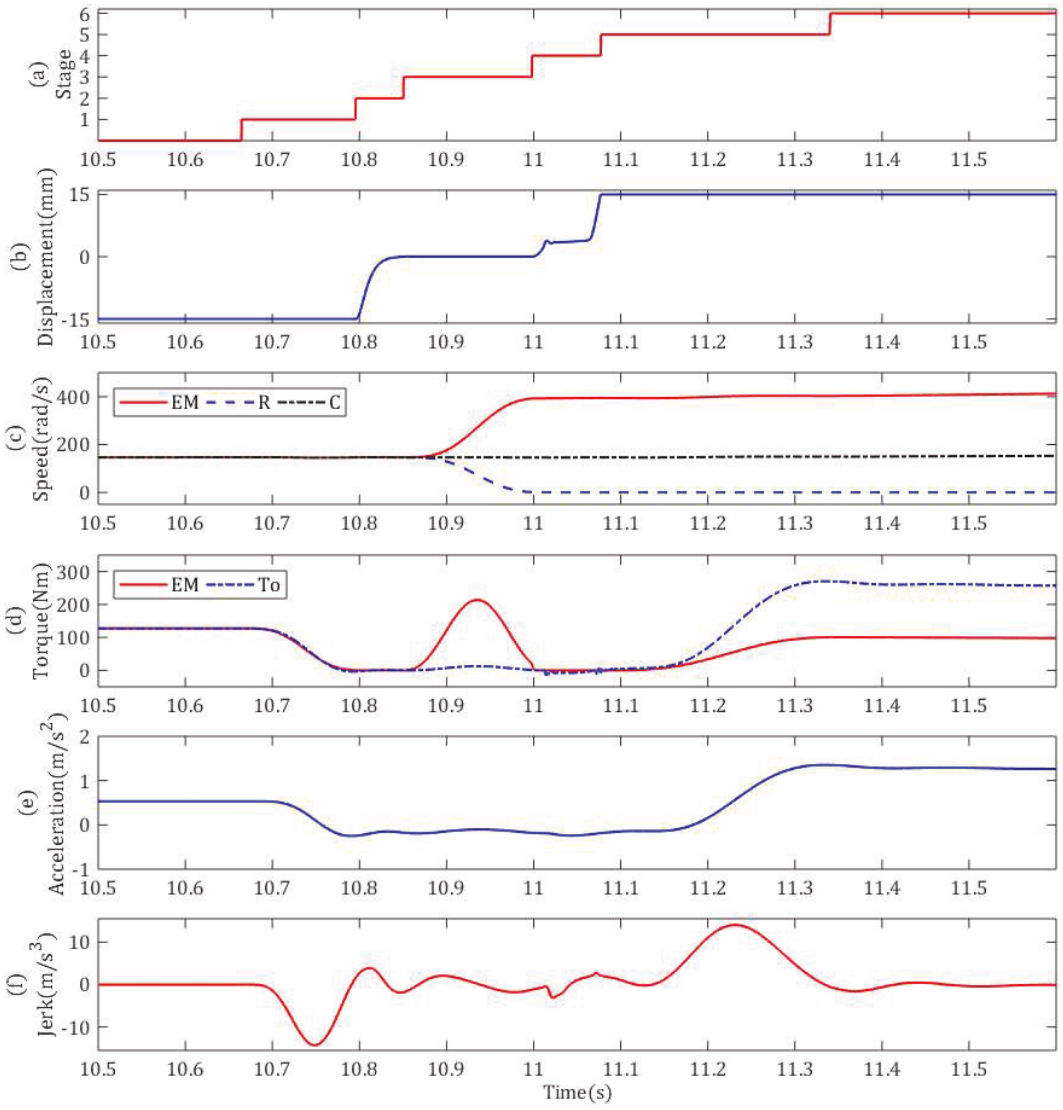

Figure 7-17: Downshift simulation results by applying SDP

7.4.3 Upshift and downshift results with the same vehicle jerk

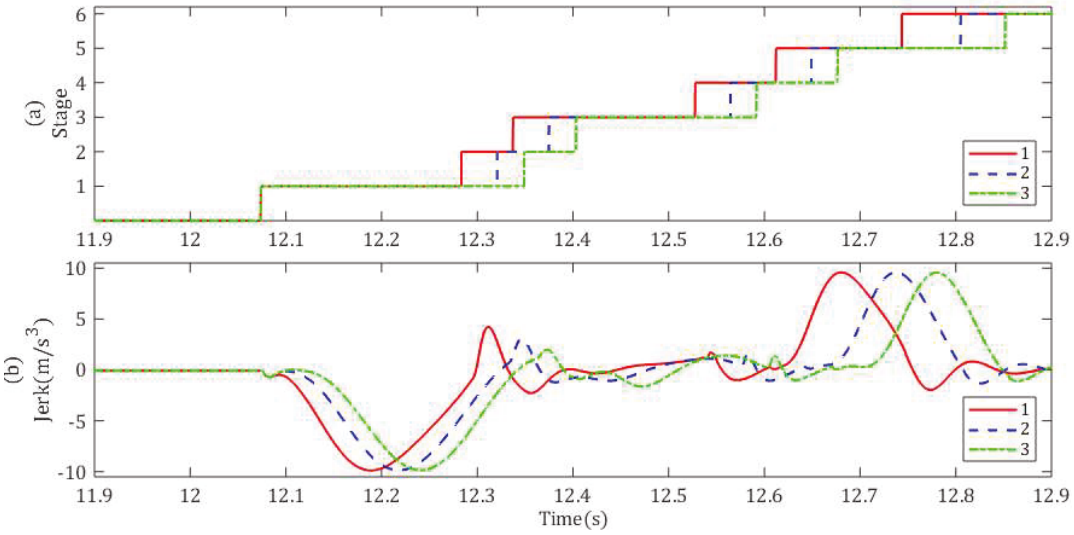

Figure 7-18: Upshift results with the same vehicle jerk

Table 7-5: Shift durations at the first stage and the fifth stage of upshift

	Time (ms)	
	Stage 1	Stage 5
TDP	209	132
TDP	247	156
TDP	274	174

In Section 7.4.1 and Section 7.4.2, through a series of comparative simulation experiments, it can be validated that TDP can achieve the least jerk response among these alternative candidate polynomials. In this section, which candidate polynomial can effectively reduce the shift duration under the condition of guaranteeing the accepted

vehicle jerk range will be verified. Herein, the parameter set is the same as that of Section. 7.4.1 and Section. 7.4.2. Firstly, the jerk results of the TDP in Table 7-2 and Table 7-4 are regard as the standard and then regulating $t_f - t_0$ to make the jerk results of adopting FDP and SDP approximately equal to those of TDP. After re-simulating, upshift and downshift simulation jerk responses are shown in Figure 7-18 and Figure 7-19 in which '1', '2' and '3' mean the results of adopting TDP, FDP, and SDP respectively. The shift durations consumed by Stage 1 and Stage 5 are abstracted into Table 7-5 and Table 7-6. According to Table 7-5, it can be found that TDP takes the least time among these alternative candidate polynomials, and SDP does the most time. Compared to the time consumption of TDP, adopting FDP consumes severally 18.18% and 18.8% more time during the first stage and fifth stage, and adopting SDP does 31.1% and 31.82% more time. Table 7-6 abstracts time consumption results of downshifting which shows the identical trend as those of upshift. So, according to the comparison, it can be found that TDP features the best performance in reducing the shift time.

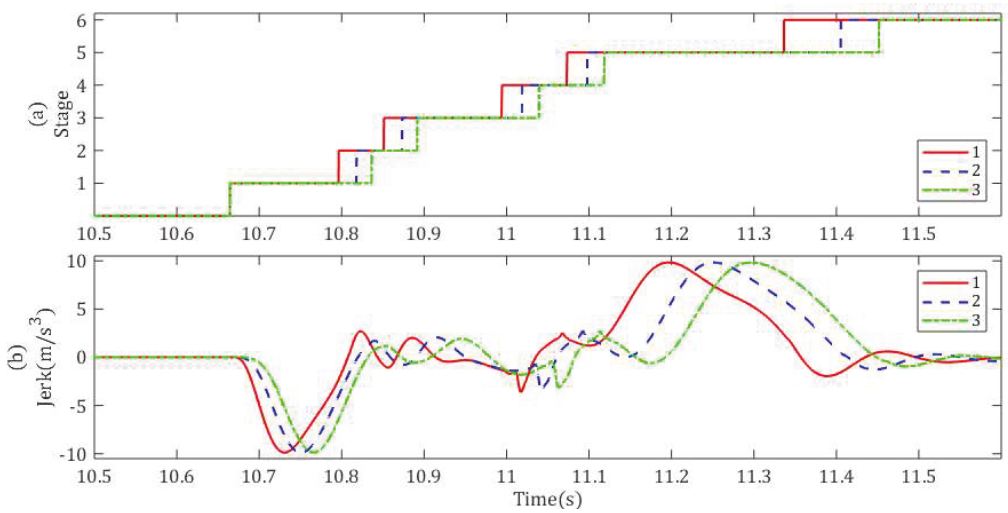

Figure 7-19: Upshift results with the same vehicle jerk

Table 7-6: Upshift results with the same vehicle jerk

	Time (ms)	
	Stage 1	Stage 5
TDP	131	263
FDP	154	308
SDP	172	333

7.5 CHAPTER CONCLUSIONS

This study proposes a novel two-speed transmission for BEVs and presents its work principles in detail. To capture the powertrain transient responses, a comprehensive and original electrified powertrain system is modeled in this chapter. To achieve gear shifting, a control strategy is designed, and divided into five stages orderly. And the corresponding controllers for the different stages are also developed respectively to achieve this strategy. To control the motor torque reduction and reinstatement at the first and the fifth stages, three alternative torque trajectories are proposed. Then, a series of control group simulations are performed to validate which candidate trajectory can obtain the optimal gearshift quality. Simulation results demonstrate that TDP based torque trajectory is the optimal trajectory which is the capacity of not only suppressing the gear shifting jerk but also reducing shift durations. This study will provide a beneficial reference for gear shifting control of clutchless automated manual transmission (CLAMT) which is widely adopted in battery electric vehicles.

Table 7-7：Powertrain system parameters

Parameter	Value	Parameter	Value
J_{EM}	0.065 kg·m^2	J_{fd1}	0.003 kg·m^2
k_I	500000 Nm/rad	J_{fd2}	1.16 kg·m^2
c_I	10 Nm·s/rad	i_{fd}	3.3750
J_S	0.000451 kg·m^2	k_H	11000 Nm/rad
J_{GR1}	0.0006 kg·m^2	c_H	50 Nm·s/rad
J_{SL}	0.0003 kg·m^2	k_T	22000 Nm/rad
J_R	0.0035 kg·m^2	c_T	100 Nm·s/rad
J_C	0.017 kg·m^2	J_V	188.3 kg·m^2
r_S	0.0279 m	m	1820 kg
r_P	0.0097 m	α	0
r_R	0.0474 m	μ	0.015
k_O	500000 Nm/rad	ρ	1.127 kg/m^3
c_O	10 Nm·s/rad	C_D	0.30
μ_D	0.3	A_S	2.08 m^2
R_C	0.125m	r_T	0.3216 m
α_C	12 deg	g	9.81 m/s^2

CHAPTER 8 : THESIS CONCLUSIONS

In this thesis, two different types of two-speed transmissions are proposed. The first is a transmission that is comprised of dual-stage planet gear sets and can achieve a gear shifting without the torque interruption, called Uninterrupted Planet-gear Automatic Transmission (UPAT). The other is made up of a single planet gear set, called Planetary Automated Manual Transmission (PAMT).

Two-speed UPAT is comprised of a compound planetary gear system with a double pinion planetary gear set and a single pinion planetary gear set. The compound planetary gear consists of ring gear (R), a carrier (C), small sun gear (SS), large sun gear (LS), inner planet pinion (IP), and outer planet pinion (OP). To ensure the power-on gearshift, a gearshift system featuring both low-cost and easy to control is applied. A one-way clutch (OWC) and two band brakes (C brake and LS brake) are adopted in the gearshift system. C brake is only taken as on-off control based on a switched component and does not work in the gearshift process. Different from C brake, LS brake, the only controlled actuator during gearshifts, needs to be precisely operated. LS brake can enable the torque applied to OWC to decrease or increase by increasing or decreasing the torque exerted on itself during the gearshifts. When the torque exerted on OWC reaches 0, C will be automatically released at the end time of the torque phase of power-on upshifts. Analogously, OWC can automatically hold C at the start time of the torque phase of power-on downshifts. Once OWC is replaced by other corresponding gearshift components that need to be actively controlled to mimic the characteristic of OWC, the transmission will require two elements to cooperate to accomplish the gear changing, which will further improve the gear control

complexity. Furthermore, when two gearshift components can not cooperate well, the untimely releasing or engaging of these components will occur, which will impair the gearshift quality. Therefore, adopting OWC as the gearshift element will reduce the gearshift control complexity of the proposed novel transmission when in comparison with some current existing transmissions. Due to the two degrees of freedom of the compound planetary gear system, two different gear ratios can be achieved. When C is grounded by OWC with C brake engaged, the first gear is achieved. The reason to engage C brake in the first gear is to prevent OWC overrunning when regenerative energy recovery condition happens. When the upshift event happens, firstly, C brake must be fully disengaged quickly, and then LS brake is controlled to engage gradually until LS speed reaches zero, which means the upshift process is finished. Therefore, only LS brake is applied in the second gear. When shifting the second gear to the first gear, the LS brake is released gradually until the torque applied on itself is zero, which means the downshift is achieved. Simultaneously, C brake should be controlled to engage quickly. In the condition of reverse gear driving, C is grounded by C brake to prevent from overrunning of OWC with the counter-clockwise ration of the traction motor. Parking gear can be obtained by engaging both C brake and LS brake.

A mathematical model of electrified powertrain equipped with two-speed UPAT is developed, including the electric motor, the proposed two-speed UPAT, one-way clutch, band brake, driveline, and the vehicle, etc. The powertrain is characterized as a front wheel drive, UPAT with band brake to engage or disengage for gear shifting between the first gear and the second gear. Vehicle resistance torque models include road incline, aerodynamic drag, and rolling resistance. During the modelling, some assumptions have

employed to simplify the model complexity. These assumptions have allowed the development of a simplified powertrain model of two-speed UPAT while still capturing the important characteristics of the powertrain, particularly with regard to transient vibration, and damping of the powertrain system.

Three model-based power-on gearshift control strategies are proposed for the novel two-speed UPAT, termed as CITGS, SCOTGS, and COTGS. In CITGS, the motor torque is maintained constant, which is an easy control method but without taking advantage of the superior controllability of the electric motor. Upshift simulation results of CITGS show that the largest vehicle jerk is attained during the inertia phase. Compared to CITGS, the motor torque is controlled according to the torque ratio of LS brake during the inertia phase in SCOTGS, in consequence, the smaller jerk is achieved by this tactic and it also generates less friction work during the upshift. COTGS takes advantage of the control flexibility of the electric motor to realize the torque coordination control with the LS brake in both the torque phase and the inertia phase. Upshift simulation results at 50% driver demand demonstrate that the smallest jerk is attained in COTGS. However, due to the increase of the motor torque in the torque phase, the most friction is generated by COTGS. It is worth noting that, in the aggressive driving condition, COTGS is ineffective to an extent in the torque phase due to the limitation of the motor torque, which brings the large jerk in the torque phase of upshift process. Downshift simulation results at 50% driver demand demonstrate that the smallest jerk is attained in COTGS. However, the least friction is generated by CITGS. At 75% driver demand, SCOTGS and COTGS are COTGS is ineffective to an extent in the inertia phase due to the limitation of the motor torque. To validate the simulation results of the proposed power-on gearshift strategies,

different power-on upshift and downshift experiment is undertaken on two-speed UPAT prototype test rig. A series of experiment results are obtained according to three different kinds of power-on gearshift control tactics in this electrified powertrain rig. It can be found that the variation trends of transmission output torque are the same as the power-on gearshift simulation results. Therefore, it can be proved that the proposed gearshift strategies are well verified by experimental results and can be applied in practice. Both the disadvantages and advantages of these strategies are clearly demonstrated, which provides beneficial knowledge and reference to the researchers undertaking the development of the transmission controller.

To comprehensively improve the gearshift quality, optimal gearshift control tactics for the torque phase and the inertia phase are proposed to reduce the vehicle jerk and friction work within the fixed gearshift duration. Model-based optimal gearshift control tactics are developed, and the simulation results demonstrate that the proposed multi-objective optimal tactic for the torque phase effectively reduces the vehicle jerk and friction work, and the optimal coordinating tactic for the inertia phase decreases the friction work to a high degree. Meanwhile, to provide unmeasurable torque information for executing the proposed optimal strategies, sliding mode theory is employed to design the torque observers which are capable of estimating the torque information sufficiently and accurately.

Two-speed PAMT features a more compact mechanical structure than clutchless automated manual transmission (CLAMT) and easier gear shifting control than power-on transmissions. The electrified drivetrain is comprised of an electric machine (EM), a two-speed PAMT, final drive, differential, half shafts, and wheels. To be more specific, the

two-speed PAMT consists of a single planetary gear train consisting of a sun gear (S), three planet gears (P), a carrier (C), and a ring gear (R). The input of PAMT is S mechanically connected to an EM via a flexible shaft. C is regarded as the output of PAMT. The gearshift actuator is a synchronizer system which is mainly comprised of gear ring 1 (GR1), spline hub (SH), sleeve (SL), gear ring 2 (GR2), etc. Specifically, GR1 is laid out on the input shaft which is also attached to S, GR2 is fixed on the transmission case and SH is connected to R. SL can be controlled to slide along SH. When SL is the neutral position, namely never engaging SH with GR1 nor engaging SH with GR2, PAMT will work at the neutral gear. When SL is controlled to engaging GR2 with SH, PAMT will be operated at the first gear. The second gear will be obtained through engaging GR1 and SH with SL. Compared to the existing literature, the first contribution of this study is that a novel planet CLAMT is proposed, called PAMT, which features a more compact mechanical layout than CLAMT and easier gear shifting control than power-on transmissions.

To capture the powertrain transient responses, a comprehensive and original electrified powertrain system equipped with two-speed PAMT is modeled. To achieve gear shifting, a control strategy is designed, and divided into five stages orderly. And the corresponding controllers for the different stages are also developed respectively to achieve this strategy. To control the motor torque reduction and reinstatement at the first and the fifth stages, three alternative torque trajectories are proposed. Then, a series of control group simulations are performed to validate which candidate trajectory can obtain the optimal gearshift quality. Simulation results demonstrate that TDP based torque trajectory is the optimal trajectory which is the capacity of not only suppressing the gear shifting jerk but

also reducing shift durations. This study will provide a beneficial reference for gear shifting control of clutchless automated manual transmission (CLAMT) which is widely adopted in battery electric vehicles.

Further Research

(1) The proposed gearshift control strategies for UPAT will be verified in a real BEV to validate the control effectiveness of these alternative strategies;

(2) The real transmission control unit for UPAT will be designed to implement the developed control code;

(3) Two-speed PAMT prototype and its control system will be developed and tested in UTS Powertrain Test Rig.

APPENDIX

Table A1: ATi 2000 series wireless torque sensor specifications

SYSTEM	
Bandwidth	DC to 1100 Hz
filtered output	DC to 100 Hz
Integral Non-Linearity	+/- .10%
Repeatability	+/- .05%
Maximum Error	<.25% Full Scale
RECEIVER	
Power	12 Volts DC
Output	+/- 2 Volts
Display	3 Digit Backlit LCD
Output Ripple	< 2 mV (Filtered) < 15 mV (Wide Band)
Induction Power Supply	500kHz Induction Power
MINIATURE CRYSTALLED TRANSMITTERS	
Power	9 Volts or Induction Power
Acceleration Limit	32,000g Static (125g Dynamic, DC -1 kHz)
Zero Drift	0.02% / Deg C
Span Drift	0.02% / Deg C
Operating Temperature Range	-40 to 140 Deg C

Table A2: Calibration data of torque sensor on the transmission input shaft

Weight (kg)	Voltage (v)
0	-4.02
1	-3.49
2	-2.92
3	-2.49
4	-1.93
5	-1.41
6	-0.84
7	-0.32
8	0.21
9	0.71
10	1.24

Bibliography

[1] P. Coppola and D. Esztergár-Kiss, *Autonomous Vehicles and Future Mobility*. Elsevier, 2019.

[2] M. Ehsani, Y. Gao, S. Longo, and K. Ebrahimi, *Modern electric, hybrid electric, and fuel cell vehicles*. CRC press, 2018.

[3] M. Lazarus and H. van Asselt, "Fossil fuel supply and climate policy: exploring the road less taken," ed: Springer, 2018.

[4] S. Bhandarkar, "Vehicular pollution, their effect on human health and mitigation measures," *VE,* vol. 1, no. 2, p. 3340, 2013.

[5] İ. A. Reşitoğlu, K. Altinişik, and A. Keskin, "The pollutant emissions from diesel-engine vehicles and exhaust aftertreatment systems," *Clean Technologies and Environmental Policy,* vol. 17, no. 1, pp. 15-27, 2015.

[6] P. Bera and M. Hegde, "Recent advances in auto exhaust catalysis," *Journal of the Indian Institute of Science,* vol. 90, no. 2, pp. 299-325, 2012.

[7] A. Goverment, "Post-2020 emissions reduction target Report of the UNFCCC Taskforce," Australia Goverment, 2015.

[8] U. S. E. P. Agency, "Progress Cleaning the Air and Improving People's Health n.d," 2018.

[9] F. F. DeCicco J, "Global warming on the road: the climate impact of America's automobiles," 2006.

[10] S. Shafiee and E. Topal, "When will fossil fuel reserves be diminished," *Energy Policy,* vol. 37, no. 1, pp. 181-189, 2009.

[11] O. o. t. P. E. Countries, "World oil outlook," 2014.

[12] R. Mounce and J. D. Nelson, "On the potential for one-way electric vehicle car-sharing in future mobility systems," *Transportation Research Part A: Policy and Practice,* vol. 120, pp. 17-30, 2019.

[13] J. E. Bistline and D. T. Young, "Emissions impacts of future battery storage deployment on regional power systems," *Applied Energy,* vol. 264, p. 114678, 2020.

[14] Z. Wu, C. Wang, P. Wolfram, Y. Zhang, X. Sun, and E. Hertwich, "Assessing electric vehicle policy with region-specific carbon footprints," *Applied Energy,* vol. 256, p. 113923, 2019.

[15] M. Ouyang, J. Du, H. Peng, H. Wang, X. Feng, and Z. Song, "Progress review of US-China joint research on advanced technologies for plug-in electric vehicles," *Science China Technological Sciences,* vol. 61, no. 10, pp. 1431-1445, 2018.

[16] J. Ruan, P. Walker, and N. Zhang, "A comparative study energy consumption and costs of battery electric vehicle transmissions," *Applied Energy,* vol. 165, pp. 119-134, 2016, doi: 10.1016/j.apenergy.2015.12.081.

[17] J. Ruan, P. D. Walker, and N. Zhang, "A comparative study energy consumption and costs of battery electric vehicle transmissions," *Applied Energy,* vol. 165, pp. 119-134, 2016.

[18] C. Chan and K. Chau, *Modern electric vehicle technology* (no. 47). Oxford University Press on Demand, 2001.

[19] B. Zhu *et al.*, "Gear shift schedule design for multi-speed pure electric vehicles," *Proceedings of the Institution of Mechanical Engineers, Part D: Journal of Automobile Engineering,* vol. 229, no. 1, pp. 70-82, 2015.

[20] A. Sorniotti *et al.*, "Analysis and simulation of the gearshift methodology for a novel two-speed transmission system for electric powertrains with a central motor," *Proceedings of the Institution of Mechanical Engineers, Part D: Journal of Automobile Engineering,* vol. 226, no. 7, pp. 915-929, 2012.

[21] B. Gao, Q. Liang, Y. Xiang, L. Guo, and H. Chen, "Gear ratio optimization and shift control of 2-speed I-AMT in electric vehicle," *Mechanical Systems and Signal Processing,* vol. 50, pp. 615-631, 2015.

[22] S. Hong, H. Son, S. Lee, J. Park, K. Kim, and H. Kim, "Shift control of a dry-type two-speed dual-clutch transmission for an electric vehicle," *Proceedings of the Institution of Mechanical Engineers, Part D: Journal of Automobile Engineering,* vol. 230, no. 3, pp. 308-321, 2016.

[23] Z. Lu, L. Yu, J. Song, S. Fang, and L. Abi, "Speed Based Power Control of Integrated Powertrain With Two-Speed Transmission for PEV," in *International*

Design Engineering Technical Conferences and Computers and Information in Engineering Conference, 2019, vol. 59216: American Society of Mechanical Engineers, p. V003T01A034.

[24] J.-O. Han, J.-W. Shin, J.-C. Kim, and S.-H. Oh, "Design 2-Speed Transmission for Compact Electric Vehicle Using Dual Brake System," *Applied Sciences,* vol. 9, no. 9, p. 1793, 2019.

[25] J. Cui, G. Tan, Z. Tian, and P. Agyeman, "Parameter Optimization of Two-Speed AMT Electric Vehicle Transmission System," SAE Technical Paper, 0148-7191, 2020.

[26] S. Kim and S. B. Choi, "Cooperative Control of Drive Motor and Clutch for Gear Shift of Hybrid Electric Vehicles with Dual-clutch Transmission," *IEEE/ASME Transactions on Mechatronics,* 2020.

[27] K. Kwon, M. Seo, and S. Min, "Efficient multi-objective optimization of gear ratios and motor torque distribution for electric vehicles with two-motor and two-speed powertrain system," *Applied Energy,* vol. 259, p. 114190, 2020.

[28] A. Ritari, J. Vepsäläinen, K. Kivekäs, K. Tammi, and H. Laitinen, "Energy Consumption and Lifecycle Cost Analysis of Electric City Buses with Multispeed Gearboxes," *Energies,* vol. 13, no. 8, p. 2117, 2020.

[29] U. Knodel, "Electric axle drives for axle-split-hybrids and EV-applications," in *9th European all-wheel drive congress*, 2009, pp. 16-17.

[30] U. Knodel and A. STRUBE, "Design and implementation of requirement-driven electric drives [J]," *ATZ World-wide,* vol. 112, no. 6, pp. 56-60, 2010.

[31] D. Paul, "Multi-speed transmissions for electric vehicle applications," in *Proc. UK Low Carbon Veh. Event*, 2011.

[32] J. Ruan, "Design and verification of novel powertrain management for multi-geared battery electric vehicles," 2016.

[33] S. Bai, J. Maguire, and H. Peng, "Dynamic Analysis and Control System Design," *SAE international,* 2013.

[34] P. Walker, B. Zhu, and N. Zhang, "Powertrain dynamics and control of a two speed dual clutch transmission for electric vehicles," *Mechanical Systems and Signal Processing,* vol. 85, pp. 1-15, 2017.

[35] M. S. R. Mousavi, A. Pakniyat, T. Wang, and B. Boulet, "Seamless dual brake transmission for electric vehicles: Design, control and experiment," *Mechanism and Machine Theory,* vol. 94, pp. 96-118, 2015.

[36] S. Fang, J. Song, H. Song, Y. Tai, F. Li, and T. S. Nguyen, "Design and control of a novel two-speed uninterrupted mechanical transmission for electric vehicles," *Mechanical Systems and Signal Processing,* vol. 75, pp. 473-493, 2016.

[37] Y. Tian, J. Ruan, N. Zhang, J. Wu, and P. Walker, "Modelling and control of a novel two-speed transmission for electric vehicles," *Mechanism and Machine Theory,* vol. 127, pp. 13-32, 2018, doi: 10.1016/j.mechmachtheory.2018.04.023.

[38] E. Galvagno, M. Velardocchia, and A. Vigliani, "Analysis and simulation of a torque assist automated manual transmission," *Mechanical Systems and Signal Processing,* vol. 25, no. 6, pp. 1877-1886, 2011.

[39] B. Gao, Y. Xiang, H. Chen, Q. Liang, and L. Guo, "Optimal trajectory planning of motor torque and clutch slip speed for gear shift of a two-speed electric vehicle," *Journal of Dynamic Systems, Measurement, and Control,* vol. 137, no. 6, 2015.

[40] G. Lucente, M. Montanari, and C. Rossi, "Modelling of an automated manual transmission system," *Mechatronics,* vol. 17, no. 2, pp. 73-91, 2007.

[41] J. Zhang, L. Chen, and G. Xi, "System dynamic modelling and adaptive optimal control for automatic clutch engagement of vehicles," *Proceedings of the Institution of Mechanical Engineers, Part D: Journal of Automobile Engineering,* vol. 216, no. 12, pp. 983-991, 2002.

[42] C.-H. Tseng and M.-F. Hsieh, "Analysis and optimization of clutch actuator on automated manual transmission system," SAE Technical Paper, 0148-7191, 2005.

[43] C.-H. Yu and C.-Y. Tseng, "Research on gear-change control technology for the clutchless automatic ‐ manual transmission of an electric vehicle," *Proceedings of the Institution of Mechanical Engineers, Part D: Journal of Automobile Engineering,* vol. 227, no. 10, pp. 1446-1458, 2013.

[44] M. Kane, "Details On BMW i8's GKN 2-Speed eAxle," Insideevs, 2014.

[45] W. Mo, P. D. Walker, Y. Fang, J. Wu, J. Ruan, and N. Zhang, "A novel shift control concept for multi-speed electric vehicles," *Mechanical Systems and Signal Processing,* vol. 112, pp. 171-193, 2018, doi: 10.1016/j.ymssp.2018.04.017.

[46] W. Mo, P. D. Walker, and N. Zhang, "Dynamic analysis and control for an electric vehicle with harpoon-shift synchronizer," *Mechanism and Machine Theory,* vol. 133, pp. 750-766, 2019, doi: 10.1016/j.mechmachtheory.2018.11.018.

[47] H. Chen and G. Tian, "Modeling and analysis of engaging process of automated mechanical transmissions," *Multibody System Dynamics,* vol. 37, no. 4, pp. 345-369, 2015, doi: 10.1007/s11044-015-9490-7.

[48] M. Z. Piracha, A. Grauers, E. Barrientos, H. Budacs, and J. Hellsing, "Model Based Control of Synchronizers for Reducing Impacts during Sleeve to Gear Engagement," presented at the SAE Technical Paper Series, 2019.

[49] M. Z. Piracha, A. Grauers, and J. Hellsing, "Feedback Control of Synchronizers for Reducing Impacts during Sleeve to Gear Engagement," presented at the SAE Technical Paper Series, 2020.

[50] B. Gao, Y. Xiang, H. Chen, Q. Liang, and L. Guo, "Optimal trajectory planning of motor torque and clutch slip speed for gear shift of a two-speed electric vehicle," *Journal of Dynamic Systems, Measurement, and Control,* vol. 137, no. 6, p. 061016, 2015.

[51] H. Kuroiwa, N. Ozaki, T. Okada, and M. Yamasaki, "Next-generation fuel-efficient automated manual transmission," *Hitachi Review,* vol. 53, no. 4, p. 205, 2004.

[52] H. Yue, C. Zhu, and B. Gao, "Fork-less two-speed I-AMT with overrunning clutch for light electric vehicle," *Mechanism and Machine Theory,* vol. 130, pp. 157-169, 2018, doi: 10.1016/j.mechmachtheory.2018.08.019.

[53] M. Goetz, M. Levesley, and D. Crolla, "Dynamics and control of gearshifts on twin-clutch transmissions," *Proceedings of the institution of mechanical engineers, Part D: Journal of Automobile Engineering,* vol. 219, no. 8, pp. 951-963, 2005.

[54] Y. Zhang, X. Chen, X. Zhang, H. Jiang, and W. Tobler, "Dynamic modeling and simulation of a dual-clutch automated lay-shaft transmission," *Transactions of the ASME-R-Journal of Mechanical Design,* vol. 127, no. 2, pp. 302-307, 2005.

[55] P. D. Walker, N. Zhang, and R. Tamba, "Control of gear shifts in dual clutch transmission powertrains," *Mechanical Systems and Signal Processing,* vol. 25, no. 6, pp. 1923-1936, 2011.

[56] B. Zhu, N. Zhang, P. Walker, W. Zhan, X. Zhou, and J. Ruan, "Two-speed DCT electric powertrain shifting control and rig testing," *Advances in Mechanical Engineering,* vol. 5, p. 323917, 2013.

[57] S. Hong, H. Son, S. Lee, J. Park, K. Kim, and H. Kim, "Shift control of a dry-type two-speed dual-clutch transmission for an electric vehicle," *Proceedings of the*

Institution of Mechanical Engineers, Part D: Journal of Automobile Engineering, vol. 230, no. 3, pp. 308-321, 2015, doi: 10.1177/0954407015585686.

[58] A. Serrarens, "Roadmap of DTI's Efficient Power shift Transmissions," in *Proceedings, CTI Symposium on Innovative Automotive Transmissions, Berlin*, 2009.

[59] M. Yamasaki, H. Konno, H. Kuroiwa, and N. Ozaki, "Automated manual transmission with torque assist mechanism for reducing shift shock," SAE Technical Paper, 0148-7191, 2005.

[60] K. Zhao, Y. Liu, X. Huang, R. Yang, and J. Wei, "Uninterrupted shift transmission and its shift characteristics," *IEEE/ASME Transactions on Mechatronics,* vol. 19, no. 1, pp. 374-383, 2014.

[61] P. Koneda and T. Stockton, "Design of a two-speed automatic transaxle for an electric vehicle," SAE Technical Paper, 0148-7191, 1985.

[62] H. Song, J. Song, S. Fang, Y. Tai, F. Li, and T. S. Nguyen, "Analysis of the Novel Two-Speed Uninterrupted Transmission With Centrifugal Clutch for Electric Vehicle," in *ASME 2015 International Design Engineering Technical Conferences and Computers and Information in Engineering Conference*, 2015: American Society of Mechanical Engineers, pp. V010T11A053-V010T11A053.

[63] J. Kim, F. Park, Y. Park, and M. Shizuo, "Design and analysis of a spherical continuously variable transmission," *Journal of Mechanical Design,* vol. 124, no. 1, pp. 21-29, 2002.

[64] T. Iino *et al.*, "Research of hydrostatic CVT for passenger vehicles," *JSAE review,* vol. 24, no. 2, pp. 227-230, 2003.

[65] G. Carbone, L. Mangialardi, and G. Mantriota, "A comparison of the performances of full and half toroidal traction drives," *Mechanism and Machine Theory,* vol. 39, no. 9, pp. 921-942, 2004.

[66] T. Hofman and C. Dai, "Energy efficiency analysis and comparison of transmission technologies for an electric vehicle," in *Vehicle Power and Propulsion Conference (VPPC), 2010 IEEE*, 2010: IEEE, pp. 1-6.

[67] A. Ge, H. Jin, H. Zhang, J. Fan, and H. Yin, "Study on automobile intelligent shift architecture," *China Mechanical Engineering,* vol. 5, no. 18, pp. 106-109, 2001.

[68] H. Yamaguchi, Y. Narita, H. Takahashi, and Y. Katou, "Automatic transmission shift schedule control using fuzzy logic," SAE Technical Paper, 0148-7191, 1993.

[69] J. Tan, X. Yin, Y. Lei, and A. Ge, "Research on a neural network model based automatic shift schedule with dynamic 3-parameters," SAE Technical Paper, 0148-7191, 2005.

[70] Y. Liu, D. Qin, H. Jiang, C. Liu, Y. Zhang, and Z. Lei, "Shift schedule optimization for dual clutch transmissions," in *Vehicle Power and Propulsion Conference, 2009. VPPC'09. IEEE*, 2009: IEEE, pp. 1071-1078.

[71] J.-q. Li, M. Lu, and Y.-q. Zhu, "The study on the gear shifting strategy for 2-speed planetary transmission of plug-in electric buses," in *2nd International*

Conference on Electronic & Mechanical Engineering and Information Technology, 2012: Atlantis Press.

[72] X. Jun-Qiang, X. Guang-Ming, and Z. Yan, "Application of automatic manual transmission technology in pure electric bus," in *Vehicle Power and Propulsion Conference, 2008. VPPC'08. IEEE*, 2008: IEEE, pp. 1-4.

[73] R. Bellman, *Dynamic programming*. Courier Corporation, 2013.

[74] D. Ngo, T. Hofman, M. Steinbuch, A. Serrarens, and L. Merkx, "Improvement of fuel economy in Power-Shift Automated Manual Transmission through shift strategy optimization-an experimental study," in *Vehicle Power and Propulsion Conference (VPPC), 2010 IEEE*, 2010: IEEE, pp. 1-5.

[75] D. Kim, H. Peng, S. Bai, and J. M. Maguire, "Control of integrated powertrain with electronic throttle and automatic transmission," *IEEE Transactions on Control Systems Technology,* vol. 15, no. 3, pp. 474-482, 2007.

[76] K. Hayashi, Y. Shimizu, Y. Dote, A. Takayama, and A. Hirako, "Neuro fuzzy transmission control for automobile with variable loads," *IEEE Transactions on Control Systems Technology,* vol. 3, no. 1, pp. 49-53, 1995.

[77] S. Bai, J. Maguire, and H. Peng, *Dynamic analysis and control system design of automatic transmissions*. SAE International Warrendale, Pennsylvania, 2013.

[78] Z.-G. Zhao, H.-J. Chen, Y.-Y. Yang, and L. He, "Torque coordinating robust control of shifting process for dry dual clutch transmission equipped in a hybrid car," *Vehicle System Dynamics,* vol. 53, no. 9, pp. 1269-1295, 2015.

[79] N. Zhang, D. Liu, J. Jeyakumaran, and L. Villanueva, "Modelling of dynamic characteristics of an automatic transmission during shift changes," *Proceedings of the Institution of Mechanical Engineers, Part I: Journal of Systems and Control Engineering,* vol. 216, no. 4, pp. 331-341, 2002.

[80] M. Cao, K. Wang, Y. Fujii, and W. Tobler, "Advanced hybrid neural network automotive friction component model for powertrain system dynamic analysis. Part 2: system simulation," *Proceedings of the Institution of Mechanical Engineers, Part D: Journal of Automobile Engineering,* vol. 218, no. 8, pp. 845-857, 2004.

[81] Y. Fujii, W. Tobler, and T. Snyder, "Prediction of wet band brake dynamic engagement behaviour Part 1: mathematical model development," *Proceedings of the Institution of Mechanical Engineers, Part D: Journal of Automobile Engineering,* vol. 215, no. 4, pp. 479-492, 2001.

[82] Y. Fujii, W. Tobler, and T. Snyder, "Prediction of wet band brake dynamic engagement behaviour Part 2: Experimental model validation," *Proceedings of the Institution of Mechanical Engineers, Part D: Journal of Automobile Engineering,* vol. 215, no. 5, pp. 603-611, 2001.

[83] M. Pettersson and L. Nielsen, "Gear shifting by engine control," *IEEE Transactions on Control Systems Technology,* vol. 8, no. 3, pp. 495-507, 2000.

[84] M. Pettersson and L. Nielsen, "Diesel engine speed control with handling of driveline resonances," *Control Engineering Practice,* vol. 11, no. 3, pp. 319-328, 2003.

[85] J. Baumann, D. D. Torkzadeh, A. Ramstein, U. Kiencke, and T. Schlegl, "Model-based predictive anti-jerk control," *Control Engineering Practice,* vol. 14, no. 3, pp. 259-266, 2006.

[86] R. Ahlawat, H. Fathy, B. Lee, J. Stein, and D. Jung, "Modelling and simulation of a dual-clutch transmission vehicle to analyse the effect of pump selection on fuel economy," *Vehicle system dynamics,* vol. 48, no. 7, pp. 851-868, 2010.

[87] J. J. Oh and S. B. Choi, "Real-time estimation of transmitted torque on each clutch for ground vehicles with dual clutch transmission," *IEEE/ASME Transactions on Mechatronics,* vol. 20, no. 1, pp. 24-36, 2015.

[88] R. Masmoudi and J. Hedrick, "Estimation of vehicle shaft torque using nonlinear observers," *Journal of dynamic systems, measurement, and control,* vol. 114, no. 3, pp. 394-400, 1992.

[89] K. Yi, B.-K. Shin, and K.-I. Lee, "Estimation of turbine torque of automatic transmissions using nonlinear observers," *Journal of dynamic systems, measurement, and control,* vol. 122, no. 2, pp. 276-283, 2000.

[90] S. Watechagit and K. Srinivasan, "Implementation of on-line clutch pressure estimation for stepped automatic transmissions," in *American Control Conference, 2005. Proceedings of the 2005*, 2005: IEEE, pp. 1607-1612.

[91] S. Watechagit and K. Srinivasan, "Online estimation of operating variables for stepped automatic transmissions," in *Control Applications, 2003. CCA 2003. Proceedings of 2003 IEEE Conference on*, 2003, vol. 1: IEEE, pp. 279-284.

[92] J.-O. Hahn and K.-I. Lee, "Nonlinear robust control of torque converter clutch slip system for passenger vehicles using advanced torque estimation algorithms," *Vehicle System Dynamics,* vol. 37, no. 3, pp. 175-192, 2002.

[93] Z. Zhao, L. He, Y. Yang, C. Wu, X. Li, and J. K. Hedrick, "Estimation of torque transmitted by clutch during shifting process for dry dual clutch transmission," *Mechanical Systems and Signal Processing,* vol. 75, pp. 413-433, 2016.

[94] J. Wu, P. D. Walker, J. Ruan, and N. Zhang, "Target torque estimation for gearshift in dual clutch transmission with uncertain parameters," *Applied Mathematical Modelling,* vol. 51, pp. 1-20, 2017.

[95] B. Gao, H. Chen, L. Tian, and K. Sanada, "A nonlinear clutch pressure observer for automatic transmission: considering drive-shaft compliance," *Journal of Dynamic Systems, Measurement, and Control,* vol. 134, no. 1, p. 011018, 2012.

[96] V. A. Neelakantan, G. N. Washington, and N. K. Bucknor, "Model predictive control of a two stage actuation system using piezoelectric actuators for

controllable industrial and automotive brakes and clutches," *Journal of Intelligent Material Systems and Structures,* vol. 19, no. 7, pp. 845-857, 2008.

[97] B. Z. Gao, H. Chen, K. Sanada, and Y. Hu, "Design of clutch-slip controller for automatic transmission using backstepping," *IEEE/ASME Transactions on mechatronics,* vol. 16, no. 3, pp. 498-508, 2011.

[98] A. Yoon, P. Khargonekar, and K. Hebbale, "Randomized algorithms for open-loop control of clutch-to-clutch transmissions," *Journal of dynamic systems, measurement, and control,* vol. 121, no. 3, pp. 508-517, 1999.

[99] H. Hu, X. Wang, and Y. Shao, "Optimization of the shift quality of dual clutch transmission using genetic algorithm," in *Natural Computation (ICNC), 2010 Sixth International Conference on*, 2010, vol. 8: IEEE, pp. 4152-4156.

[100] Z. Zhao, H. Chen, and Y. Yang, "Fuzzy determination of target shifting time and torque control of shifting phase for dry dual clutch transmission," *Mathematical Problems in Engineering,* vol. 2014, 2014.

[101] X. Song and Z. Sun, "Pressure-based clutch control for automotive transmissions using a sliding-mode controller," *IEEE/ASME Transactions on mechatronics,* vol. 17, no. 3, pp. 534-546, 2012.

[102] L. Chen, G. Xi, and C. Yin, "Model referenced adaptive control to compensate slip-stick transition during clutch engagement," *International Journal of Automotive Technology,* vol. 12, no. 6, pp. 913-920, 2011.

[103] L. Glielmo, L. Iannelli, V. Vacca, and F. Vasca, "Gearshift control for automated manual transmissions," *IEEE/ASME transactions on mechatronics,* vol. 11, no. 1, pp. 17-26, 2006.

[104] Y. Dong, X. Jiao, and D. Chen, "Adaptive control for clutch engagement on starting up of vehicle," in *Intelligent Control and Automation (WCICA), 2012 10th World Congress on*, 2012: IEEE, pp. 1230-1234.

[105] P. D. Walker, Y. Fang, and N. Zhang, "Dynamics and control of clutchless automated manual transmissions for electric vehicles," *Journal of Vibration and Acoustics,* vol. 139, no. 6, p. 061005, 2017.

[106] T. Jin, P. Li, and G. Zhu, "Optimal decoupled control for dry clutch engagement," in *American Control Conference (ACC), 2013*, 2013: IEEE, pp. 6740-6745.

[107] F. Meng, P. Shi, H. R. Karimi, and H. Zhang, "Optimal design of an electro-hydraulic valve for heavy-duty vehicle clutch actuator with certain constraints," *Mechanical Systems and Signal Processing,* vol. 68, pp. 491-503, 2016.

[108] A. V. D. Heijden, A. Serrarens, M. Camlibel, and H. Nijmeijer, "Hybrid optimal control of dry clutch engagement," *International Journal of Control,* vol. 80, no. 11, pp. 1717-1728, 2007.

[109] T. Szabo, M. Buchholz, and K. Dietmayer, "Optimal control of a gearshift with a dual-clutch transmission," *ASME Paper No. DSCC2011-6028,* 2011.

[110] A. Haj-Fraj and F. Pfeiffer, "Optimal control of gear shift operations in automatic transmissions," *Journal of the Franklin Institute,* vol. 338, no. 2, pp. 371-390, 2001.

[111] X. Song, M. A. M. Zulkefli, Z. Sun, and H.-C. Miao, "Modeling, analysis, and optimal design of the automotive transmission ball capsule system," *Journal of dynamic systems, measurement, and control,* vol. 132, no. 2, p. 021003, 2010.

[112] X. Song, M. A. M. Zulkefli, Z. Sun, and H.-C. Miao, "Automotive transmission clutch fill control using a customized dynamic programming method," *Journal of Dynamic Systems, Measurement, and Control,* vol. 133, no. 5, p. 054503, 2011.

[113] F. Garofalo, L. Glielmo, L. Iannelli, and F. Vasca, "Optimal tracking for automotive dry clutch engagement," *IFAC Proceedings Volumes,* vol. 35, no. 1, pp. 367-372, 2002.

[114] B. Tepes, J. Kasac, and J. Deur, "Optimal control of automated transmission engagement process," in *Control Applications (CCA), 2012 IEEE International Conference on*, 2012: IEEE, pp. 329-335.

[115] P. D. Walker, N. Zhang, W. Zhan, and B. Zhu, "Modelling and simulation of gear synchronisation and shifting in dual-clutch transmission equipped powertrains," *Proceedings of the Institution of Mechanical Engineers, Part C: Journal of Mechanical Engineering Science,* vol. 227, no. 2, pp. 276-287, 2013.

[116] M. Géradin and D. J. Rixen, *Mechanical vibrations: theory and application to structural dynamics*. John Wiley & Sons, 2014.

[117] Y. Fu, Y. Liu, L. Cui, and X. Xu, "Dynamic analysis and control strategy of wet clutches during torque phase of gear shift," *Journal of Mechanical Science and Technology,* vol. 30, no. 4, pp. 1479-1496, 2016.

[118] A. R. Crowther, R. Singh, N. Zhang, and C. Chapman, "Impulsive response of an automatic transmission system with multiple clearances: Formulation, simulation and experiment," *Journal of Sound and Vibration,* vol. 306, no. 3-5, pp. 444-466, 2007.

[119] Y. Fujii, W. Tobler, E. Clausing, T. Megli, and M. Haghgooie, "Application of dynamic band brake model for enhanced drivetrain simulation," *Proceedings of the Institution of Mechanical Engineers, Part D: Journal of Automobile Engineering,* vol. 216, no. 11, pp. 873-881, 2002.

[120] T. Minowa, T. Ochi, H. Kuroiwa, and K.-Z. Liu, "Smooth gear shift control technology for clutch-to-clutch shifting," SAE Technical Paper, 0148-7191, 1999.

[121] S. Bai, R. L. Moses, T. Schanz, and M. J. Gorman, "Development of a new clutch-to-clutch shift control technology," *SAE Transactions,* pp. 1663-1672, 2002.

[122] J. E. Marano, S. P. Moorman, M. D. Whitton, and R. L. Williams, "Clutch-to-clutch transmission control strategy," SAE Technical Paper, 0148-7191, 2007.

[123] S. Kim, J. Oh, and S. Choi, "Gear shift control of a dual-clutch transmission using optimal control allocation," *Mechanism and Machine Theory,* vol. 113, pp. 109-125, 2017, doi: 10.1016/j.mechmachtheory.2017.02.013.

[124] M. Kulkarni, T. Shim, and Y. Zhang, "Shift dynamics and control of dual-clutch transmissions," *Mechanism and machine theory,* vol. 42, no. 2, pp. 168-182, 2007.

[125] dSPACE, *dSPACE MicroAutoBox Manual*.

[126] "What is Rapid Prototyping?" https://tech-labs.com/rapid-prototyping (accessed.

[127] "Rapid Control Prototyping." https://www.dspace.com/en/pub/home/applicationfields/our_solutions_for/bussimulation/bussimulation_usecases/rapid_control_prototyping.cfm (accessed.

[128] Z. Bubnicki, *Modern control theory*. Springer, 2005.

[129] R. Bellman and R. E. Kalaba, *Dynamic programming and modern control theory*. Citeseer, 1965.

[130] L. D. Berkovitz, *Optimal control theory*. Springer Science & Business Media, 2013.

[131] M. Roozegar and J. Angeles, "The optimal gear-shifting for a multi-speed transmission system for electric vehicles," *Mechanism and Machine Theory,* vol. 116, pp. 1-13, 2017.

[132] K. D. Mishra and K. Srinivasan, "Robust control and estimation of clutch-to-clutch shifts," *Control Engineering Practice,* vol. 65, pp. 100-114, 2017.

[133] V. I. Utkin, "Scope of the theory of sliding modes," in *Sliding modes in control and optimization*: Springer, 1992, pp. 1-11.

[134] V. Utkin, J. Guldner, and J. Shi, *Sliding mode control in electro-mechanical systems*. CRC press, 2009.

[135] J. J. Uicker, G. R. Pennock, and J. E. Shigley, *Theory of machines and mechanisms*. Oxford University Press New York, NY, 2011.

[136] L. Lovas, D. Play, J. Márialigeti, and J.-F. Rigal, "Mechanical behaviour simulation for synchromesh mechanism improvements," *Proceedings of the Institution of Mechanical Engineers, Part D: Journal of Automobile Engineering,* vol. 220, no. 7, pp. 919-945, 2006.

[137] P. Walker, N. Zhang, R. Tamba, and S. Fitzgerald, "Synchroniser modeling with application specific to the dual clutch transmission," in *Asia Pacific Vibration Conference*, 2009: University of Canterbury, Christchurch, New Zealand.

[138] P. D. Walker and N. Zhang, "Engagement and control of synchroniser mechanisms in dual clutch transmissions," *Mechanical systems and signal processing,* vol. 26, pp. 320-332, 2012.

[139] H. Chen, X. Cheng, and G. Tian, "Modeling and analysis of gear-shifting process of motor-transmission coupled drive system," *Journal of Computational and Nonlinear Dynamics,* vol. 11, no. 2, p. 021013, 2016.

[140] Z. Zhao, L. He, Z. Zheng, Y. Yang, and C. Wu, "Self-adaptive optimal control of dry dual clutch transmission (DCT) during starting process," *Mechanical Systems and Signal Processing,* vol. 68-69, pp. 504-522, 2016, doi: 10.1016/j.ymssp.2015.06.012.